Inelastic Light Scattering from Correlated Electrons

Thomas P. Devereaux[*]

Department of Physics, University of Waterloo, Waterloo, ON, Canada N2L 3G1

Rudi Hackl[†]

Walther Meissner Institute, Bavarian Academy of Sciences, 85748 Garching, Germany

(Dated: July 16, 2006)

Inelastic light scattering is an intensively used tool in the study of electronic properties of solids. Triggered by the discovery of high temperature superconductivity in the cuprates and by new developments in instrumentation, light scattering both in the visible (Raman effect) and the X-ray part of the electromagnetic spectrum has become a method complementary to optical (infrared) spectroscopy while providing additional and relevant information. The main purpose of the review is to position Raman scattering with regard to single-particle methods like angle-resolved photoemission spectroscopy (ARPES), and other transport and thermodynamic measurements in correlated materials. Particular focus is placed on photon polarizations and the role of symmetry to elucidate the dynamics of electrons in different regions of the Brillouin zone. This advantage over conventional transport (usually measuring averaged properties) indeed provides new insights into anisotropic and complex many-body behavior of electrons in various systems. We review recent developments in the theory of electronic Raman scattering in correlated systems and experimental results in paradigmatic materials such as the A15 superconductors, magnetic and paramagnetic insulators, compounds with competing orders, as well as the cuprates with high superconducting transition temperatures. We present an overview of the manifestations of complexity in the Raman response due to the impact of correlations and developing competing orders. In a variety of materials we discuss which observations may be understood and summarize important open questions that pave the way to a detailed understanding of correlated electron systems.

Contents

[*]Electronic address: d@ ̄ ̄a y a e ̄ .ca
[†]Electronic address: ha ̄ @ i.bad .de

I. INTRODUCTION

A. Overview

Raman scattering is a photon-in photon-out process with energy transfered to a target material. Most of the light is elastically scattered from the sample, a fraction is color-shifted and collected at the detector.

Light couples to electronic charge in solids and can scatter inelastically from many types of excitations in a sample, as shown schematically for $YBa_2Cu_3O_{6.5}$ in Figure 1. Optical phonons produce sharp peaks at well known positions and orientations of the incoming and outgoing photon polarizations, while a large broad feature centered at much higher energies due to two-magnon scattering occurs in compounds with antiferromagnetic correlations. This review article largely places emphasis on the electronic Raman scattering continuum upon which the phonons and magnons are superimposed.

Light scatters off of electrons by creating variations of electronic charge density in the illuminated region of a sample. By observing the frequency shift and polarization change of the outgoing photon compared to the incoming photon, the properties of charge density relaxation is measured. However, measuring the Raman effect of photons scattering from electrons is a difficult proposal to carry forward. It is made difficult precisely because of the coupling of the real photon vector potential and the exchange of virtual photons which mediate the Coulomb forces between electrons. In simple metals, variations of the charge density will be largely screened by the mobile electrons, and the system of electrons responds collectively at a characteristic plasma frequency of several electron volts. In semiconductors or well-developed band insulators, the creation of charge density fluctuations occurs only via the population of excited states across a band gap - again on the scale of several electron volts. Therefore it is difficult to investigate the behavior of electrons at low energies. In fact, hardly *any* measurements of electronic Raman scattering in simple metals exist precisely for this reason, and focus on semiconductors is usually placed on plasma excitations. Since the dynamics of electrons lying near the Fermi surface govern the behavior of transport in most systems, this would give the impression that Raman would have but little to offer in simple metals and insulators.

Yet the Raman effect is extremely well suited to study electrons in systems with non-trivial electron dynamics. First well-studied in the context of breaking Cooper pairs in superconductors in the period from 1980 to 1990, the field of Raman scattering from electronic excitations has grown tremendously over the past few decades to study the evolution of electron correlations in a variety of systems in which many-body interactions are essential to the physics of new materials and their potential device applications.

Raman spectroscopy has become an indispensable tool in the arsenal for understanding many-body physics. One of the most celebrated achievements of electronic Raman scattering has been the ability to focus on the nature of electron dynamics in different regions of the Brillouin zone. This distinguishes Raman scattering from most other transport and thermodynamic measurements, allowing the study of the development of correlations in projected regions of the Brillouin zone. By simply aligning the polarization orientations of the incoming and outgoing photons, charge excitations can be selectively mapped and analyzed using group-theoretical symmetry arguments. The search for conventional as well as exotic excitations in strongly correlated matter has been greatly enhanced. Raman spectroscopy has provided new and valuable insights into unconventional superconductivity and collective modes, excitations in charge, spin and/or orbitally ordered systems as well as the competition between the various ordered phases. In addition, new insights into electron dynamics of metal-insulator transitions, quantum phase transitions, and the concomitant quantum critical behavior could be obtained. The purpose of this article is to review the essence of these new developments in a "snapshot" of the current state of investigation.

The overall agenda of the paper is to provide a vehicle to sort through the extensive literature, learn about the outstanding problems, and become aware of the level of consensus. In order to present a detailed picture of the current status of electronic light scattering, other types of excitations, such as phonons and magnons, are mainly ignored. There have been many reviews on inelastic light scattering from phonons and magnons. The reader is referred to earlier reviews by Klein (1982b) for a fundamental treatment of scattering from phonons, while studies of phonons in high temperature superconductors are summarized by Thomsen (1989) and Sherman *et al.* (2003). Recently Lemmens *et al.* (2003) and Gozar *et al.* (2005b) reviewed magnetic light scattering in low-dimensional quantum spin systems and cuprates. Due to space limitations we cannot give adequate commentary on these exciting and developing fields.

The outline of our review is as follows. After a brief historical summary, the fundamental experimental aspects and theoretical developments for electronic Raman scattering are presented in the first part of the article. A general treatise on the theory of electronic Raman scattering is given in Section II with a view toward the formalism for both weak and strong correlations. Results from model-specific calculations can be found in Section II.D. Readers who are more interested in summaries of experimental work may want to skim these sections and skip to Section III, where a review of Raman scattering measurements in a variety of correlated materials is given with a view toward common features manifest from strong correlations. The presentation is generally organized in systems with increasing complexity of correlations and competing orders.

In this framework, the canon of work on the high temperature superconductors in the last part of our review is
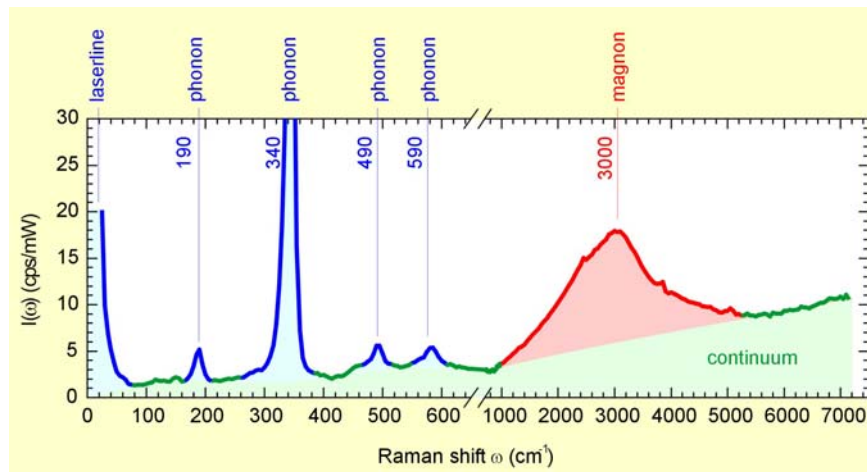
FIG. 1 Characteristic Raman scattering spectrum taken on $YBa_2Cu_3O_{6.5}$ showing light scattering from phonons (blue lines), magnons (red), and electrons (green). Courtesy of Matthias Opel.

presented in Section IV. This detailed part of the review is organized in conceptual issues of correlations, superconductivity, normal state properties, and the propensity toward charge and spin ordering in various families of the cuprates. In all subsections in this part, data on a variety of cuprate materials are summarized.

The review closes with a general discussion of open questions for both experimental and theoretical developments in Raman scattering, and points out new directions in which our understanding of electronic correlations may be further enhanced.

B. Historical Review

Inelastic scattering of light was discovered independently in organic liquids by Raman and Krishnan (1928) and in quartz by Landsberg and Mandelstam (1928) who properly explained the observed effect: The energy of the incoming photon is split between the scattered one and an elementary excitation in the solid. Shortly thereafter in 1930 C. V. Raman was awarded the Nobel prize, and his name was associated with the effect (Fabelinskiĭ, 1998; Ginzburg, 1998; Pleijel, 1930). Although the phenomenological description by Smekal (1923) in terms of a periodically modulated polarizability qualitatively captures the relevant physics including the selection rules, the effect is genuinely quantum mechanical as described first and ahead of the experimental discovery by Kramers and Heisenberg (1925) in context of the dispersion in dielectrics.

Soon after the observation of light scattering from vibrational excitations, Verkin and Lazarev (1948) and Khaĭkin and Bykov (1956) attempted to use the new technique for studying electronic excitations. They picked one of the most ambitious subjects, i.e., light scattering from superconducting gap excitations in conventional metals. It is not at all surprising that they

could not succeed. In a seminal paper Abrikosov and Fal'kovskiĭ (1961) not only calculated the Raman response of a typical elemental superconductor but also demonstrated that the sensitivity in the early experiments was by approximately 5 or 6 orders of magnitude too low. In 1980 light was finally scattered successfully from superconducting electrons in $2H - NbSe_2$ (Sooryakumar and Klein, 1980). Balseiro and Falicov (1980) and Littlewood and Varma (1981, 1982) argued that the superconducting excitations in this system become Raman active mainly via their coupling to a charge-density wave mode (CDW). After the observation of gap excitations in the A15 compounds Nb_3Sn and V_3Si (Dierker *et al.*, 1983; Hackl *et al.*, 1982, 1983; Klein, 1982a) it was clear that light can be scattered directly by Cooper pairs (Dierker *et al.*, 1983; Klein and Dierker, 1984). Tüttő and Zawadowski (1992) demonstrated that both types of coupling contribute.

Collective excitations of normal electrons were first observed in semiconductors (Mooradian and Wright, 1966) following theoretical studies by Pines (1963), Platzman and Tzoar (1964). As a function of doping the plasmon peak moves across the phonon energies leading to strong electron-lattice interactions. In heavily doped silicon, with the plasma energy well beyond the vibration spectrum, the evolution of the phonon line shape (Cerdeira *et al.*, 1973; Fano, 1961) clearly demonstrated the existence of an electron continuum. In 1977, fluctuations of electrons between pockets of the Fermi surface of silicon were observed by Chandrasekhar *et al.* (1977) and explained subsequently by Ipatova *et al.* (1981). In magnetic fields, transitions between Landau levels were found (Worlock *et al.*, 1981)[1]. Strong phonon renormalization

---

[1] The subject has been reviewed in detail by Abstreiter *et al.*

effects also occur in metallic alloys with A15 structure (Schicktanz *et al.*, 1980; Wipf *et al.*, 1978). The origin of the broad continuum, which interacts with phonons and is redistributed below the superconducting transition (Klein and Dierker, 1984), is certainly electronic but as of today is still not fully understood.

The full power of the method became apparent after the discovery of copper-oxygen compounds (Bednorz and Müller, 1986) with superconducting transition temperatures above 100 K. It turned out that, in contrast to infrared spectroscopy, momentum dependent transport properties can be measured with Raman spectroscopy, since different regions of the Brillouin zone can be projected out independently by appropriately selecting the polarizations of the incident and scattered photons (Devereaux *et al.*, 1994a). New theoretical ideas were not only applied to the superconducting but also to the normal state. The spectra extend over energy ranges as large as electron Volts (eV) (Bozovic *et al.*, 1987; Cooper *et al.*, 1988a,b; Kirillov *et al.*, 1988) and are similar to those in the A15s or in rare earth elements (Klein *et al.*, 1991). Both elastic (Zawadowski and Cardona, 1990) and inelastic (Itai, 1992; Kostur, 1991; Virosztek and Ruvalds, 1992) relaxation of electrons indeed produces light scattering over such a broad range of energies. It soon became clear that a continuum extending over an eV cannot originate from elastic scattering, but only from inelastic processes or interband transitions. However, it has not been straightforward to pin down the types of interactions.

At very low energies, spin- (Yoon *et al.*, 2000) and charge-ordering fluctuations were reported in manganites and, respectively, in ladder compounds (Blumberg *et al.*, 2002) and in the cuprates (Venturini *et al.*, 2002b). The response should not be confused with that of an ordered spin/charge-density-wave (SDW/CDW) state (Benfatto *et al.*, 2000; Klein, 1982c; Zeyher and Greco, 2002). Since a characteristic energy decreases rather than increases upon cooling (Blumberg *et al.*, 2002; Caprara *et al.*, 2002, 2005; Venturini *et al.*, 2002b; Yoon *et al.*, 2000), which is in clear contrast to typical order parameter behavior.

Along with the early studies of charge excitations, Fleury and coworkers observed Raman scattering from spin waves in antiferromagnetically ordered FeF_2, MnF_2, and K_2NiF_4 (Fleury *et al.*, 1966, 1967, 1970). Elliot and Loudon (1963) and Fleury and Loudon (1968) presented a detailed theoretical description which allowed them to semi-quantitatively understand the spectral shape and the cross section. With the discovery of the cuprates by Bednorz and Müller (1986) also this field experienced a renaissance in particular for the study at low doping close to the antiferromagnetic Néel state (Gozar *et al.*, 2004, 2005b; Lyons *et al.*, 1988; Sugai *et al.*, 1988; Sulewski *et al.*, 1991). Raman scattering is probably the most

precise method for determining the exchange coupling J though the theoretical understanding is still incomplete. In this context, spin-Peierls systems (Loosdrecht *et al.*, 1996) and ladder compounds (Abrashev *et al.*, 1997) shifted very much into the focus of interest (Dagotto, 1999).

Very recently, light scattering from "orbitons", i.e. from a propagating reorientation of orbitals, has been proposed to explain new modes in the the Raman spectra (Saitoh *et al.*, 2001). However, there is no agreement yet on whether or not orbitons can be observed independent of phonons or other excitations (Choi *et al.*, 2005; Grüninger *et al.*, 2002; Krüger *et al.*, 2004).

C. What Can One Learn from Electronic Raman Scattering?

We give now a qualitative introduction into the relationship between Raman spectroscopy and other experimental techniques. We begin by drawing the distinction between one-particle and many-particle properties.

Typically, electronic states in solids are characterized by their energy dispersions as well as the characteristic lifetime of an electron placed into such a state. This state is characterized by the single particle propagator or Green's function for the electron,

$$G(\mathbf{k},\omega) = \frac{1}{\omega - \xi_\mathbf{k} - \Sigma(\mathbf{k},\omega)}. \qquad (1)$$

Here $\xi_\mathbf{k}$ denotes the bare energy band dispersion calculated from a solvable model. Σ represents the electron self-energy which encompasses all the information pertaining to interactions of the single electron in state $\mathbf{k}$ to all other excitations of the system. Usually the self energy can only be obtained via approximate methods. Some of these approximations are quite good - such as electron-phonon interactions in metals (known as Migdal's approach (Migdal, 1958)) for example, while others are more difficult - such as the Coulomb interaction between other electrons. The self energy is a complex function, $\Sigma = \Sigma' + i\Sigma''$, which, in general, depends on temperature, momentum and energy. The real part of the self energy determines how the energy dispersion $\xi_\mathbf{k}$ is renormalized by the interactions while the imaginary part determines the lifetime of the quasiparticle placed into the state $\mathbf{k}$.

The spectral function is directly related to the analytically continued electron's Green's function for frequencies on the real axis via the replacement $i\omega \to \omega + i\delta$

$$A(\mathbf{k},\omega) = -\frac{1}{\pi}\lim_{\delta\to 0} G''(\mathbf{k},\omega+i\delta) \qquad (2)$$

which is measurable via modern angle-resolved photoemission (ARPES) techniques and has provided an immense amount of information in strongly correlated systems (Campuzano *et al.*, 2002; Damascelli *et al.*, 2003). For non-interacting electrons, $A(\mathbf{k},\omega)$ is a δ-function

peaked at the pole of the propagator when the frequency ω equals the bare band energy $\xi_{\mathbf{k}}$. Interactions broaden the spectral function and give it non-trivial temperature and frequency dependences as well as non-trivial anisotropies in momentum-space if the interactions among electrons are anisotropic. The spectral function describes real electrons, hence integrals over all energies must obey sum rules, such as (i) $\int d\omega A(\mathbf{k}, \omega) = 1$ and (ii) $\int d\omega f(\omega) A(\mathbf{k}, \omega) = n(\mathbf{k})$ with the Fermi Dirac distribution $f(\omega)$ and the momentum distribution function $n(\mathbf{k})$.

If the electronic interactions are weak, one usually uses the nomenclature of Landau and refers to dressed quasiparticles replacing the electron as the fundamental excitation in the solid. These interactions may be characterized by the residue of the pole (usually denoted by $Z_{\mathbf{k}}$) and the quasiparticle effective mass $m^*/m_{\mathrm{b}} = (Z_{\mathbf{k}})^{-1}$ with m_{b} the bare band mass for quasiparticles lying near the Fermi surface. $Z_{\mathbf{k}}$ is related to the real part of the self energy Σ' which can be expanded for electrons near the Fermi surface as $\Sigma'(\mathbf{k}, \omega) \simeq \Sigma_0'(\mathbf{k}) + \omega \partial \Sigma'(\mathbf{k}, \omega = 0)/\partial\omega$. According to Luttinger's theorem, the Fermi surface average of $\Sigma_0'(\mathbf{k})$ vanishes. The enhancement of the quasiparticle mass over the band mass can be written as $m^*/m_{\mathrm{b}} = (1 - \partial\Sigma'/\partial\omega)$. One often defines $m^*/m_{\mathrm{b}} = 1 + \lambda$ with the dimensionless coupling constant $\lambda \geq 0$ (see, e.g., (Ashcroft and Mermin, 1976)). $Z_{\mathbf{k}} = (1 - \partial\Sigma'/\partial\omega)^{-1}$ is always smaller than 1, reflecting the fact that even for $\omega = 0$ and $T = 0$ only a fraction $Z_{\mathbf{k}}$ of the spectral weight (coherent part) is in the pole of $A(\mathbf{k}, \omega)$ while $1 - Z_{\mathbf{k}}$ (incoherent part) is distributed over larger energy scales. Equivalently, $Z_{\mathbf{k}} \leq 1$ is the discontinuity at $\mathbf{k}_F$ of the zero-temperature momentum distribution function $n(\mathbf{k})$. If $Z_{\mathbf{k}}$ approaches zero $(\propto 1/\ln\omega)$ the system is referred to as a marginal Fermi liquid (Varma *et al.*, 1989a), and sum rule (i) is exhausted only at energies much larger than $\xi_{\mathbf{k}}$. Thus, knowledge of the self energy is an important requisite to understanding many-body interactions.

For this reason, single particle methods such as ARPES, electron tunneling and specific heat measurements have been applied extensively to study correlated electron systems. Very much stimulated by the discovery of superconductivity in the cuprates (Bednorz and Müller, 1986) ARPES and tunneling spectroscopy have developed more rapidly than any other method in the last decade. ARPES data has given unprecedented insight into momentum-resolved single electron properties and their many body effects (Campuzano *et al.*, 2002; Damascelli *et al.*, 2003), while tunneling measurements have provided information on pairing (Mandrus, 1991; Renner, 1995; Zasadzinski *et al.*, 2002) and have recently elucidated many issues of nanoscale inhomogeneities in the cuprates and their connection to superconductivity (Fang *et al.*, 2006; Hanaguri *et al.*, 2004; Hoffman *et al.*, 2002; Howald *et al.*, 2003; Kivelson *et al.*, 2003; McElroy *et al.*, 2003, 2005; Vershinin *et al.*, 2004). Detailed knowledge of phase transitions in the cuprates has been obtained from specific heat studies (Loram and Tallon,

2001; Moler *et al.*, 1994; Roulin *et al.*, 1998). Due to space limitations we only have listed some of the later references of important experimental papers which we hope serve as an entry point for the reader to search backwards in time to follow the developments.

Yet knowledge of the spectral function and single-particle excitation spectra do not yield information about how the electrons may transport heat, current, entropy, or energy. For this one needs two-particle correlation functions for charge or spin which can be measured by, e.g., ordinary and heat transport, optical spectroscopy, neutron and light scattering. As an example for such a correlation function we consider a standard expression for the generalized Kubo susceptibility $\chi_{a,b}''(\Omega)$ of weakly interacting, isotropic normal electrons (see, e.g., Mahan (2000)),

$$\chi_{a,b}''(\Omega) = \frac{2}{V} \sum_{\mathbf{k}} a_{\mathbf{k}} b_{\mathbf{k}} \int_{-\infty}^{\infty} \frac{d\omega}{\pi} G''(\mathbf{k}, \omega) G''(\mathbf{k}, \omega + \Omega)$$
$$\times [f(\omega) - f(\omega + \Omega)]. \tag{3}$$

Here V is the volume, $a_{\mathbf{k}}, b_{\mathbf{k}}$ are the bare vertices representing quasiparticle charge ($a_{\mathbf{k}} = 1$) or current ($a_{\mathbf{k}} = j_{\mathbf{k}} = e\mathbf{k}$) correlation functions, and the factor 2 accounts for spin degeneracy. The absorptive part of the conductivity $\sigma' = \chi_{\mathrm{j,j}}''(\Omega)/\Omega$ measures essentially a convolution of occupied and unoccupied states. For electrons weakly interacting with impurities the conductivity can readily be calculated to exhibit a Lorentzian dependence on Ω represented by

$$\sigma'(\Omega) = \sigma_0 \frac{1}{1 + (\Omega\tau)^2} \tag{4}$$

where σ_0 is the dc ($\Omega = 0$) conductivity, and the relaxation time $\tau = -\hbar(2\Sigma'')^{-1}$ controls both the width of the spectral function and the conductivity as a function of frequency.[2] A very similar expression is found for light scattering[3]. Thus in the case non-interacting electrons, single and two-particle correlation functions give similar results.

This is also true by and large if weak but essentially isotropic interactions lead to an energy dependent $\Sigma''(\omega)$ and, for causality, to a finite $\Sigma'(\omega)$. Götze and Wölfle (1972) and, more phenomenologically, Allen and Mikkelsen (1977) (for a more recent reference see (Basov and Timusk, 2005)) discuss how this generalization modifies the response given by Eq. (4), which is then often referred to as the extended Drude model. However, interacting systems require some care. For example, in

---

[2] Note that Eq. (3) does not return the proper transport lifetime τ_t which differs by a factor of typically $1 - \cos\theta$ with the scattering angle θ since events with $\theta \approx 0$ do not contribute to the resistivity. This deficit must be taken care of by vertex corrections (Mahan, 2000).

[3] The case of Raman scattering is described in detail in reference (Opel *et al.*, 2000) and touched upon briefly in section IV.D.1.

superconductors, both the single and the two-particle responses yield the energy gap. Yet two-particle correlation functions also have coherence factors which can be crucially important to determine the gap symmetry in unconventional systems. Generally, collective modes (such as the plasmon or excitons) appear directly in two-particle correlation functions but only indirectly in the spectral function.

Sometimes the results from single- and two-particle measurements can be qualitatively different, even for non-interacting electrons. As an illustration, we consider first the metal-insulator transition occurring in a system of otherwise non-interacting electrons in a disordered environment (Anderson transition). Here, backscattering of electrons from impurities leads to destructive phase interference, and the electrons become localized once a critical concentration of impurities is in place in three dimensions. Thus while the conductivity is critical and vanishes at the metal-insulator transition, the spectral function, or equivalently the density of states, is uncritical. This distinction becomes even more pronounced if the electron interactions are strong and anisotropic, and the bare vertices along with the Green's functions entering into Eq. (3) must be renormalized by the strong interactions.

As a second example, in the spinless Falicov-Kimball model light $d-$electrons strongly interact with localized $f-$electrons and are characterized by the Hamiltonian (Falikov and Kimball, 1969)

$$H = -\frac{t^*}{2\sqrt{D}} \sum_{\langle i,j \rangle} (c_i^\dagger c_j + c_j^\dagger c_i) + E_f \sum_i w_i$$
$$-\mu \sum_i (c_i^\dagger c_i + w_i) + U \sum_i c_i^\dagger c_i w_i \qquad (5)$$

where $c_i^\dagger$ (c_i) create (destroy) a conduction electron at site i, w_i is a classical variable (representing the localized electron number at site i) that equals 0 or 1, t^* is a renormalized hopping matrix element that is nonzero between nearest neighbors on a hypercubic lattice in D-dimensions, and U is the local screened Coulomb interaction between conduction and localized electrons. $\langle i,j \rangle$ denotes a sum over sites i and nearest neighbors j. $E_{\rm f}$ and μ are adjusted to set the average filling of conduction and localized electrons. This model has been solved exactly for electrons on a hypercubic lattice in the limit of large coordination number (Freericks and Zlatic, 2003b). The system undergoes a metal-insulator transition (MIT) at half-filling (one electron per site) if the interaction U is beyond a critical value $U_{\rm c}$. On either side of the metal-insulator transition, the density of states is temperature independent (van Dongen, 1992), while the conductivity has a strong temperature dependence (Pruschke et al., 1995) showing the development of the MIT.

In systems with strong and anisotropic interactions, the differences between single and two-particle properties are inescapable. This is been borne out in the cuprates by the large amount of work using optical (Homes et

al., 2004) and thermal conductivities (Sutherland et al., 2005), resistivities (Ando et al., 2004), nuclear magnetic resonance (NMR) (Alloul et al., 1989) and electron spin resonance (ESR) (Jánossy et al., 2003). These experiments have revealed basic properties of strongly correlated systems and have emerged as key elements to characterize the complex behavior of the high-T_c cuprates.

Yet these two-particle measurements are largely insensitive of anisotropies, as they measure Brillouin zone averaged quantities. As a result they reveal the behavior of quasiparticles having the highest velocities which, in the cuprates, are the quasiparticles near the nodal regions of the Brillouin zone. As far as carriers are concerned, the momentum dependence of neutron scattering serves mainly to measure spin dynamics in different regions of the Brillouin zone.

In this review, we illustrate that Raman spectroscopy gives complementary information to all of these measurement techniques, and also may provide detailed information of charge and spin dynamics of electrons in different regions of the Brillouin zone. This is due to the polarization selection rules. As with phonon scattering (Hayes and Loudon, 2005), simple group theoretic symmetry arguments can be used to focus on electron dynamics in different regions of the Brillouin zone. For Raman scattering $(a_{\mathbf{k}} b_{\mathbf{k}})$ is replaced with $\gamma_{\mathbf{k}}^2$ which, in certain limits, may be represented by $\gamma_{\mathbf{k}} = \sum_{\mu,\nu} e_\mu^i e_\nu^s \partial^2 \xi_{\mathbf{k}} / \hbar^2 \partial k_\mu \partial k_\nu$, with $\mathbf{e}^{i,s}$ the incident, scattered light polarization vectors.[4] Apart from energy-independent scaling factors and vertices with different $\mathbf{k}$ dependences there is an extra factor $1/\Omega$ between Raman and infrared response. It has been shown first by Shastry and Shraiman (1990) and explicitly demonstrated within Dynamical Mean Field Theory (DMFT) by Freericks and Devereaux (2001) that, under certain restrictions, there is a simple correspondence between conductivity and Raman response,

$$\Omega \sigma'(\Omega) \propto \chi''_{\gamma\gamma}(\Omega), \qquad (6)$$

highlighting that electronic Raman scattering measures transport properties. However, even the simple form of the vertices given above shows that a coincidence can be expected only for an isotropic material. In anisotropic systems, light scattering can sample parts of the Fermi surface which are unaccessible for infrared spectroscopy.

D. State of the Art Experimental Technique

Over decades Raman scattering was predominantly used for the study of molecular and lattice vibrations which produce isolated and typically narrow lines in the spectra (see Fig. 1). The lines are used as probes which sensitively react to changes in the environment of the vi-

---

[4] For a microscopic derivation see section II.A.

brating atoms. Similar considerations are at the heart of magnetic resonance techniques such as NMR and ESR.

If light is scattered from electrons in solids, the spectra are usually continuous (Fig. 1). To study their evolution as a function of a control parameter, such as temperature, doping, magnetic field or pressure, is rather involved since the overall shape and not the position of well-defined lines matters. In addition, typical cross sections per unit solid angle and energy interval are smaller by several orders of magnitude than those of vibrations. Electronic Raman scattering in a metal typically produces one energy-shifted photon per s, meV, and sr (unit solid angle steradian) out of 10^{13} incoming ones. The low efficiency is particularly demanding in studies at high pressure since additional losses and complications such as fluorescence and birefringence arise from the windows, which are typically diamond anvils. Although there were successful early experiments (Zhou *et al.*, 1996) the availability of synthetic diamonds brought substantial advances (Goncharov and Struzhkin, 2003).

There are three inventions which finally produced the required sensitivity: (i) the laser as an intense light source providing lines of high spectral purity in a wide energy range, (ii) as an early application of the laser, holographically fabricated gratings without secondary images (ghosts) and an extremely low level of diffusely scattered light and, finally, (iii) the invention of charge-coupled devices (CCD) as a location-sensitive detector with an efficiency at the quantum limit and negligible dark count rate.

Gratings have an extremely well defined number of lines per unit length (cm in the cgs system). This is the origin of the energy unit cm^{-1}. The following conversions are frequently used:

$$1 \text{ meV} = 11.604 \text{ K}$$
$$1 \text{ meV} = 8.0655 \text{ cm}^{-1}$$
$$k_\text{B} = 0.69504 \frac{\text{cm}^{-1}}{\text{K}}$$

Since the CCD has a high spatial resolution down to a few μm it is a superior replacement of the photographic plate. It facilitates recording complete spectra in a single exposure with energy ranges from meV up to approximately 1 eV, depending on the desired resolution.

The essentials of a setup for inelastic light scattering with polarized photons are shown schematically in Fig. 2. The coherent light at energy $\hbar\omega_i$ from the laser (Ar$^+$ and Kr$^+$ gas lasers are still very popular) is spatially filtered. A prism monochromator (PMC) selects the desired frequency and suppresses incoherent photons from the laser medium. A combination of a $\lambda/2$ retarder and a polarizer (P1) facilitates the preparation of a photon flux of a well-defined polarization state and intensity. For excitation, the polarization inside the sample counts. The same holds for the selection of the proper polarization for the scattered photons at $\hbar\omega_s$. The best results are obtained by using a crystal polarizer (P1, e.g. of Glan-Thompson type) and a Soleil-Babinet compensator for
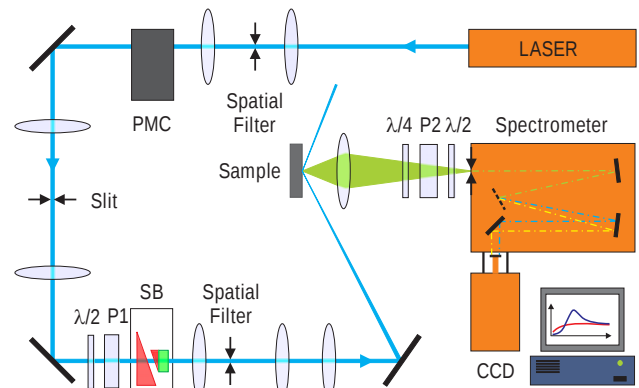

FIG. 2 Schematic drawing of the light path. The laser light with energy $\hbar\omega_i$ is first spatially filtered. A prism monochromator (PMC) is to suppress the plasma lines of the laser medium, only the coherent one at $\hbar\omega_i$ passes the slit. The polarization is prepared with polarizer P1 and the Soleil-Babinet compensator (SB). The $\lambda/2$ retarder in front of P1 allows one to adjust the power. Before hitting the sample the light is once again spatially filtered to maintain an approximately Gaussian intensity profile in the spot. If the angle of incidence is not close to zero phase shift effects at the sample surface must be taken into account since the polarization inside the sample is important. High speed optics collects the scattered light. The polarization state is selected by a $\lambda/4$ retarder and polarizer P2. The $\lambda/2$ retarder in front of the entrance slit rotates the light polarization for maximal transmission of the spectrometer (here single stage). Except for the compensator most retarders and polarizers work also for light propagating at small angles (up to approximately $\pm5°$) with respect to the optical axis. The configuration shown here is usually referred to as back-scattering geometry since incoming and outgoing photons have essentially opposite momenta in the sample.

the incoming light and an achromatic $\lambda/4$ retarder and another crystal polarizer (P2) for the scattered light. In this way all states, including circularly polarized ones, can be prepared. The $\lambda/2$ retarder in front of the entrance slit of the spectrometer rotates the polarization into the direction of highest sensitivity.

Since we wish to discriminate between the 10^{10-15} elastically scattered photons at $\hbar\omega_i$ and the few Raman photons at $\hbar\omega_s$ at very small shifts $\hbar\Omega = |\hbar\omega_i - \hbar\omega_s| < 1$ meV, a single monochromator is insufficient. A modern instrument for Raman scattering in metallic samples has three stages consisting of essentially independent grating monochromators. The first two are usually subtractively coupled and select a band from the spectrum of inelastically scattered photons. The third stage disperses the band transmitted through the two stages of the premonochromator into a spectrum which is recorded by the CCD. In this configuration, the dispersion is given only by the third stage while the first two discriminate the elastically scattered laser light. If all stages are coupled additively, the resolution is improved by a factor of 3. Because of losses at the mirrors and gratings, only 15 to 20 % of the photons entering the spectrometer arrive at the detector.

Since very interesting physics is going on at energies even below 1 meV (see, e.g., section IV.D.3) the discrimination is a cardinal point. Out of the two options only the premonochromator gives satisfactory results below 10 meV. The price one has to pay is a loss of intensity of approximately 60 %. Alternatively, for energy shifts above 10 meV an interferometric notch filter can be used. The latter device is widely used for commercial applications which develop rapidly since the introduction of the CCD. The main fields are quality control and analytics.

At finite temperatures, $T > 0$, inelastically scattered light is found on either side of $\hbar\omega_i$. As a consequence of time-reversal symmetry and for phase space arguments the energy gain (Anti-Stokes) and loss (Stokes) spectra are related by the principle of detailed balance (equivalent to the fluctuation-dissipation theorem) (Landau and Lifshitz, 1960; Placzek, 1934)

$$\frac{\dot{N}_{\text{AS}}}{\dot{N}_{\text{ST}}} = \left(\frac{\omega_i + \Omega}{\omega_i - \Omega}\right)^2 \exp\left(-\frac{\hbar\Omega}{k_{\text{B}}T}\right) \qquad (7)$$

with $\dot{N}_{\text{ST(AS)}}$ and $\hbar\Omega$ the rate of photons per unit time collected on the Stokes (Anti-Stokes) side and the energy transferred to the system, respectively. Equation (7) can be used to determine the temperature of the laser spot.

If spectra are measured in large energy ranges, the sensitivity of the instrument has to be taken into account. To this end, the spectral response of the whole system, including all optical elements between the sample and the entrance slit of the spectrometer, the spectrometer itself, and the detector, must be calibrated. This is best done by replacing the sample with a continuous light source of the same size as the laser spot with a known spectral emissivity. A continuous source is of crucial importance for including the energy dependence of the dispersion in addition to the bare transmission. In addition, the frequency dependence of the sample's index of refraction, $\sqrt{\varepsilon} = n + ik$, requires attention in order to get the internal cross section.

The main limitations of present commercial systems come from geometrical aberrations of the spectrometer optics and from the relatively low total reflectivity of the large number of mirrors. It is a matter of resources to improve these caveats. Recently, an improved type of triple spectrometer with aspherical optics has been described by Schulz et al. (2005). CCDs and gratings are close to the theoretical limits.

For many studies, light sources with continuously adjustable lines in an extended energy range would be desirable. This holds particularly true for organic materials (e.g. carbon nanotubes or proteins) which have relatively sharp resonances in the visible and the ultraviolet. The synchrotron, free electron "lasers", as well as dye and solid-state lasers are developing rapidly and will gain influence on the field of Raman spectroscopy in the near future. The same holds for near-field techniques (Hartschuh et al., 2003) which are capable of improving spatial resolution by at least an order of magnitude below the diffraction limit.

II. THEORY OF ELECTRONIC RAMAN SCATTERING

A. Electronic Coupling to Light

The aim of this section is to formulate the theoretical treatments for inelastic light scattering in general. Much has been done in the development of theories for Raman scattering, particularly in semiconductors and superconductors. Excellent and early reviews of electronic Raman scattering have been given by Klein (1983) and Abstreiter et al. (1984) focusing on semiconductors. More recent reviews by Devereaux and Kampf (1997) and Sherman et al. (2003) have focused on theory in superconductors with applications towards the cuprates. We outline the general formalism for treating systems with weak and strong correlations and return to a discussion of various theoretical models in connection with materials in the following section.

1. General Approach

We first consider a Hamiltonian for N electrons coupled to the electromagnetic fields (Blum, 1970; Pines and Nozières, 1966):

$$H = \sum_i^N \frac{[\hat{\mathbf{p}}_i + (e/c)\hat{\mathbf{A}}(\mathbf{r}_i)]^2}{2m} + H_{\text{Coulomb}} + H_{\text{fields}}, \quad (8)$$

where $\hat{\mathbf{p}} = -i\hbar\boldsymbol{\nabla}$ is the momentum operator, e is the magnitude of the elementary charge (the electronic charge is $q_e = -e$) and c the speed of light. $\hat{\mathbf{A}}(r_i)$ is the vector potential of the field at space-time point $\mathbf{r_i}$ and m the electron mass. H_{Coulomb} represents the Coulomb interaction and H_{fields} the free electromagnetic part. We use the symbol $\hat{A}$ to denote operators. We expand the kinetic energy to obtain

$$\begin{aligned} H &= H' + \frac{e}{2mc}\sum_i \left[\hat{\mathbf{p}}_i \cdot \hat{\mathbf{A}}(\mathbf{r}_i) + \hat{\mathbf{A}}(\mathbf{r}_i) \cdot \hat{\mathbf{p}}_i\right] \\ &\quad + \frac{e^2}{2mc^2}\sum_i \hat{\mathbf{A}}(\mathbf{r}_i) \cdot \hat{\mathbf{A}}(\mathbf{r}_i), \end{aligned} \qquad (9)$$

with $H' = H_0 + H_{\text{fields}}$ and $H_0 = (1/2m)\sum_i \hat{\mathbf{p}}_i^2 + H_{\text{Coulomb}}$. Generally we choose $|\alpha\rangle$ to denote eigenstates of H_0 with eigenvalues E_α: $H_0|\alpha\rangle = E_\alpha|\alpha\rangle$. The eigenstate is labeled by all the relevant quantum numbers for the state, such as combinations of band index, wavevector, orbital and/or spin quantum numbers, for example. The eigenstates may be considered to be Bloch electrons when the electron-ion interaction is included in H_0, as plane-wave states if it is neglected, or may represent Hubbard states if H_{Coulomb} is taken to include short-range Hubbard-like interactions between electrons.

The electromagnetic vector potential can be expanded into Fourier modes $\hat{\mathbf{A}}(\mathbf{r}_i) = \sum_{\mathbf{q}} e^{i\mathbf{q}\cdot\mathbf{r}_i}\hat{\mathbf{A}}_{\mathbf{q}}$. In second quantized notation, the electromagnetic field operator

takes the form (Mahan, 2000)

$$\hat{\mathbf{A}}_{\mathbf{q}} = \sqrt{\frac{hc^2}{\omega_{\mathbf{q}}V}}[\hat{\mathbf{e}}_{\mathbf{q}}a_{-\mathbf{q}} + \hat{\mathbf{e}}_{\mathbf{q}}^*a_{\mathbf{q}}^\dagger], \qquad (10)$$

with V the volume and $a_{\mathbf{q}}^\dagger, a_{\mathbf{q}}$ are the creation, annihilation operators of transversal photons with energy $\hbar\omega_{\mathbf{q}} = \hbar c|\mathbf{q}|$ having a polarization direction denoted by the complex unit vector $\hat{\mathbf{e}}_{\mathbf{q}}$.

Electronic Raman scattering measures the total cross section for scattering from all the electrons illuminated by the incident light. The differential cross section is determined by the probability that an incident photon ω_i is scattered into a solid-angle interval between Ω and $\Omega + d\Omega$ and a frequency window between ω_s and $\omega_s + d\omega_s$. A general expression for the differential light scattering cross-section is given via the transition rate R of scattering an incident $(\mathbf{q}_i, \omega_i, \hat{\mathbf{e}}_{\mathbf{q}}^{(i)})$ photon into a outgoing state $(\mathbf{q}_s, \omega_s, \hat{\mathbf{e}}_{\mathbf{q}}^{(s)})$,

$$\frac{\partial^2\sigma}{\partial\Omega\partial\omega_s} = \hbar r_0^2 \frac{\omega_s}{\omega_i}R. \qquad (11)$$

Here, $r_0 = e^2/mc^2$ is the Thompson radius, and R is determined via Fermi's Golden Rule,

$$R = \frac{1}{\mathcal{Z}}\sum_{I,F} e^{-\beta E_I} \mid M_{F,I} \mid^2 \delta(E_F - E_I - \hbar\Omega), \qquad (12)$$

with $\beta = 1/k_{\mathrm{B}}T$, $\mathcal{Z}$ the partition function, and $M_{F,I} = \langle F|M|I \rangle$ where M is the effective light scattering operator. The sum represents a thermodynamic average over possible initial and over final states with $\mathbf{k}$ vectors in the solid angle element $d\Omega$ of the many-electron system having energies E_I, E_F, respectively. Here $\Omega = \omega_i - \omega_s$ is the transferred frequency and we denote $\mathbf{q} = \mathbf{q}_i - \mathbf{q}_s$ the net momentum transfered by the photon. Multiplying Eq. (11) by the incident photon flux gives the number of scattered photons per second into the solid angle increment $d\Omega$ within the frequency range $d\omega_s$, while multiplying Eq. (11) by ω_s/ω_i gives the power scattering cross section (Klein, 1983).[5]

From here on we consider the case relevant to Raman scattering in the visible range with photon energies of typically 2 eV. Since the momentum transferred to the electrons, $q \sim 1/\delta$, with δ the skin depth at the light energies (Abrikosov and Fal'kovskiǐ, 1961), is much less

than the relevant momentum scale of order k_{F}, the Fermi momentum in metallic systems, the limit $q \to 0$ is a good approximation in practically all cases.[6] However, finite q should be considered if incident light from frequency-doubled or synchrotron radiation is used where transitions between initial and final states at finite q can be probed. Then the structure of the Landau particle-hole continuum in weakly correlated systems or transitions across a finite q Mott gap in strongly correlated insulators can be studied.[7]

$M_{F,I}$ has contributions from either of the last three terms in Eq. (9): the first two terms coupling the electron's current to a single photon and the third term coupling the electron's charge to two photons. This is shown in the schematic cartoon in Figures 3 and 4. Here we consider two bands - one partially filled and the other completely filled - in which the incident photon excites an electron from either the partially or the completely filled band, shown in Figures 3 and 4, respectively. In the nonresonant intraband case, the photon gives up part of its energy to leave behind a particle-hole pair, while in the interband case, an intermediate state is involved, which decays via a particle from the partially filled band into the hole left behind in the filled band. The latter scattering may be resonant if the incident or emitted photon energy corresponds to that of the energy gap separation, otherwise it is non-resonant. In this simple cartoon, one can see that excitations lying near the Fermi surface are predominantly probed by non-resonant intraband scattering while excitations involving transition between different bands - such as the lower and upper Hubbard band for example - are probed by intermediate state scattering. The Feynman diagrams representing these contributions to $M_{F,I}$ are shown in Figure 5.
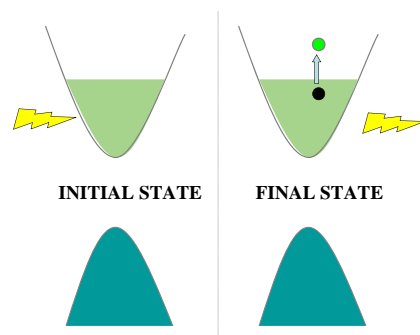
Referring to Eq. (9), the current coupling has odd spa-

FIG. 3 Cartoon showing light scattering via non-resonant intraband scattering.

---

[5] We note that Eqs. (11) and (12) describe scattering inside the material. Trivial (Fresnel-formulas) and non-trivial (q_z integration) (Abrikosov and Fal'kovskiǐ, 1961; Fal'kovskiǐ, 1990, 1991) transformations, which we do not discuss here, are required to fully describe the cross section outside. The q_z integration originates from the lack of momentum conservation perpendicular to the surface of an absorbing medium and can change the spectra qualitatively. From here on, $\hbar\Omega$ is always the energy transferred to the system.

[6] The applicability of the $q = 0$ limit is discussed in more detail at the beginning of section III.

[7] For a review of relevant work in this regard, the reader is referred to references (Devereaux et al., 2003a,c; Kotani and Shin, 2001; Platzman and Isaacs, 1998).

tial symmetry and involves single photon emission or absorption, while the second term is even in parity and involves two photon scattering of emission followed by absorption and vice-versa. The cross-section or the transition rate is thus determined via Fermi's Golden rule by the square of the matrix elements shown in Figure 5.

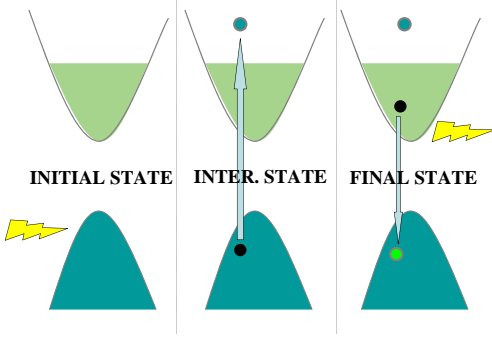The resulting Feynman diagrams of the contributions to the cross section are shown in Figure 6. However, not

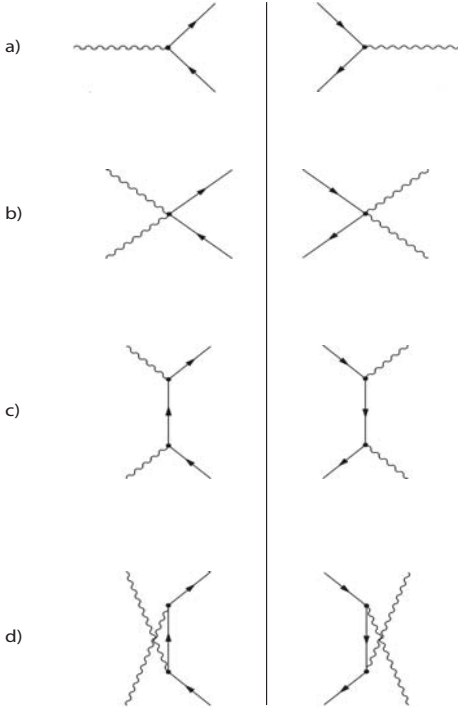FIG. 4 Cartoon showing light scattering via interband transitions.

FIG. 5 Feynman diagrams contributing to the effective light scattering operator M. The top diagram represents single-photon absorption, the second two photon scattering, while photon emission (absorption) followed by absorption (emission) is shown in the 3rd (4th) diagram from top. The panels on the right are the time-reversed partners of the left diagrams.

all of them give rise to inelastic light scattering. Some of these terms vanish either because they represent contributions to the renormalized photon propagator (Figure 6 (a)), or due to parity arguments (Figures 6 (b)-(d)) in the limit of small q scattering. The remaining terms can be classified as non-resonant (Figure 6 (e)), resonant (Figure 6 (h)-(j) and mixed terms (Figure 6 (f)-(g)), since in the former case the initial and final states must share a large sub-set of quantum numbers, while the other terms can involve transitions through intermediate states well separated in energy and distinct from the initial and final states. However, we remark that the response is only truly resonant if the photon energies are tuned to the energy gap between intermediate and initial or final states.

To obtain a general expression for the matrix element $M_{F,I}$ for Raman scattering, we use second quantized notation for the fermions in which the single-particle wave function and it's conjugate are given by $\psi(\mathbf{r}) = \sum_\alpha c_\alpha \varphi_\alpha(\mathbf{r})$ and $\psi^\dagger(\mathbf{r}) = \sum_\alpha c_\alpha^\dagger \varphi_\alpha^*(\mathbf{r})$, with φ, φ^* the eigenstates of the Hamiltonian H_0. Electron states α, β are created, annihilated by $c_\alpha^\dagger, c_\beta$ respectively, and the indices refer to the quantum number associated with the state, such as the momenta and/or spin states. The ma-
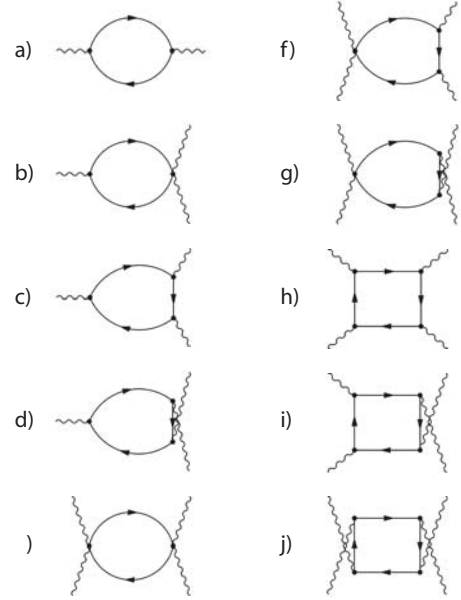

FIG. 6 Feynman diagrams contained in the cross-section. (a) gives a renormalized photon propagator in the solid, while (b)-(d) vanish due to parity and thus (a)-(d) do not contribute to inelastic light scattering. Of the remaining contributions, (e) refers to intra-band (sometimes "non-resonant") scattering within a single band, (f) and (g) are referred to as "mixed" contributions while (h)-(j) describe transitions within a single or between different bands via intermediate band states. If the light energy is equal or close to the energy difference of the states involved resonance effects with a strong enhancement of the cross section occur. Therefore the contributions themselves are sometimes referred to as "resonant".

trix element $M_{F,I}$ can thus be written as

$$M_{F,I} = \mathbf{e}_i \cdot \mathbf{e}_s \sum_{\alpha,\beta} \rho_{\alpha,\beta}(\mathbf{q}) \langle F | c_\alpha^\dagger c_\beta | I \rangle$$
$$+ \frac{1}{m} \sum_\nu \sum_{\alpha,\alpha',\beta,\beta'} p_{\alpha,\alpha'}(\mathbf{q}_s) p_{\beta,\beta'}(\mathbf{q}_i)$$
$$\times \left(\frac{\langle F | c_\alpha^\dagger c_{\alpha'} | \nu \rangle \langle \nu | c_\beta^\dagger c_{\beta'} | I \rangle}{E_I - E_\nu + \hbar\omega_i} \right.$$
$$\left. + \frac{\langle F | c_\beta^\dagger c_{\beta'} | \nu \rangle \langle \nu | c_\alpha^\dagger c_{\alpha'} | I \rangle}{E_I - E_\nu - \hbar\omega_s} \right). \quad (13)$$

Here $|I\rangle, |F\rangle, |\nu\rangle$ represent the initial, final and intermediate many-electron states having energies $E_{I,F,\nu}$, respectively. The many-electron states could be labeled by band index and momentum as, for example, for Bloch electrons. They may also consist of core and valence electrons on selected atoms for x-ray scattering, or may represent states of the many-band Hubbard model for correlated electrons. $\rho_{\alpha,\beta}(\mathbf{q}) = \int d^3 r \varphi_\alpha^*(\mathbf{r}) e^{i\mathbf{q}\cdot\mathbf{r}} \varphi_\beta(\mathbf{r}) = \langle \alpha | e^{i\mathbf{q}\cdot\mathbf{r}} | \beta \rangle$ is the matrix element for single-particle density fluctuations involving states α, β. The momentum density matrix element is given by $p_{\alpha,\beta}(\mathbf{q}_{i,s}) = \langle \alpha | \mathbf{p} \cdot \mathbf{e}_{i,s} e^{\pm i\mathbf{q}_{i,s}\cdot\mathbf{r}} | \beta \rangle$. The first term in the expression arises from the two-photon scattering term in Eq. (9) in first order perturbation theory. The remaining terms arise from the single-photon scattering term in Eq. (9) in second order via intermediate states ν and involve different time orderings of photon absorption and emission. The $\mathbf{p} \cdot \mathbf{A}$ coupling does not enter to first order since the average of the momentum operator is zero.

2. Importance of Light Polarization

At this point, little progress can be made in evaluating the matrix elements for Raman scattering without specifying the quantum numbers of the electronic many-body states. Yet, from Eq. (13), one can apply symmetry arguments to view what types of excitations can be created by the incident photons. In this subsection, we employ a general set of symmetry classifications and put specific emphasis on models in later subsections.

The first term in Eq. (13) only arises if the incident and scattering polarization light vectors are not orthogonal, as electronic charge density fluctuations are created and destroyed along the polarization directions of the incident and scattered photons. Thus, for instance, this term does not probe electron dynamics in which the charge density relaxes in a direction orthogonal to the incident polarization direction.

In the limit of small momentum transfer $\mathbf{q} \to 0$, the matrix element simplifies to $\rho_{\alpha,\beta}(\mathbf{q} \to 0) = \delta_{\alpha,\beta}$ and thus this term gives rise to scattering from fluctuations of the isotropic electronic number density.

The remaining terms in Eq. (13) have contributions regardless of photon polarization directions. However, one

can further classify scattering contributions by separating the sum over intermediate states $|\nu\rangle$ into states which share some quantum numbers with the initial many-body state, such as band index, and states which do not. Since the photon momenta are much smaller than the relevant electron momenta, contributions of the terms where the intermediate states include the initial states are roughly a factor of v_F/c smaller than the first term in Eq. (13) and can be neglected (Pines and Nozières, 1966; Wolff, 1966). However contributions where $|\nu\rangle$ includes higher bands cannot in general be neglected, particularly if the energy of the incident or scattering light lies near the energy of a transition from the initial state E_I to an intermediate state E_ν. These terms thus give rise to "mixed" and "resonant" Raman scattering.

The polarization dependence of Raman scattering can be generally classified using arguments of group theory. In essence, the charge density fluctuations brought about by light scattering are modulated in directions determined by the polarizations of the incident and scattered photons. These density fluctuations thus have the symmetry imposed on them by the way in which the light is oriented, and the charge density fluctuations obey the symmetry rules governing the scattering geometry. This is manifest in the dependence of the Raman matrix elements on the initial and final fermion states. In general, the Raman matrix element $M_{F,I} = M_{I,F}^{\alpha,\beta} e_i^\alpha e_s^\beta$ can be decomposed into basis functions of the irreducible point group of the crystal Φ_μ (Devereaux, 1992; Hayes and Loudon, 2005; Klein and Dierker, 1984; Monien and Zawadowski, 1990; Shastry and Shraiman, 1991)

$$M_{F,I}(\mathbf{q} \to 0) = \sum_\mu M_\mu \Phi_\mu, \quad (14)$$

with μ representing an irreducible representation of the point group of the crystal. Which set of μ contributes to the sum is determined by the orientation of incident and scattered polarization directions. As an example, if we consider the D_{4h} group of the tetragonal lattice, as in the cuprates, the decomposition can be written as

$$M_{F,I} = \frac{1}{2} O_{A_{1g}^{(1)}}(e_i^x e_s^x + e_i^y e_s^y)$$
$$+ \frac{1}{2} O_{A_{1g}^{(2)}}(e_i^z e_s^z)$$
$$+ \frac{1}{2} O_{B_{1g}}(e_i^x e_s^x - e_i^y e_s^y)$$
$$+ \frac{1}{2} O_{B_{2g}}(e_i^x e_s^y + e_i^y e_s^x)$$
$$+ \frac{1}{2} O_{A_{2g}}(e_i^x e_s^y - e_i^y e_s^x)$$
$$+ \frac{1}{2} O_{E_g^{(1)}}(e_i^x e_s^z + e_i^z e_s^x)$$
$$+ \frac{1}{2} O_{E_g^{(2)}}(e_i^y e_s^z + e_i^z e_s^y), \quad (15)$$

with O_μ the corresponding projected operators and $e_{i,s}^\alpha$ the light polarizations. This classification demonstrates
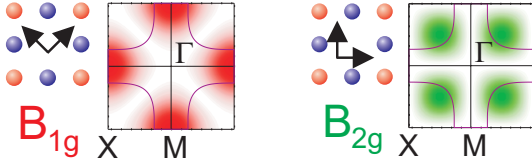
FIG. 7 Schematic weighting of the light scattering transition for polarization orientations transforming as B_{1g} and B_{2g} for a D_{4h} crystal. High symmetry points are indicated. Here a typical Fermi surface for optimally doped cuprates is represented by the solid line, and the orientations of the incident and scattered polarization light vectors are shown with respect the to copper-oxygen bond directions.

that there is no mixing of representations for $q = 0$, i.e. the correlation functions read $R \sim \langle O_\mu^\dagger O_{\mu'} \rangle = R_\mu \delta_{\mu,\mu'}$ and there are 6 independent correlation functions, each selected by combinations of polarization orientations.

Following Shastry and Shraiman (1990), we list in Table I some common experimentally used polarization geometries in relation to the elements of the transition rate R selected. One observes that a complete characterization of M can be made from a subset of the polarization orientations listed in the table. However, additional polarization orientations can be useful to calibrate data and compare symmetry decompositions from different combinations of orientations. For geometries with polarizations in the $(a-b)$ plane in D_{4h} crystals, the irreducible representations cannot be accessed individually and must be separated by proper subtraction procedures. As a minimum set, four independent configurations are required, while additional polarizations may be used for consistency checks.

In addition, we have listed in Table I the representative basis functions $\Phi_\mu(\mathbf{k})$ taken from the complete set of Brillouin zone (BZ) harmonics for D_{4h} space group (Allen, 1976). This directly points out the connection between polarizations and the coupling of light to electrons. By virtue of the $\mathbf{k}$-dependence of the light scattering transition rate, excitations on certain regions of the BZ can be correspondingly projected out by orienting the incident and scattered light polarization vectors. Thus, Raman is one of the few spectroscopic multi-particle probes (the other being inelastic X-ray scattering) able to examine charge excitations in different regions of the BZ.

For example, as demonstrated in Figure 7, for crossed polarizations transforming as B_{1g}, light couples to charge excitations along the BZ axes (k_x or $k_y = 0$), while for B_{2g}, excitations along the BZ diagonals ($k_x = \pm k_y$) are projected accordingly. Operators like $O_{A_{2g}}$ cannot be accessed independently by linear polarizations alone. Only sums including circular polarizations allow the isolation of A_{2g} components. Light scattering in this orientation can be coupled to chiral excitations. These important symmetry classifications have been ex-

tremely useful to point out anisotropic electron dynamics in correlated insulators (Devereaux *et al.*, 2003a,c; Shastry and Shraiman, 1990), superconductors (Devereaux *et al.*, 1994a), disordered (Devereaux, 1992; Zawadowski and Cardona, 1990) and correlated metals (Einzel and Manske, 2004; Freericks and Devereaux, 2001; Freericks *et al.*, 2001). More recently they have been related to sum rules referring to BZ-projected potential energies in correlated systems (Freericks *et al.*, 2005). In the remaining part of this review, such symmetry classifications will be featured prominently.

B. Formalism: Single-Particle Excitations and Weak Correlations

We now consider specific cases where simplifications can be made to Eq. (13). First we assume that the intermediate many-particle states only differ from the initial and final states by single electron excitations. This is exact in the limit of non-interacting electrons, yet ignores the effects of many-body correlations, and specifically the role of Coulomb interactions on the reorganization of the initial state into the intermediate states by creating many-particle excitations. We now focus on weakly interacting systems, where single-particle excitations are relatively well defined, and discuss strongly correlated systems in later sections.

1. Particle-hole Excitations

Eq. (13) can be simplified by replacing E_ν in the denominators by $E_I - E_{\beta'} + E_\beta$ and $E_I - E_{\alpha'} + E_\alpha$ in the first and second terms, respectively, and use the closure relation $\sum_\nu |\nu\rangle\langle\nu| = 1$. Commutator algebra eliminates the four fermion matrix element,

$$M_{F,I} = \sum_{\alpha,\beta} \gamma_{\alpha,\beta} \langle F \mid c_\alpha^\dagger c_\beta \mid I \rangle, \qquad (16)$$

where

$$\gamma_{\alpha,\beta} = \rho_{\alpha,\beta}(\mathbf{q})\hat{\mathbf{e}}_i \cdot \hat{\mathbf{e}}_s \; + \; \frac{1}{m}\sum_{\beta'}\left(\frac{p_{\alpha\beta'}^s p_{\beta'\beta}^i}{E_\beta - E_{\beta'} + \hbar\omega_i}\right.$$
$$\left. + \frac{p_{\alpha,\beta'}^i p_{\beta',\beta}^s}{E_\beta - E_{\beta'} - \hbar\omega_s}\right). \quad (17)$$

Specifying to states α, β indexed by momentum quantum numbers (such as Bloch electrons), from Eq. (11), the Raman response simplifies to a correlation function $\tilde{S}$ of an effective charge density $\tilde{\rho}$,

$$\frac{\partial^2\sigma}{\partial\Omega\partial\omega_s} = \hbar r_0^2 \frac{\omega_s}{\omega_i}\tilde{S}(\mathbf{q}, i\Omega \to \Omega + i0). \qquad (18)$$

Geometry	$\hat{e}_i$	$\hat{e}_s$	R	Basis Functions $\Phi_\mu(\mathbf{k})$
$xx,\ yy$	$\hat{x},\hat{y}$	$\hat{x},\hat{y}$	$R_{A_{1g}} + R_{B_{1g}}$	$\frac{1}{2}[\cos(k_x a) + \cos(k_y a)] \pm \frac{1}{2}[\cos(k_x a) - \cos(k_y a)]$
$x'x'$	$\frac{1}{\sqrt{2}}(\hat{x}+\hat{y})$	$\frac{1}{\sqrt{2}}(\hat{x}+\hat{y})$	$R_{A_{1g}} + R_{B_{2g}}$	$\frac{1}{2}[\cos(k_x a) + \cos(k_y a)] + \sin(k_x a)\sin(k_y a)$
$x'y'$	$\frac{1}{\sqrt{2}}(\hat{x}+\hat{y})$	$\frac{1}{\sqrt{2}}(\hat{x}-\hat{y})$	$R_{B_{1g}} + R_{A_{2g}}$	$\frac{1}{2}[\cos(k_x a) - \cos(k_y a)][1 + \sin(k_x a)\sin(k_y a)]$
xy	$\hat{x}$	$\hat{y}$	$R_{B_{2g}} + R_{A_{2g}}$	$\sin(k_x a)\sin(k_y a)\left\{1 + \frac{1}{2}[\cos(k_x a) - \cos(k_y a)]\right\}$
LR	$\frac{1}{\sqrt{2}}(\hat{x}+i\hat{y})$	$\frac{1}{\sqrt{2}}(\hat{x}+i\hat{y})$	$R_{B_{1g}} + R_{B_{2g}}$	$\frac{1}{2}[\cos(k_x a) + \cos(k_y a)] + \sin(k_x a)\sin(k_y a)$
LL	$\frac{1}{\sqrt{2}}(\hat{x}+i\hat{y})$	$\frac{1}{\sqrt{2}}(\hat{x}-i\hat{y})$	$R_{A_{1g}} + R_{A_{2g}}$	$\frac{1}{2}\left\{\cos(k_x a) + \cos(k_y a) + [\cos(k_x a) - \cos(k_y a)]\sin(k_x a)\sin(k_y a)\right\}$
xz	$\hat{x}$	$\hat{z}$	$R_{E_{1g}}$	$\sin(k_x a)\sin(k_z c)$
yz	$\hat{y}$	$\hat{z}$	$R_{E_{1g}}$	$\sin(k_y a)\sin(k_z c)$
zz	$\hat{z}$	$\hat{z}$	$R_{A_{1g}^{(2)}}$	$\cos(k_z c)$

TABLE I Elements of the transition rate R for experimentally useful configurations of polarization orientations (given in Porto notation) along with the symmetry projections for the D_{4h} point group relevant for the cuprates. Here we use notations in which x and y point in directions along the Cu-O bonds in tetragonal cuprates, while x' and y' are directions rotated by 45°. L and R denote left and right circularly polarized light, respectively. In our convention left circular light has positive helicity. (In a right-handed system the polarization rotates from x to y while the wavefront travels into positive z direction by $\lambda/4$.) Note that in back-scattering configuration (see Fig. 2) with $\hat{e}_{i,s}$ pinned to the coordinate system of the crystal axes the representation for incoming and outgoing photons with circular polarizations change sign in order to maintain the proper helicity.

Here the Raman effective density-density correlation function is

$$\tilde{S}(\mathbf{q}, i\Omega) = \sum_I \frac{e^{-\beta E_I}}{\mathcal{Z}} \int d\tau\, e^{i\Omega\tau} \langle I \mid T_\tau \tilde{\rho}(\mathbf{q},\tau)\tilde{\rho}(-\mathbf{q},0) \mid I\rangle, \quad (19)$$

T_τ is the complex time τ ordering operator and

$$\tilde{\rho}(\mathbf{q}) = \sum_{\mathbf{k},\sigma} \gamma(\mathbf{k},\mathbf{q}) c^\dagger_{\mathbf{k}+\mathbf{q},\sigma} c_{\mathbf{k},\sigma}. \quad (20)$$

The scattering amplitude γ is determined from the Raman matrix elements and incident/scattered light polarization vectors as

$$\gamma(\mathbf{k},\mathbf{q}) = \sum_{\alpha,\beta} \gamma_{\alpha,\beta}(\mathbf{k},\mathbf{q}) e_i^\alpha e_s^\beta, \quad (21)$$

with

$$\gamma_{\alpha,\beta}(\mathbf{k},\mathbf{q}) = \delta_{\alpha,\beta} + \frac{1}{m}\sum_{\mathbf{k}_\nu}\left[\frac{\langle \mathbf{k}+\mathbf{q} \mid p_s^\beta \mid \mathbf{k}_\nu\rangle\langle \mathbf{k}_\nu \mid p_i^\alpha \mid \mathbf{k}\rangle}{E_\mathbf{k} - E_{\mathbf{k}_\nu} + \hbar\omega_i}\right.$$
$$\left. + \frac{\langle \mathbf{k}+\mathbf{q} \mid p_i^\alpha \mid \mathbf{k}_\nu\rangle\langle \mathbf{k}_\nu \mid p_s^\beta \mid \mathbf{k}\rangle}{E_{\mathbf{k}+\mathbf{q}} - E_{\mathbf{k}_\nu} - \hbar\omega_s}\right]. \quad (22)$$

Here, $p_{i,s}^\alpha = p^\alpha e^{\pm i\mathbf{q}_{i,s}\cdot\mathbf{r}}$. The effective dynamical density-density correlation function or Raman response $\tilde{S}$ can be written in terms of a dynamical effective density susceptibility $\tilde{\chi}$ via the fluctuation-dissipation theorem,

$$\tilde{S}(\mathbf{q},\Omega) = -\pi^{-1}\{1 + n(\Omega,T)\}\tilde{\chi}''(\mathbf{q},\Omega),$$

with $n(\Omega,T)$ the Bose-Einstein distribution and

$$\tilde{\chi}(\mathbf{q},\Omega) = \langle[\tilde{\rho}(\mathbf{q}), \tilde{\rho}(-\mathbf{q})]\rangle_\Omega. \quad (23)$$

Thus, for non-interacting electrons, the Raman response is given as a two-particle effective density correlation function and can be calculated easily using, e.g., diagrammatic techniques or via the kinetic equation (Devereaux and Einzel, 1995a). This reduces to evaluating the bubble diagram depicted in Figure 6 with vertices γ depending upon the incident and scattered photon frequencies.[8]

The vertex γ depends on polarization, but does not depend sensitively on $\mathbf{q}$ for $q \ll k_F$. This can be made more obvious if we consider the sum over intermediate states $\mathbf{k}_\nu$ in Eq. (22). The sum over intermediate states includes both the band index of the states created from the initial state (i.e. the conduction band) as well as intermediate states separated from the conduction band. The matrix elements of the former are proportional to the momentum transferred by the photon, which in the limit $q \ll k_F$ are smaller by a factor of $(v_F/c)^2$ than the other terms, with v_F (c) the Fermi (light) velocity, and can be neglected (Pines and Nozières, 1966). For the remaining sum over the intermediate states separated from the conduction band, we assume that $\omega_{i,s} \ll \mid E_{\mathbf{k}_\nu} - E_\mathbf{k} \mid$ and recover the widely used effective mass approximation[9]

$$\gamma_{\alpha,\beta}(\mathbf{k}, q \to 0) = \frac{1}{\hbar^2}\frac{\partial^2 E_\mathbf{k}}{\partial k_\alpha k_\beta}. \quad (24)$$

The symmetry classifications listed in Table I thus can connect excitations created by certain polarization orien-

---

[8] We remark that technically these expression must be modified if a resonant condition is satisfied. In that case one needs to expand to higher terms in the vector potential to capture resonance effects as perturbation theory breaks down. Yet for low energy Raman scattering, in most cases this is not crucially important since in real materials the intermediate states reached via a direct resonance are quite broadened by interactions and the resonant terms are not orders of magnitude larger than the non-resonant terms. Thus this treatment may be of more general utility.

[9] This is derived in Appendix E of Ashcroft and Mermin (1976).

tations to properties of the band structure. Yet it must be kept in mind that this connection can only be made in the limit of small $\omega_{i,s}$.

2. Im$(1/\epsilon)$ and Sum Rules

We consider first the case when the incident polarization is parallel to the scattered polarization and the band $E_{\mathbf{k}}$ is isotropic and parabolic, as for the electron gas or lightly-filled isotropic band metal. The scattering amplitude γ is then independent of $\mathbf{k}$ and the effective density $\tilde{\rho}(\mathbf{q})$ is simply proportional to the pure charge density ρ. Using the definition of the complex dielectric function (Mahan, 2000; Pines and Nozières, 1966)

$$\epsilon(\mathbf{q}, \Omega) = 1 + v_q \chi_{sc}(\mathbf{q}, \Omega) \qquad (25)$$

is obtained with v_q the bare Coulomb interaction, and χ_{sc} is the screened or irreducible polarizability. It is determined from the full polarizability χ via

$$\chi_{sc}(\mathbf{q}, \Omega) = \frac{\chi(\mathbf{q}, \Omega)}{1 - v_{\mathrm{q}}\chi(\mathbf{q}, \Omega)}, \qquad (26)$$

but is most easily identified diagrammatically as all contributions to the polarizability which are irreducible with respect to the interaction. The dynamical density-density correlation function (or structure factor) follows as

$$S(\mathbf{q}, \Omega) = \frac{1}{\pi v_q}[1 + n(\Omega)] \, Im\left[\frac{1}{\epsilon(\mathbf{q}, \Omega)}\right]. \qquad (27)$$

The Raman response $\tilde{S}$ is proportional to S with a constant of proportionality determined by the ratio of effective to free electron mass.

Inelastic light scattering occurs via the creation of charge fluctuations inside the unit cell which are coupled via the Coulomb interaction to charge fluctuations in other unit cells. These intercell excitations are therefore well screened by the Coulomb interaction and reduce the scattering cross section at small q. In particular, for small q, $\chi(q, \Omega) \sim N_{\mathrm{F}} v_{\mathrm{F}}^2 q^2/\Omega^2$, and the response is governed by the plasma frequency. The Raman response thus obeys the longitudinal sum rule resulting from particle-number conservation (Pines and Nozières, 1966),

$$\int_0^\infty d\Omega \; \Omega \; Im\left[\frac{1}{\epsilon(\mathbf{q}, \Omega)}\right] = \frac{\pi}{2}\Omega_{\mathrm{pl}}^2 = \frac{2\pi^2 N e^2}{m}, \qquad (28)$$

where Ω_{pl} is the plasma frequency and N is the number of electrons of mass m and charge $-e$ in the system. Thus the only contribution for $q \to 0$ comes from exciting the plasmon being the only charge excitation available for light scattering at small q in a free-electron gas.

3. Intra- vs. Inter-cell Charge Fluctuations

In the more general case of light scattering in solids, the Raman response may have other contributions coming from intra-cell charge fluctuations, provided the band structure is non-parabolic, as pointed out by Platzman (1965) and Wolff (1968). Then light can create anisotropic charge fluctuations which are zero on average inside the unit cell and thus are not screened via the long-range Coulomb interaction, as pointed out by Abrikosov and Genkin (1973). The general expression for the screened Raman response function $\chi_{\gamma,\gamma}^{sc}$ can be written as (Devereaux and Einzel, 1995a; Monien and Zawadowski, 1990)

$$\chi_{\gamma,\gamma}^{sc} = \chi_{\gamma,\gamma} - \frac{\chi_{\gamma,1}\chi_{1,\gamma}}{\chi_{1,1}} + \frac{\chi_{\gamma,1}\chi_{1,\gamma}}{\chi_{1,1}^2}\chi_{sc}, \qquad (29)$$

where $\chi_{sc} = \chi_{1,1}(1 - v_q\chi_{1,1})^{-1}$. This is an exact expression, where the subscript γ denotes the effective Raman density and 1 denotes the pure charge density, obtained when the usually momentum dependent vertex γ is replaced by a constant. The respective χ-s describe the full density-density, density-Raman density, and Raman density-Raman density susceptibilities which are again each irreducible with respect to the interaction.

The first term in Eq. (29) is the bare response for a neutral system, and the other terms represent the backflow needed to enforce particle number conservation of charge density fluctuations and gauge invariance. These terms are important for light scattering configurations which transform according to the symmetry of the lattice, such as A_{1g} in $D_{4\mathrm{h}}$ crystals. In particular, if we consider scattering from pure charge density fluctuations where γ is a constant independent of momentum, which is an A_{1g} representation, the first two terms in Eq. (29) cancel and χ_{sc} and Eq. (27) are recovered. This is inescapable for $q = 0$, since then the scattering operator is given in terms of the total density of electrons, which commutes with the bare Hamiltonian and therefore cannot give inelastic scattering channels to light. On the other hand, if we consider the scattering vertex γ to depend on wavevector, the backflow terms are not capable of completely canceling the bare Raman response.

Momentum dependence of the vertex γ is quite general for electrons in solids. In particular, for crossed light polarizations projecting out representations of lower symmetry than that of the lattice $\chi_{\gamma,1}$ is identically zero by symmetry for $q = 0$ and the backflow terms make no correction to the Raman cross-section. This occurs for B_{1g}, B_{2g}, and E_g scattering geometries in $D_{4\mathrm{h}}$ systems such as the cuprates, for example. While there is no conservation law for light scattering from the excitations created by crossed polarizations (Kosztin, 1991), there are sum rules which relate the Raman intensity to model-dependent potential energies projected in different regions of the BZ (Freericks et al., 2005).

C. Formalism: Strong Correlations

1. General Approach to Treating Correlations

Section II.B outlined a general approach to inelastic light scattering when the intermediate states differ from the initial and final states only by individual single electron energies. This holds in the limit of weakly interacting electrons. In this section we show that the formalism is also valid in the Heisenberg limit of the Hubbard model including the manifold of zero and 1 doubly occupied sites. These are two limits in which either the kinetic energy or the potential energy of the electrons is dominant. However, the more general case of interest to most systems is tackling the problem when both kinetic and potential energies are roughly equal. The interactions are sufficient to give broad spectral functions as measured by ARPES, where the incoherent part of the spectral function is manifest from the strong many-body interactions mixing individual electron states.

In this situation, one must resort back to Eq. (13), and correlation functions involving two, three and four particles are needed, as depicted in Figure 6. Yet usually one is not interested in treating many-body correlations over various bands and puts focus on a few bands close to the Fermi level having strong correlations. For example in the cuprates, one usually takes downfolded Hamiltonians involving only Cu $3d_{x^2-y^2}$ and O $2p_{x,y}$ orbitals, with short-range Coulomb interactions for two electrons in on-site or neighboring orbital states. The downfolding procedure, such as that described by Löwdin (1951), removes all other bands (effectively moving them infinitely far away in energy from the focus bands), such as the apical oxygen, Cu $4s$ and other Cu d orbitals, and treats the electrons in the bands of interest as having renormalized energy dispersion. In the cuprates the downfolding results in either a few bands from local density approximation (LDA) approaches in one case or cell perturbation theory in the strongly interacting case. Thus we consider a downfolded tight-binding Hamiltonian

$$H_0 = \sum_{\langle i,j\rangle,\sigma} t_{i,j} c_{i,\sigma}^\dagger c_{j,\sigma} + H_{\text{int}}, \qquad (30)$$

where $t_{i,j}$ are the effective hopping integrals resulting from the downfolding procedure, and H_{int} describes the relevant interactions. For example, we may consider a square lattice of electrons with strong on-site repulsion U much greater than the electron hopping t in the Hubbard model,

$$H = -t \sum_{\langle i,j\rangle,\sigma} c_{i,\sigma}^\dagger c_{j,\sigma} + U \sum_i n_{i,\uparrow} n_{i,\downarrow}, \qquad (31)$$

where $\langle i,j\rangle$ denotes a sum over nearest neighbors.

The electronic eigenstates fall into two bands for large U at $1/2$ filling - e.g., the occupied lower and unoccupied upper Hubbard bands - separated by an energy U for double occupancies. Away from $1/2$ filling, quasiparticles

develop. The microscopic Hamiltonians can be viewed as families of models related to the Hubbard model, such as the Falicov-Kimball model, Anderson model, or Anderson-Fano model, without loss of generality.

In essence, the sums over intermediate states in Eq. (13) are separated into groups of bands lying far away in energy from the initial and final states (i.e. the bands projected out) and bands lying nearby the initial and final states (considered bands with correlations). The former grouping of intermediate states are considered as in Section II.B to be approximated by the effective mass contribution, Eq. (24). The remaining terms involve matrix elements of the current operator between the remaining band of interest[10].

The interaction of light with these downfolded electrons can be treated via the Peierls construction, in which the creation and annihilation operators develop a phase,

$$c_{i,\sigma} \to c_{i,\sigma} e^{-i\frac{e}{\hbar c}\int_{-\infty}^{\mathbf{r}_i} \mathbf{A}\cdot d\ell}. \qquad (32)$$

The resulting scattering Hamiltonian obtained by expanding in powers of $\mathbf{A}$ reads

$$H_{\text{int}} = \frac{e}{\hbar c}\hat{\mathbf{j}}\cdot\mathbf{A} + \frac{e^2}{2\hbar^2 c^2}\sum_{\alpha\beta} A_\alpha \hat{\gamma}_{\alpha\beta} A_\beta, \qquad (33)$$

where

$$\hat{j}_\alpha(\mathbf{q}) = \sum_{\mathbf{k}} \frac{\partial\varepsilon(\mathbf{k})}{\partial k_\alpha} c_\sigma^\dagger(\mathbf{k}+\mathbf{q}/2)c_\sigma(\mathbf{k}-\mathbf{q}/2), \qquad (34)$$

is a component of the current operator $\hat{\mathbf{j}}$ and

$$\hat{\gamma}_{\alpha\beta}(\mathbf{q}) = \sum_{\mathbf{k}} \frac{\partial^2\varepsilon(\mathbf{k})}{\partial k_\alpha \partial k_\beta} c_\sigma^\dagger(\mathbf{k}+\mathbf{q}/2)c_\sigma(\mathbf{k}-\mathbf{q}/2) \qquad (35)$$

is the stress tensor operator. Both operators are thus formed from the energy dispersion of the downfolded band structure. The matrix element can be written in compact form:

$$\begin{aligned} M_{F,I}(\mathbf{q}) &= \sum_{\alpha,\beta} e_\alpha^i e_\beta^s M^{\alpha,\beta}(\mathbf{q}), \\ M^{\alpha\beta}(\mathbf{q}) &= \langle F|\hat{\gamma}_{\alpha,\beta}(\mathbf{q})|I\rangle \\ &+ \sum_\nu \left(\frac{\left\langle F\left|\hat{j}_\beta(\mathbf{q}_s)\right|\nu\right\rangle \left\langle\nu\left|\hat{j}_\alpha(\mathbf{q_i})\right|I\right\rangle}{E_\nu - E_I - \hbar\omega_i} \right. \\ &+ \left. \frac{\left\langle F\left|\hat{j}_\alpha(\mathbf{q}_i)\right|\nu\right\rangle\left\langle\nu\left|\hat{j}_\beta(\mathbf{q}_s)\right|I\right\rangle}{E_\nu - E_I + \hbar\omega_s} \right), \end{aligned} \qquad (36)$$

---

[10] We remark that this is not exact as it inaccurately treats resonant scattering processes occurring within the conduction band. Since these processes are usually taken to be damped, even though this approach is strictly speaking not exact, it provides a good starting point for considering Raman scattering in correlated single-band systems, and as such, has been widely used (Shastry and Shraiman, 1991).

with the sum over intermediate states ν of the Hamiltonian Eq. (30). The Raman cross section can be separated into non-resonant, mixed, and resonant contributions:

$$R(\Omega) = R_N(\Omega) + R_M(\Omega) + R_R(\Omega), \qquad (37)$$

where the nonresonant contribution is

$$R_N(\Omega) = \sum_{I,F} \frac{\exp(-\beta E_I)}{\mathcal{Z}} \, \tilde{\gamma}_{I,F}^{i,s} \, \tilde{\gamma}_{F,I}^{s,i} \, \delta(E_F - E_I - \hbar\Omega),$$
$$(38)$$

the mixed contribution is

$$\begin{aligned}
R_M(\Omega) \;=\; & \sum_{I,F,\nu} \frac{\exp(-\beta E_I)}{\mathcal{Z}} \\
\times \; & \left[\tilde{\gamma}_{I,F}^{i,s} \left(\frac{\tilde{j}_{F,\nu}^{(s)} \tilde{j}_{\nu,I}^{(i)}}{E_\nu - E_I - \hbar\omega_i} + \frac{\tilde{j}_{F,\nu}^{(i)} \tilde{j}_{\nu,I}^{(s)}}{E_\nu - E_I + \hbar\omega_s} \right) \right. \\
+ \; & \left. \left(\frac{\tilde{j}_{I,\nu}^{(i)} \tilde{j}_{\nu,F}^{(s)}}{E_\nu - E_I - \hbar\omega_i} + \frac{\tilde{j}_{I,\nu}^{(s)} \tilde{j}_{\nu,F}^{(i)}}{E_\nu - E_I + \hbar\omega_s} \right) \tilde{\gamma}_{F,I}^{s,i} \right] \\
\times \; & \delta(E_F - E_\nu - \hbar\Omega),
\end{aligned}$$
$$(39)$$

and the resonant contribution is

$$\begin{aligned}
R_R(\Omega) \;=\; & \sum_{I,F,\nu\nu'} \frac{\exp(-\beta E_I)}{\mathcal{Z}} \\
\times \; & \left(\frac{\tilde{j}_{I,\nu}^{(i)} \tilde{j}_{\nu,F}^{(s)}}{E_\nu - E_I - \hbar\omega_i} + \frac{\tilde{j}_{I,\nu}^{(s)} \tilde{j}_{\nu,F}^{(i)}}{E_\nu - E_I + \hbar\omega_s} \right) \\
\times \; & \left(\frac{\tilde{j}_{F,\nu'}^{(s)} \tilde{j}_{\nu',I}^{(i)}}{E_{\nu'} - E_I - \hbar\omega_i} + \frac{\tilde{j}_{F,\nu'}^{(i)} \tilde{j}_{\nu',I}^{(s)}}{E_{\nu'} - E_I + \hbar\omega_s} \right) \\
\times \; & \delta(E_F - E_I - \hbar\Omega).
\end{aligned}$$
$$(40)$$

We have introduced the symbols

$$\tilde{\gamma}^{i,s} = \sum_{\alpha\beta} e_\alpha^i \hat{\gamma}_{\alpha\beta}(\mathbf{q}) e_\beta^s, \qquad \tilde{j}^{(i,s)} = \sum_\alpha e_\alpha^{i,s} \hat{j}_\alpha(\mathbf{q}_{i,s}),$$
$$(41)$$

and denote $\hat{O}_{\kappa,\lambda}$ as the matrix element $\langle \kappa | \hat{O} | \lambda \rangle$. Some of the contributions are depicted diagrammatically in Figures 8, 9, and 10 for the non-resonant, the mixed, and the resonant terms, respectively. In the limit $D \to \infty$ these are the main diagrams to consider. Additional diagrams involving multi-particle vertex renormalizations generally contribute for finite dimensions (not shown). In general, the matrix elements that enter into Eqs. (38–40) are not easy to calculate for an interacting system, so the summations are problematic to evaluate. In particular, one needs to evaluate the irreducible stress and current vertices, depicted in Figures 8-10 by the hatched symbols. Contributions to these vertex dressings include many-particle renormalizations. A particularly complicated one is shown in Figure 11 which represents 4-particle vertex corrections. Moreover, analytic continuation must be performed to obtain the Raman response

$R(\Omega)$ on the real axis from the imaginary axis. While this is relatively straightforward for the non-resonant case, mixed and resonant cases are problematic because of the complicated dependences on each of the frequencies $\omega_{i,s}, \Omega$ which have to be analytically continued. While the continuation has been worked out recently for the general case, evaluating these diagrams for general interactions has proved elusive.

The overall complexity of the problem limits the evaluation of the light scattering cross section to generic interacting systems. Only recently, these diagrams have been evaluated exactly in a DMFT treatment of the Falicov-Kimball model (Shvaika *et al.*, 2004, 2005).

2. Correlated Insulators - Heisenberg Limit

To emphasize the generality of Eq. (13) we now consider the large U limit for the insulating half-filled two-dimensional Hubbard model. Following Shastry and Shraiman (1991) we consider a system with N interacting electrons in which the manifold of states can be classified by the number n of doubly occupied sites. The well-
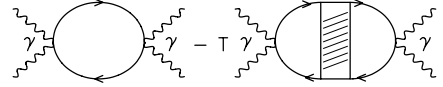

FIG. 8 Feynman diagrams for non-resonant Raman scattering. The wavy and the solid lines denote photon and electron propagators, respectively. The cross-hatched rectangle is the *reducible* charge vertex. The symbol γ denotes the stress-tensor vertex of the corresponding electron-photon interaction. From Shvaika *et al.* (2005).
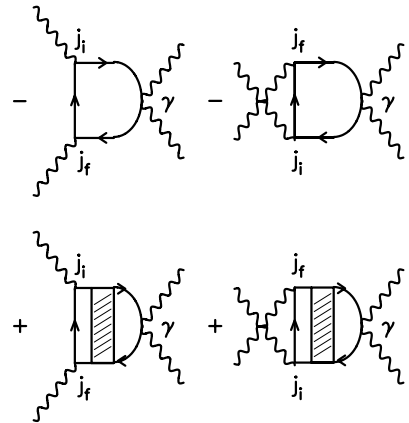

FIG. 9 Feynman diagrams for the mixed contributions to Raman scattering. The symbols j_f and j_i remind us to include the relevant vertex factors from the current operator in the electron-photon interaction. From Shvaika *et al.* (2005).

known Heisenberg Hamiltonian emerges from projecting the Hubbard model down onto the reduced Hilbert space

containing no double occupancies:

$$H_{\text{Heisenberg}} = J \sum_{i,\delta} \mathbf{S}_i \cdot \mathbf{S}_{i+\delta}, \tag{42}$$

with $J = 4t^2/U$ the Heisenberg exchange constant. Higher manifolds containing empty holes and doubly occupied states can be labeled according to the net spin configuration $\{\sigma\}$ of the $N - 2n$ singly occupied sites, as well as the locations $\{\mathbf{R}\}$ of the empty $\mathbf{r}_{\text{hole}}$ and doubly occupied $\mathbf{r}_{\text{double}}$ sites. We denote these states as $|n; \{\sigma\}, \{\mathbf{R}\}\rangle$. These states are connected to each other via

$$|1; \{\sigma'\}; \{\mathbf{R}\}\rangle = c_\sigma^\dagger(\mathbf{r}_{\text{double}}) c_\sigma(\mathbf{r}_{\text{hole}}) |0; \{\sigma\}\rangle, \tag{43}$$

where $|0; \{\sigma\}\rangle = \Pi_{\mathbf{r}} c_{\sigma_r}^\dagger(\mathbf{r}) |\text{vac}\rangle$ and $|\text{vac}\rangle$ denotes the vacuum.

Light scattering thus occurs via transitions out of the manifold of singly-occupied states. To leading order for large U, only the $n = 0$ and $n = 1$ manifold of states contributes to light scattering via Eq. (13), with $n = 0$ denoting the ground state and $n = 1$ the manifold of intermediate states having one doubly occupied and one empty site. The first term containing $m_{\alpha,\beta}$ cannot contribute for the half-filled lattice, and thus only interband scattering between the upper and lower Hubbard bands occurs via the $\mathbf{p} \cdot \mathbf{A}$ term. The energy difference between these excitations is U to lowest order in t/U, allowing us to write the matrix element Eq. (13) in the form
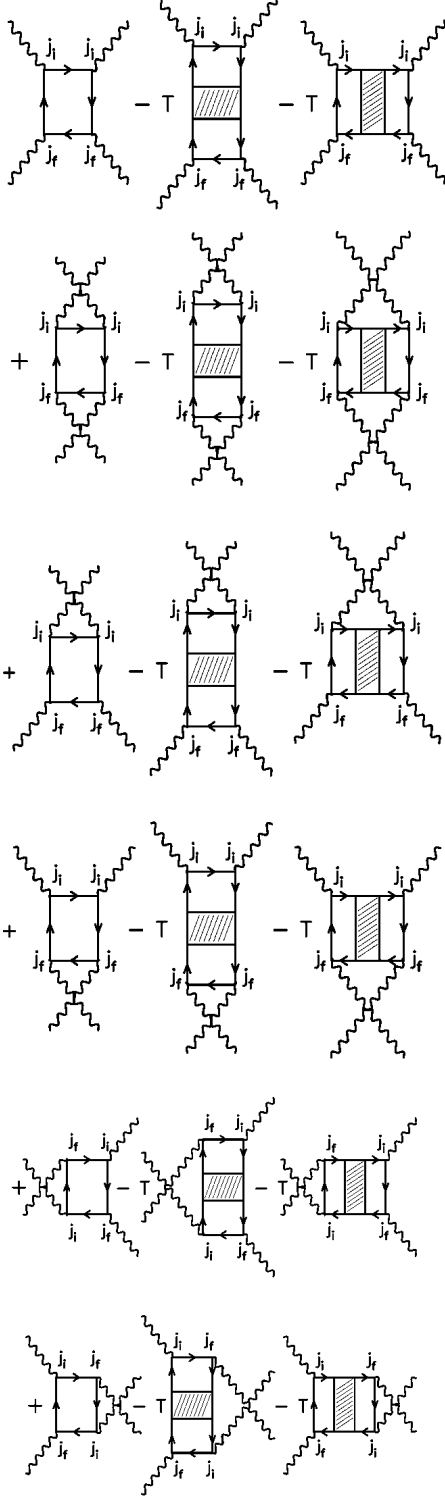

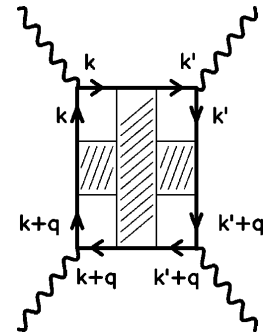FIG. 10 Feynman diagrams for the resonant contributions to Raman scattering. From Shvaika et al. (2005).

FIG. 11 Feynman diagrams for a typical parquet-like renormalization. This resonant diagram has a simultaneous horizontal and vertical renormalization by the two-particle reducible charge vertex. From Shvaika et al. (2005).

$$M_{F,I} = \sum_{\nu,\boldsymbol{r},\boldsymbol{r'},\boldsymbol{\delta},\boldsymbol{\delta'}} \langle 0, \{\sigma_I\} \mid \hat{j}_s(\boldsymbol{r}) \hat{\mathbf{e}}_s \cdot \boldsymbol{\delta} \mid 1; \{\sigma_\nu\}; \mathbf{R}_\nu \rangle \langle 1; \{\sigma_\nu\}; \mathbf{R}_\nu \mid \hat{\mathbf{e}}_i \cdot \boldsymbol{\delta'} \hat{j}_i(\boldsymbol{r'}) \mid 0, \{\sigma_F\} \rangle \left[\frac{1}{U - \hbar\omega_i} + \frac{1}{U + \hbar\omega_s} \right], \quad (44)$$

with the current operator defined as

$$\hat{j}_{i,s}(\mathbf{r}) = i\,t[c_\sigma^\dagger(\mathbf{r} + \boldsymbol{\delta} a \cdot \hat{\mathbf{e}}_{i,s})c_\sigma(\mathbf{r}) - c_\sigma^\dagger(\mathbf{r})c_\sigma(\mathbf{r} + \boldsymbol{\delta} a \cdot \hat{\mathbf{e}}_{i,s})]. \quad (45)$$

Here $\boldsymbol{\delta}$ is a unit vector connecting a site with its nearest neighbors. The intermediate states ν represent a sum over spin configurations and locations of both the doubly occupied and the hole sites. Substituting Eq. (43) into Eq. (44) collapses the intermediate state sum, leaving four terms connecting initial and final states. Using the identity $1/2 - 2\mathbf{S}_i \cdot \mathbf{S}_j = c^\dagger(\mathbf{r} + \boldsymbol{\delta} a)c(\mathbf{r})c^\dagger(\mathbf{r})c(\mathbf{r} + \boldsymbol{\delta} a)$ valid in the manifold of singly occupied states, one obtains the light scattering Hamiltonian of Elliot and Loudon (1963) and Fleury and Loudon (1968),

$$H_{\mathrm{EFL}} = \sum_{\mathbf{r},\boldsymbol{\delta}} \mathbf{S_r} \cdot \mathbf{S_{r+\delta a}}(\hat{\mathbf{e}}_\mathbf{s} \cdot \boldsymbol{\delta})(\hat{\mathbf{e}}_\mathbf{i} \cdot \boldsymbol{\delta}) \left[\frac{1}{U - \hbar\omega_i} + \frac{1}{U + \hbar\omega_s} \right]. \quad (46)$$

We note that the polarization dependence is crucial as well. For $xx + yy$ polarizations projecting the fully symmetric components, the light scattering Hamiltonian commutes with the nearest neighbor Heisenberg Hamiltonian and thus does not give inelastic scattering in the A_{1g} channel. Moreover, B_{2g} (xy) is also identically zero. As a result, a large signal appears only in the B_{1g} channel ($xx - yy$). These restrictions are lifted however if longer range spin interactions are considered (Shastry and Shraiman, 1991).

The collapse of the intermediate states allowed us to replace the operators with projected spin operators confined to the restricted Hilbert space of the $n = 0, 1$ manifolds. Thus, in this limited Hilbert space, the formalism is similar to non-interacting electrons in that the operators appearing in the scattering matrix may be simplified. If the Hilbert space is enlarged to include larger manifolds, then this would no longer be the case, and thus including terms to higher order in t/U becomes highly non-trivial and is still one of the challenges to merge a weakly interacting picture into a strongly interacting one.

We note that Equation (46) was derived effectively as an expansion in $t/(U - \hbar\omega_i)$. Therefore, the scattering Hamiltonian is limited to cases when both the number of holes and double occupied sites are restricted and off-resonance conditions apply, with the incident photon energy $\hbar\omega_i$ far away from U. Efforts to extend the treatment to more general conditions involve understanding the motion of holes or doubly occupied sites in an arbitrary spin background. This has proved to be a hard task.

D. Electronic Charge Relaxation

In Sections II.B and II.C we reviewed the general formalism of the theory of Raman scattering for weakly and strongly correlated systems. In this subsection we now specify the electronic states from which light can be scattered and review the various theoretical treatments for specific models of interacting electrons. Emphasis is placed upon how symmetry can be used to highlight electron dynamics on regions of the BZ, and general features for each model system will be presented. We first consider the case where the correlations among electrons are weak.

1. Weakly-Interacting Electrons

In this subsection, we consider electrons as having very well defined eigenstates labeled by energy and momentum and having sharp spectral functions. Apart from the form of the energy dispersion $\xi_\mathbf{k}$, the results are rather general and governed largely by phase space considerations. We must, however, consider the long-range Coulomb interaction in order to account for charge backflow and screening, and we utilize the results derived in Section II.B and the general expression Eq. (29).

The use of χ_{sc} rather than χ takes into account the most drastic manifestation of the long-range Coulomb interaction, viz. screening. For weakly interacting electrons, the Random Phase Approximation (RPA) is acceptable, which replaces χ_{sc} by the Lindhard function for non-interacting electrons. The response functions are determined by the Lindhard kernel,

$$\chi_{a,b}(\mathbf{q}, \Omega) = \frac{2}{V} \sum_\mathbf{k} a_{\mathbf{k},\mathbf{q}} b_{\mathbf{k},\mathbf{q}} \frac{f(\xi_\mathbf{k}) - f(\xi_{\mathbf{k+q}})}{\xi_\mathbf{k} - \xi_{\mathbf{k+q}} + \hbar\Omega - i\delta}, \quad (47)$$

for general vertices a, b appearing in Eq. (29). In a free electron gas, the Raman response is given by Eq. (27) or equivalently, the last term in Eq. (29). For large q, collective excitations are unimportant and light scattering occurs via creation of particle-hole excitations in the Landau continuum. However, as the only phase space

for creating particle-hole pairs comes from finite q transferred from the photons, the resulting response is a continuum varying linearly with Ω at small frequencies and extending up to a cut-off $\Omega_c = v_F q$ from the borders of the continuum (Mahan, 2000). The low-energy intensity is proportional to q^2, and the only excitation left at $q = 0$ is the collective plasmon. The Raman response for the free electron gas is shown in Figure 12.

For electrons in a solid, however, the non-parabolicity of the energy dispersion results in charge fluctuations which are anisotropic in the small q limit and thus can survive screening and give more weight at low energy transfers. Formally, an additional contribution to the response is given by the first two terms in Eq. (29). Yet phase space restrictions still produce an inescapable cutoff at $\Omega_c = v_F q$ (Wolff, 1968), and the response resembles that shown in Figure 12. This is also the case if scattering occurs for the 2 dimensional electron-gas (2DEG) in the absence of a magnetic field (Jain and Das Sarma, 1987; Mishchenko, 1999) or for complex Fermi surfaces (Ipatova *et al.*, 1983). An RPA treatment for resonant scattering has been given by Wang and Das Sarma (1999, 2002).

Recently, substantial progress has been made in understanding the Raman response in the integer or fractional quantum Hall regimes of the 2DEG. Space limitations do not allow us to review these systems; so for brevity, we cite only a recent reference (Richards, 2000).

2. Impurities

Excitations at low energies in non-interacting electronic systems can arise for small q via electronic scattering from impurities, where momentum contributed by impurity scattering can provide phase space for electron-hole creation which is anisotropic in the Brillouin zone. For example, if one considers a general electron-impurity interaction of the form
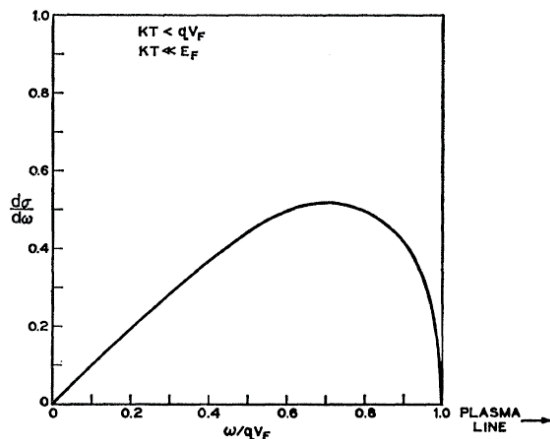
$$H_{\mathrm{imp}} = \sum_{\mathbf{k},\mathbf{k}',\sigma} V_{\mathbf{k},\mathbf{k}'} c_{\mathbf{k},\sigma}^\dagger c_{\mathbf{k}',\sigma}, \qquad (48)$$

with an anisotropic interaction $V_{\mathbf{k},\mathbf{k}'}$, the gauge invariant Raman response is given via the diagrams presented in Figure 8. If we make a symmetry decomposition of the scattering amplitude $\gamma(\mathbf{k}) = \sum_L \gamma_L \Phi_L(\mathbf{k})$ in terms of basis functions Φ_L of the Brillouin zone, the resulting response in channel L corresponding to a particular light polarization orientation has a Drude Lorentzian form (Devereaux, 1992; Fal'kovskiǐ, 1989; Zawadowski and Cardona, 1990):

$$\chi''(\mathbf{q}, \Omega) = N_F \gamma_L^2 \frac{\Omega \tau_L^*}{1 + (\Omega \tau_L^*)^2}, \qquad (49)$$

with N_F the density of states at the Fermi level. $1/\tau_L^* = 1/\tau + Dq^2 - 1/\tau_L$ is the effective scattering rate where

$$1/\tau = 1/\tau_{L=0} = n_i N_F \int \frac{dS_{\mathbf{k}}}{S} \int \frac{dS_{\mathbf{k}'}}{S} \mid V_{\mathbf{k},\mathbf{k}'} \mid^2, \quad (50)$$

involving an integration of the Fermi surface $S_{\mathbf{k}}$ normalized to the Fermi area S. Here n_i is the impurity concentration, $D = \frac{1}{3} v_F^2 \tau$ is the diffusion constant. The anisotropy of the impurity scattering is characterized via orthonormal basis functions Φ_L

$$V_{\mathbf{k},\mathbf{k}'} = \sum_{L,L'} \Phi_L^*(\mathbf{k}) \Phi_L(\mathbf{k}') V_{L,L'}, \qquad (51)$$

using an intelligent basis where the interaction is diagonal $V_{L,L'} = \delta_{L,L'} V_L$. Then, $1/\tau_L = 2\pi n_i N_F V_L$ and $1/\tau_{L=0}$ is the dominant contribution.

The resulting Raman spectrum (Figure 13) grows linearly with frequency Ω, decays as $1/\Omega$, and has a peak when $\Omega \tau_L^*$ equals 1. The width of the Lorentzian reflects the rate for which charge density excitations having symmetry L decay into all other channels. The light polarizations select the type of excitation L created, and thus allow a way to probe the anisotropy of the impurity-electron interaction. The decay of the charge density

FIG. 12 Raman response of an electron gas. From Platzman (1965).
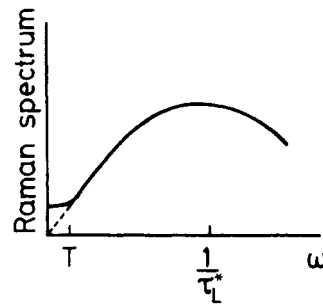

FIG. 13 Raman response from impurity scattering in an otherwise non-interacting system. From Zawadowski and Cardona (1990).

fluctuations can occur via finite q through the diffusion term and all contributions other than V_L which relax electrons out of the state L. Put another way, $Dq^2 + 1/\tau$ are "scattering out" processes, while $1/\tau_L$ is a "scattering in" process, giving an effective scattering rate $1/\tau_L^*$. This is a consequence of a gauge invariant treatment including

(t")9$\bar{c}$38n6392.b 1((t"(s)-1.9(c)261k))-1.fl 1((to)2392.w(r)-223.((h)7.C)300.5(o)-1.u 1((tl(e)4.om))-33.b ointtionss ellssonig ererscatterimputerc 2aer).(g)]TJ49.1499 -1.1563 TD11 TcΩns, the36382.limi7(t)5782.9(o582.(of)4414.1)-3aa5261ksca52616(tter505.6()-7.ving5-3.9(,3

tions in the Hubbard (Freericks *et al.*, 2001, 2003a) and Falicov-Kimball models (Freericks and Devereaux, 2001).

Two aspects of the Raman response are generally in the main focus: the frequency dependence of the broad continuum extending well past qv_F, and the polarization dependence. We discuss first the spectral response.

In the context of the cuprates, Varma and coworkers pointed out that a flat, nearly frequency independent response could be obtained if the imaginary part of the electron self-energy depended linearly on frequency (Varma *et al.*, 1989a; Varma, 1989b). The response is then given in terms of the scale-invariant ratio of $\hbar\omega/k_B T$ and approaches a constant at large frequency transfers. This can be understood phenomenologically by replacing $1/\tau_L^*$ with $1/\tau_L^*(\Omega, T) \propto \max(k_B T, \hbar\Omega)$ in Eq. (49).[11] A scale-invariant response at low frequencies is a general consequence of systems in proximity to a quantum-critical point, but this scale invariance is broken outside the quantum critical regime. "Marginal Fermi liquid" behavior emerges for instance when scattering is considered in a nested Fermi liquid (Virosztek and Ruvalds, 1991, 1992), low Fermi-energy systems (Dahm *et al.*, 1999; Devereaux and Kampf, 1999), and slave-boson systems (Bang, 1993). A broad background very similar to "marginal" behavior is also found for strongly coupled electron-phonon systems (Itai, 1992; Kostur, 1991, 1992). As a representative example, we show the response calculated by Virosztek and Ruvalds (1992) for a nested Fermi liquid in Figure 14.
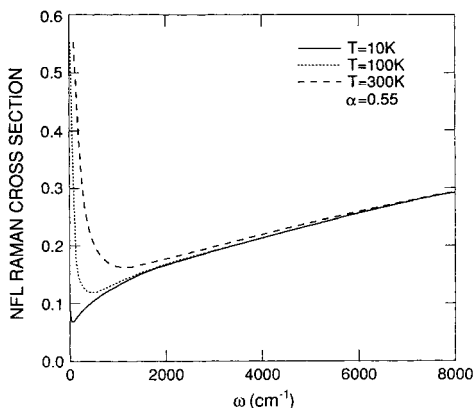
Low energy electron dynamics can be extracted by

FIG. 14 Raman response as a function of temperature obtained by Virosztek and Ruvalds (1992) for a system with a nested Fermi surface. The upturn at low frequencies is to the $(\log(\Omega))$ frequency dependence of the effective mass in this model.

studying the Raman response in the limit $\Omega \to 0$. Neglecting vertex corrections, the low frequency response reads (Devereaux and Kampf, 1999; Venturini *et al.*, 2002a)

$$\chi_\mu''(\Omega \to 0) = \Omega N_F \times$$
$$\times \left\langle \frac{\gamma_\mu^2(\mathbf{k}) \int d\xi \left(-\frac{\partial f^0}{\partial \xi}\right) Z_{\mathbf{k}}^2(\xi, T)}{2\Sigma_{\mathbf{k}}''(\xi, T)} \right\rangle. \quad (54)$$

Here, N_F is the density of electronic levels at the Fermi energy E_F, $\Sigma_{\mathbf{k}}''$ is the imaginary part of the single-particle self energy related to the electron lifetime as $\hbar/2\Sigma_{\mathbf{k}}''(\omega, T) = \tau_{\mathbf{k}}(\omega, T)$, $Z_{\mathbf{k}}(\omega, T) = (1 - \partial\Sigma_{\mathbf{k}}'(\omega, T)/\partial\omega)^{-1}$ is the quasiparticle residue, f^0 is the equilibrium Fermi distribution function, and $\langle\cdots\rangle$ denotes an average over the Fermi surface. Thus the inverse of the Raman slope

$$\Gamma_\mu(T) = \left[\frac{\partial\chi_\mu''(\Omega)}{\partial\Omega}\right]^{-1} \quad (55)$$

measures the effective "scattering rate" of the quasiparticles in a correlated metal, and can be best thought of as a "Raman resistivity".

In systems with isotropic interactions, the polarization dependence drops out and the slope of the low-frequency Raman response is given in terms the low energy quasiparticle scattering lifetime, $\Gamma_\mu(T) \propto \hbar/\tau(T)$, as an extension of Eq. (49). Yet, in strongly correlated systems, the quasiparticle residue Z and, importantly, vertex corrections, enter as well. In a correlated or a strongly disordered metal (near an Anderson transition, e.g.), however, a finite energy might be necessary to move an electron from one site to another one. Thus, in spite of a non-vanishing density of states at the Fermi level, as observed in an ARPES experiment for instance, no current can be
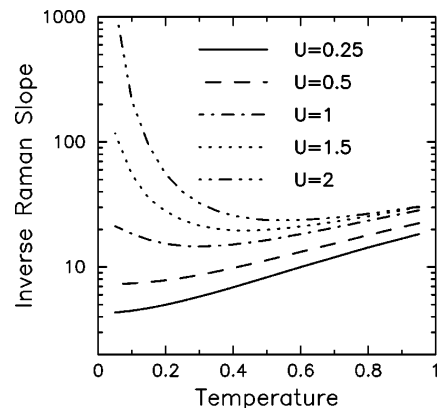

FIG. 15 Inverse Raman slope (see Eq. (55)) close to a metal-insulator transition at a value $U = \sqrt{2}$ in the Falicov-Kimball model for $D = \infty$ (Freericks and Devereaux, 2001). All energies and temperatures are measured in terms of the hopping t.

---

[11] This is only an approximation since $1/\tau_L^*(\Omega, T)$ depends now on energy. Causality requires that the relaxation function has real and imaginary part, $M(\Omega, T) = \Omega\lambda + i/\tau_L^*$ (Götze and Wölfle, 1972; Opel *et al.*, 2000).

transported and $\Gamma_\mu(T) \gg \hbar/\tau(T)$. This is an important difference between single- and two-particle properties.

Figure 15 displays the inverse Raman slope defined in Eq. (55), as determined via a DMFT treatment of the Falicov-Kimball model in the vicinity of a metal-insulator transition, as a function of the Coulomb repulsion U (Freericks and Devereaux, 2001). It provides an illustrative example of how Fermi-liquid-like features evolve as the lifetime of putative quasiparticles increases due to decreased role of correlations. For small U, the correlated metal displays an inverse slope $\propto T^2$ as a canonical Fermi liquid in the metallic state. A pseudogap opening in the density of states with increasing U drives the inverse slope into insulating behavior, increasing as the temperature decreases.

As a second important application Eq. (55) can illuminate the anisotropy of electron dynamics due to the momentum-dependent weighting factors of the polarization orientations and self energies. The geometry of light scattering orientations, as given by the form factors listed in Table I, project out the ratio of quasiparticle residues and scattering rates in different regions of the BZ. As a consequence, the Raman spectra show polarization dependent behavior determined largely by the self energies and vertex corrections near the regions projected by the scattering vertices γ. Figure 16 plots the B_{1g} and B_{2g} Raman response calculated in a spin-fermion model in which electron scattering is most pronounced involving antiferromagnetic reciprocal lattice momentum transfers $\mathbf{Q} = (\pi, \pi)$, leading to "hot" quasiparticles near the BZ axes (projected by B_{1g} form factors) and "cold" quasiparticles along the BZ diagonals (projected by B_{2g} form factors). Therefore, the Raman response has a sharp quasiparticle peak for B_{2g} scattering at low energies due to the long quasiparticle lifetimes, while the response in B_{1g} is dominated by strong incoherent scattering leading to a suppression of the quasiparticle peak at low energies and an essentially structureless continuum.

Lastly, we note that the non-resonant Raman response has also been calculated for exchange of fluctuation modes at wavevectors $\mathbf{Q}$ and $-\mathbf{Q}$ for systems near a spin-density wave instability (Brenig and Monien, 1992; Kampf and Brenig, 1992; Venturini *et al.*, 2000) and a charge-density wave instability (Caprara *et al.*, 2005). Here, the Raman response is sensitive to the light polarizations and has a peak centered at twice the energy of the fluctuating mode.

4. Interacting Electrons - Resonant Response

In addition to the non-resonant response, one has the mixed and resonant contributions to consider. Typically these diagrams are neglected in the weak correlation limit, as they can be summed into two-particle response functions as discussed in Section II.B. In the insulating case, only the resonant terms are kept, as the studies focus on excitations across a charge-transfer or Hubbard gap. This has been calculated in systems exhibiting 1D-Luttinger behavior (Kramer and Sassetti, 2000; Sassetti and Kramer, 1998; Sassetti *et al.*, 1999; Wang *et al.*, 2004) where bosonization techniques can be applied. Yet, generally treating all diagrams on equal footing is technically demanding. Only recently, an exact evaluation in DMFT has been performed (Shvaika *et al.*, 2004, 2005).

It is well known that many of the Raman signals in correlated metals and insulators display complicated dependences on incoming photon frequency ω_i. For example, the B_{1g} two-magnon feature at roughly 350 meV in the thoroughly studied insulating parent cuprates has a resonance for incident photon energies near 3 eV. As a reaction to the experimental results in the cuprates, much theoretical work has been devoted to Raman scattering in a two-dimensional Heisenberg antiferromagnet using the Fleury-Loudon model Eq. (46).

In the nearest neighbor Heisenberg antiferromagnet, one treats the spin operators using a Dyson-Maleev representation of magnons with dispersion $2J$. Due to the B_{1g} form factor, in the absence of magnon-magnon interactions at T=0, a sharp peak at $4J$ appears as the top of the magnon dispersion is projected out, and the response abruptly drops to zero for large Raman shifts (Sandvik *et al.*, 1998). However, since the light scattering is localized to neighboring spins, magnon-magnon interactions must be included, and the peak becomes more symmetric and shifts to $\sim 3J$ via breaking exchange bonds between local neighbors, as shown in Figure 17.

There have been many developments on the Fleury-Loudon model, which has been addressed via critical fluctuation analysis (Halley, 1978), series expansions (Singh *et al.*, 1989), lower (Morr and Chubukov, 1997; Parkinson, 1969) and higher (Canali and Girvin, 1992; Chubukov and Frenkel, 1995b) order spin wave theories, $t-J$ studies at finite doping (Prelovšek and Jaklič, 1998), exact diagonalizations of small clusters (Tohyama *et al.*, 2002), excitonic cluster approaches (Hanamura *et al.*, 2000), finite temperature Quantum Monte Carlo methods (Sandvik *et al.*, 1998), and studies of bilayer effects (Morr *et al.*, 1996), 2-leg spin ladders (Jurecka *et al.*,
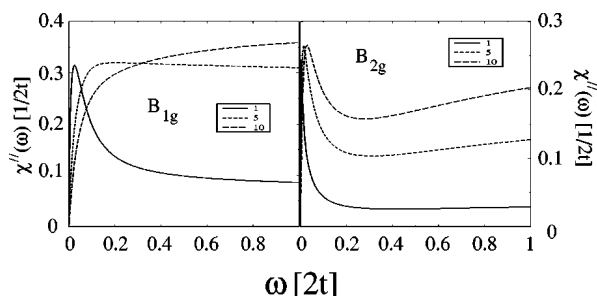

FIG. 16 Polarization-dependent Raman response in a spin-fermion model for a fixed temperature for three different values of the coupling constant. From Devereaux and Kampf (1999).

2001) and ... (Kampf, 2003),
giving a th... non scattering
from spin d... onant regime.
Scattering ... nd describing
the anisotr... ave been ad-
dressed via ... ractions and
by exact di... to phonons
(Freitas an... pproach of
Lorenzana ... t develop-
ments conc... f freedom
(Okamoto ... resonant
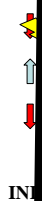
FIG. 17 C... rocess in a
2D Heisenb... hoton causes
an electron ... and creating a
double occu... with energy $\propto U$.
One partic... σ hops back to the
hole site lik... gy $\sim U - zJ\sigma$, leaving
behind a l... magnet with z exchange
bonds brok... as indicated by the dotted
lines.

(a)
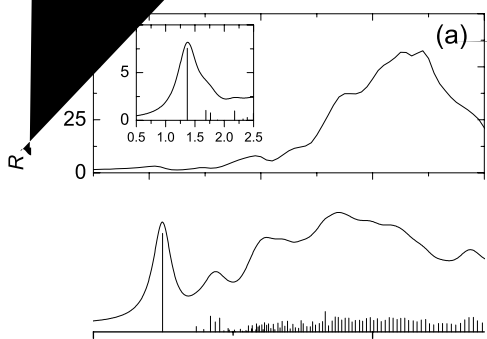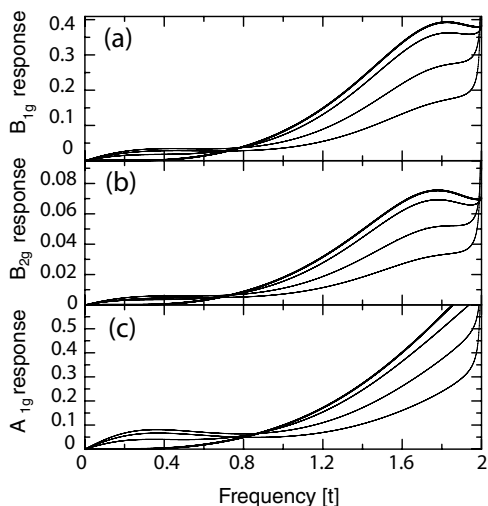
FIG. 19 Raman response in the 1/2-filled Falicov-Kimball model ($U = 2t$) as a function of transfered frequency for various temperatures for fixed incident photon frequency $\omega_i = 2t$. The thickest curve is $T/t = 0.05$, and the temperature increases to 0.2, 0.5, and 1 as the curves are made thinner. From Shvaika et al. (2004).

incident photon frequency is slightly larger than the frequency of the non-resonant feature. The resulting Raman response is a complicated function of the correlations, the temperature, the incident photon energy, and the transfered energy. It was found that resonance effects are different in different scattering geometries, corresponding to different symmetries of the charge excitations scattered by the light.

Resonance effects were found as a function of both the incoming and the outgoing photon frequencies $\omega_{i,s}$. A double resonance - occurring when the energy denominators of two pairs of the Greens functions, appearing in the bare response shown in Figure 10, approach zero - gives the strongest resonant enhancement of the response(Shvaika et al., 2004). In addition, an interesting resonance effect on both the charge-transfer peak and the low-energy peak was found when the incident photon frequency is of the order of the interaction strength, showing that in general the total response cannot be well described as a uniform resonance enhancement of the separable non-resonant response. In agreement with the results of Tohyama et al. (2002), for an antiferromagnetic system this is a direct consequence of the inseparability of energy scales in the correlated electron problem, in contrast to non-interacting electrons.

Shown in Figure 19 is the temperature and symmetry-dependent Raman response, including non-resonant, resonant, and mixed terms in the Falikov-Kimball model. In the insulating phase, spectral weight is depleted for small energy transfers and piles up into the excitations at energies of order U as the temperature is lowered. The transfer of spectral weight from lower to higher energies occurs across a temperature independent so-called isosbestic point. An isosbestic point also appears in studies of the Hubbard model (Freericks et al., 2001, 2003a), implying that it is a generic feature of the insulating phase, regardless of the microscopic origin of the phase. We note that isosbestic behavior already appears in the non-resonant contributions for B_{1g} scattering. In the A_{1g} and B_{2g} symmetries, it emerges only if resonant terms are included.

The local treatment of self energies in the single-site DMFT approach imposes limitations on the theory of light scattering in correlated systems. In particular, the full polarization dependence of the Raman spectra would uncover the way in which correlations affect electron dynamics in regions of the BZ, providing a two-particle complement to ARPES, for example. Progress here most likely will come from cluster dynamical mean field theory able to treat nonlocal and anisotropic interactions in a coarse-grained manner.

6. Superconductivity

As discussed in Section II.D.1, in the absence of interactions, there is no phase-space for low energy Raman scattering for $\mathbf{q} = 0$ momentum transfers. In the superconducting state, phase space restrictions are lifted since light can break $\mathbf{q} = 0$ Cooper pairs if the energy of the light is greater than 2Δ. Thus the Raman response becomes non-trivial, yet easily formulated, in BCS theory. As a consequence, there has been an enormous amount of theoretical work devoted to light scattering for temperatures below T_c as an extension of the theory for non-interacting electrons in the normal state. We review that work here.

In the superconducting state, focus has been traditionally placed on the two-particle non-resonant response in BCS theory. Formally the Raman response is given by generalizing Eqs. (52-53) in particle-hole space using Pauli matrices $\tau_{i=0..3}$ in Nambu notation (Nambu, 1960):

$$\chi(\mathbf{q} = 0, i\Omega) = -\frac{2}{V\beta} \sum_{i\omega} \sum_{\mathbf{k}} Tr\left[\hat{\gamma}(\mathbf{k})\hat{G}(\mathbf{k}, i\omega)\hat{\Gamma}(\mathbf{k}; i\omega; i\Omega)\hat{G}(\mathbf{k}, i\omega + i\Omega)\right],$$ (56)

where Tr denotes the trace, and

$$\hat{\Gamma}(\mathbf{k};i\omega;i\Omega) = \hat{\gamma}(\mathbf{k}) + \frac{1}{V\beta}\sum_{i\omega'}\sum_{\mathbf{k}'}V_i(\mathbf{k}-\mathbf{k}',i\omega-i\omega')\hat{\tau}_i\hat{G}(\mathbf{k}',i\omega')\hat{\Gamma}(\mathbf{k}';i\omega';i\Omega)\hat{G}(\mathbf{k}',i\omega'+i\Omega)\hat{\tau}_i. \qquad (57)$$

Here the bare Raman vertex of coupling to charge is $\hat{\gamma} = \hat{\tau}_3\gamma$ and the interaction V_i determines the channel of the vertex corrections. For example $V_{i=3}$ corresponds to interactions coupling electronic charge, while $V_{i=0}$ corresponds to spin interactions.

For the case of weak correlations, the Green's functions appearing in Eqs. (56) and (57) are given by the BCS expression

$$\hat{G}(\mathbf{k},i\omega) = \frac{i\omega\hat{\tau}_0 + \epsilon(\mathbf{k})\hat{\tau}_3 + \Delta(\mathbf{k})\hat{\tau}_1}{(i\omega)^2 - E^2(\mathbf{k})}, \qquad (58)$$

with $E^2(\mathbf{k}) = \xi^2(\mathbf{k}) + \Delta^2(\mathbf{k})$ the quasiparticle energies. In the weak coupling limit for the BCS approximation, $V_{i=3} = -V$ for phonon-mediated pairing.

By far, the superconducting state has received the largest amount of attention from theory, starting from the seminal contribution of Abrikosov and Fal'kovskiĭ (1961), which predated the observation of the effect by 19 years. The main focus in the early years was to study the 2Δ features in conventional $s-$wave superconductors with small and large coherence lengths (Abrikosov and Fal'kovskiĭ, 1961, 1987; Abrikosov and Falkovsky, 1988; Klein and Dierker, 1984), including the effects of Coulomb screening (Abrikosov and Genkin, 1973) and examining the temperature dependence (Tilley, 1972). If one neglects vertex corrections, the $\mathbf{q}$-dependent Raman response in a superconductor is given by a projected Maki-Tsuneto function (Maki and Tsuneto, 1962),

$$\chi''_{a,b}(\mathbf{q},\Omega+i\delta) = \frac{1}{N}\sum_{\mathbf{k}}a_{\mathbf{k},\mathbf{q}}b_{\mathbf{k},\mathbf{q}}$$

$$\times\Bigg\{A_+(\mathbf{k},\mathbf{q})\left[f(E(\mathbf{k})) - f(E(\mathbf{k}+\mathbf{q}))\right]\left(\frac{1}{\Omega+i\delta-E(\mathbf{k})+E(\mathbf{k}+\mathbf{q})} - \frac{1}{\Omega+i\delta+E(\mathbf{k})-E(\mathbf{k}+\mathbf{q})}\right)$$

$$+A_-(\mathbf{k},\mathbf{q})\left[1-f(E(\mathbf{k})) - f(E(\mathbf{k}+\mathbf{q}))\right]\left(\frac{1}{\Omega+i\delta+E(\mathbf{k})+E(\mathbf{k}+\mathbf{q})} - \frac{1}{\Omega+i\delta-E(\mathbf{k})-E(\mathbf{k}+\mathbf{q})}\right)\Bigg\}, \quad (59)$$

with the coherence factors $A_\pm(\mathbf{k},\mathbf{q}) = 1 \pm \frac{\xi(\mathbf{k})\xi(\mathbf{k}+\mathbf{q})-\Delta(\mathbf{k})\Delta(\mathbf{k}+\mathbf{q})}{E(\mathbf{k})E(\mathbf{k}+\mathbf{q})}$. A more common expression is the Raman response for $\mathbf{q} = 0$ which simplifies to

$$\chi''_{a,b}(\mathbf{q}=0,\Omega+i\delta) = \frac{2}{N}\sum_{\mathbf{k}}a_{\mathbf{k}}b_{\mathbf{k}}\left[\frac{|\Delta(\mathbf{k})|}{E(\mathbf{k})}\right]^2\tanh\left(\frac{E(\mathbf{k})}{2T}\right)\left(\frac{1}{2E(\mathbf{k})+\Omega+i\delta} + \frac{1}{2E(\mathbf{k})-\Omega-i\delta}\right), \qquad (60)$$

The full Raman response, including charge screening, is once again given by Eq. (29), in which the vertices a,b are replaced by the Raman $(a,b = \gamma)$ and pure charge $(a,b = 1)$ vertices (Abrikosov and Genkin, 1973).

For the case of an isotropic gap $(\Delta(\mathbf{k}) = \Delta)$ and momentum transfers $\mathbf{q} = 0$, a threshold and a square-root discontinuity appears at twice the gap edge Δ, reflecting the two-particle density of states. For finite $\mathbf{q}$, the singularity is cut-off due to breaking Cooper pairs with finite momentum, and the peak is shifted out to frequencies of roughly v_Fq as in the normal state (Figure 20). Qualitatively similar behavior is obtained for disordered $s-$wave superconductors (Devereaux, 1992) in which $1/\tau_L^*$ (see Eq. (49)) assumes the role of v_Fq .

Further advances in the theory for conventional $s-$wave superconductors were made for energy gaps with small anisotropy (Klein and Dierker, 1984), coexistence with charge-density wave order (Balseiro and Falicov, 1980; Littlewood and Varma, 1981, 1982; Tüttő and Zawadowski, 1992), layered superconductors (Abrikosov, 1991), impurities (Devereaux, 1992, 1993), and final-state interactions (Devereaux, 1993; Devereaux and Einzel, 1995a; Klein and Dierker, 1984; Monien and Zawadowski, 1990).

We note in particular that the variation with $\mathbf{k}$ of the Raman vertices $\gamma(\mathbf{k})$ is coupled to the $\mathbf{k}$-dependence of the energy gap $\Delta(\mathbf{k})$ (see, e.g., Eq. (60)), leading to a strong polarization dependence of the spectra. For isotropic s-wave superconductors, the vertex does not affect the lineshape, and thus the spectrum is polarization independent, apart from an overall prefactor. For this case, a polarization dependence can be generated in BCS

theory by taking into account channel-dependent final-state interactions (Bardasis and Schrieffer, 1961) and/or impurity scattering. However, for the most part this only produces a channel dependence in the vicinity of the gap edge, and thus the main feature of the response is the uniform gap existing for all polarizations. For anisotropic energy gaps, the symmetry dependence of the spectra is a direct consequence of the **k**-summation (angular averaging), which couples gap and Raman vertex and leads to constructive (destructive) interference if the vertex and the gap have the same (different) symmetry.

Generally, in superconductors with nodes of the energy gap, power-laws in the low frequency and/or temperature variation of transport and thermodynamic quantities emerge, replacing threshold or Arrhenius behavior ubiquitous in isotropic superconductors. However, due to the averaging over the entire Fermi surface, the power-laws themselves do not uniquely identify the ground state symmetry of the order parameter, but only can give the topology of the gap nodes along the Fermi surface, e.g., whether the gap vanishes on points and/or lines. Thus, one cannot distinguish between different representations

For $d_{x^2-y^2}$ superconductors, the interplay of polarizations and gap anisotropy can be simply drawn. Referring to Figure 7, B_{1g} orientations project out excitations around the principle directions (M-points or anti-nodal regions) of the BZ where the superconducting gap is maximal and where the van Hove singularity is located, while B_{2g} orientations project the nodal regions along the diagonals. As a consequence, the Raman response has a peak at $2\Delta_{\max}$ for B_{1g} and at slightly lower energy for B_{2g}. The polarization dependence also enters the low frequency behavior. Since line nodes yield a linear dependence on energy of the density of states, the B_{2g} response depends linearly on $\hbar\Omega$ in the limit $\Omega \to 0$ for a gap vanishing on the diagonals. For B_{1g} orientations, in contrast, the Raman vertex vanishes along with the energy gap at the same points in the BZ. This yields an additional Ω^2 contribution from the line nodes of the vertex, and the resulting response varies as Ω^3. The unscreened A_{1g} response measures an overall average throughout the BZ and thus picks up the gap maxima as well as the linear density of states. This is shown quantitatively in Figure 21. The frequency power laws also translate in low temperature power laws of the response in the small frequency limit (Devereaux and Einzel, 1995a).

Disorder effects generally smear peak features at larger energies and change the B_{1g} exponent to 1, similar to the change in the low temperature NMR rate for d-wave superconductors (Devereaux, 1995b). Moreover, similarities between the in-plane conductivity and B_{2g} Raman follows from the BZ weighting around the nodes, while the B_{1g} response is qualitatively similar to the c-axis conductivity due to the weighting around the antinodes (Devereaux, 2003b). For example the residual in-plane conductivity as $T \to 0$ is universal and given by $\sigma(T = 0) = ne^2/m\pi\Delta_0$, the slope of the B_{2g} response $2N_F/\pi\Delta_0$ is also universal and insensitive to impurity effects, while the B_{1g} channel and c-axis conductivity are non-universal, having additional impurity dependent prefactors (Devereaux, 1995b; Devereaux and Kampf, 1997; Devereaux, 2003b). The slope of the B_{2g} response follows the temperature dependence of the in-plane conductivity, and both possess a peak at intermediate temperatures due to a balance of DOS and lifetime effects as temperatures are lowered from T_c. Yet, both the out-of-plane conductivity and the B_{1g} response do not show a peak due to the more rapid variation of the projected DOS coming from antinodal portions of the BZ.

We note that for a d_{xy} energy gap, the above discussion applies accordingly, with the role of B_{1g} and B_{2g} symmetry reversed. It was indeed an important development to show that Raman scattering is unique in determining two-particle electron dynamics independently in *different* regions of the BZ in the superconducting state.

While the low frequency power-laws are insensitive to band structure (such as the shape of the Fermi surface), the polarization selection rules can select features of the band structure at higher energies. For example, in the cuprates, the van Hove singularities from $(\pi, 0)$ and re-lated points yields a peak at twice the quasiparticle energy $E(\mathbf{k})$ in A_{1g} and B_{1g} channels, as shown in Figure (21). For multiple bands, including the case of several Fermi surface sheets, the responses for crossed polarizations are simply additive, yet for A_{1g} channels due to backflow effects an additional interference term can be present if the charge fluctuations are different for the different sheets (Devereaux *et al.*, 1996; Krantz and Cardona, 1994).

Quite generally the backflow yields substantial reorganization of spectral weight around $2\Delta_{\max}$ compared to the bare response(Branch and Carbotte, 1995; Dahm *et al.*, 1999). This is because the term $\chi_{\gamma,1}$, which contributes in channels having the symmetry of the lattice, is peaked and large at the same position as the unscreened term $\chi_{\gamma,\gamma}$. Not surprisingly, the reorganization depends delicately on the relative momentum dependences of the Raman vertices and energy gap (number of BZ harmonics for example, as shown in Figure 22), as well as on details of the band structure (Branch and Carbotte, 1996; Devereaux *et al.*, 1994a; Krantz and Cardona, 1994; Strohm and Cardona, 1997).

For the cuprates, Raman vertices have been calculated using LDA (Strohm and Cardona, 1997), but limited progress has been made in including the contributions of substantial electronic correlations. In most other cases, either the effective mass approximation has been used in calculations or simply a symmetry classification has been made. While a detailed lineshape analysis can be applied based purely on symmetry as explained above, it must be kept in mind that even a comparison of overall intensities between different geometries can at best be qualitative.

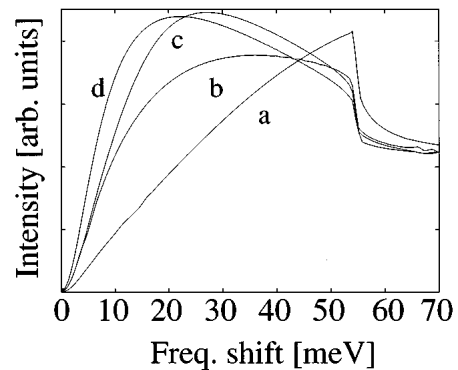Yet, the continuation of these treatments from the su-

FIG. 22 Comparison of the screened A_{1g} response obtained for different number of $d_{x^2-y^2}$ gap harmonics $\Delta(\mathbf{k}) = \Delta_0\{[\cos(k_x a) - \cos(k_y a)]/2 + \Delta_1[\cos(k_x a) - \cos(k_y a)]^3/8 + \Delta_2[\cos(k_x a) - \cos(k_y a)]^5/32\}$. Here $a - d$ correspond to the set $\Delta_{1,2} = (0,0), (1,0), (0,1)$, and $(1,1)$, respectively, and Δ_0 has been rescaled to give the same value for the maximum gap. Generally the large peak at 2Δ (as shown in Figure 21) is suppressed by the backflow terms. From Devereaux *et al.* (1996).

perconducting to the normal state is not straightforward. As can be seen directly from Eq. (60), the intensity vanishes proportional to Δ^2 as T approaches T_c. Hence, to avoid phase space limitations in the absence of Cooper pairs, an additional source for electronic scattering, such as the one mediating the formation of Cooper pairs, must be included. While strong coupling extensions of Raman scattering in $d-$wave superconductors have recently been presented (Dahm *et al.*, 1999; Devereaux and Kampf, 2000; Jiang and Carbotte, 1996), a merging of the normal and the superconducting states is poorly understood. This would require a not yet existing microscopic description of the formation of $d-$wave superconductivity from the normal state.

7. Collective Modes

Raman scattering has the almost unique ability to sort out collective modes of the two-particle response in different symmetry channels, owing to the freedom to independently adjust the two polarization vectors. The collective mode spectrum one obtains depends upon which interactions are included in Eq. (57). We first discuss the general consequences based on gauge-invariance and focus on exciton-like modes.

In order to form a fully gauge-invariant theory, the interactions responsible for superconductivity appear not only in $\hat{G}$, but must also be included as vertex renormalizations $\hat{\Gamma}$. In this way, the Raman response from pure charge density fluctuations in the superconducting state yields the Goldstone mode from the broken gauge symmetry - the phase or Anderson-Bogoliubov mode (Anderson, 1958; Bogoliubov *et al.*, 1959; Nambu, 1960). In the absence of the long-range Coulomb interaction, this mode is a soft sound mode, yet the Coulomb interactions - inescapable for $\mathbf{q}=0$ - push the sound mode up to the plasma frequency via the Higgs mechanism. As a result, particle-number conservation is satisfied in the superconducting state and $\chi_{sc}(\mathbf{q} = 0, \Omega) = 0$, independent of whether one considers Bloch states (Abrikosov and Genkin, 1973; Klein and Dierker, 1984; Monien and Zawadowski, 1990) or Anderson exact eigenstates of the disordered problem (Devereaux, 1993).

However, additional modes of excitonic origin may appear if one considers further interactions between electrons in clean (Bardasis and Schrieffer, 1961) and disordered (Fulde and Strassler, 1965; Maki and Tsuneto, 1962) conventional superconductors. These excitons appear split off from the continuum at $\hbar\Omega < 2\Delta$ if the interaction occurs in higher momentum channels orthogonal to the BCS condensate.

Since Raman scattering couples to anisotropic charge density fluctuations with symmetry selectivity to different channels L, the light polarizations can be used to determine the exact nature of bound states. Balseiro and Falicov (1980) considered the formation of a phonon-Cooper pair bound state due to electron-phonon coupling

though neglecting channels higher than $L = 0$. However, this mode is canceled by the backflow applying generically to all systems. Finite L exciton formation in clean and disordered superconductors, and the resulting appearance in Raman scattering, have been considered explicitly by Monien and Zawadowski (1990) and Devereaux (1993), respectively, bringing the symmetry of the exciton and the polarization dependence to light.

We show in Section III.B below that the effect of final state interactions can be substantial in strongly coupled conventional superconductors. This demonstrates the strength of the electron-phonon coupling, not only in general, but also specifically in channels orthogonal to the ground state. Interestingly, the lattice instability found in some of these materials has the same symmetry as the collective mode and the electronic states which apparently drive the transition (Weber, 1984).

For $d_{x^2-y^2}$ superconductors, the collective mode spectra have been investigated thoroughly by Devereaux and Einzel (1995a) and others (Dahm *et al.*, 1998; Manske *et al.*, 1997, 1998; Strohm *et al.*, 1998a; Wu and Griffin, 1995a,b). It was shown that the Anderson-Bogoliubov mode appears in A_{1g} channels and massive modes can appear in other channels. Since the pair state has only one representation in the D_{4h} group, massive collective modes arise when one considers interactions in orthogonal channels. Recently, it has been suggested that the presence of collective modes may allow one to distinguish charge- or spin-mediated $d-$wave pairing (Chubukov *et al.*, 1999, 2006), highlighting the possible importance in the context of the cuprates.

Generally, the collective mode spectrum can be quite diverse in unconventional superconductors. In principle, additional broken continuous symmetries can exist, such as SO_3^S spin rotational symmetry in spin-triplet systems and SO_3^L orbital rotational symmetry in spin-singlet systems, if the gap does not possess the full symmetry of the lattice. Furthermore, massive collective modes can arise if the energy gap is degenerate or has an admixture of different representations of the point group. The massive modes can in principle lie below the gap edge, and can thus be relevant for the low frequency dynamics of correlation functions. In fact, Raman-active modes in spin-triplet superconductors such as Sr_2RuO_4 have drawn recent theoretical interest (Kee *et al.*, 2003), although the experimental challenges are not negligible because of the low T_c and the related small energy gap in these materials.

Though very interesting, spin-triplet pairing or spin-orbit effects are rare and more on the exotic side in superconductivity. Competing ground states, however, are quite common whenever correlation effects come into play. This is not at all confined to the cuprates, but occurs also in, e.g., spin (SDW) and charge (CDW) density wave systems. Usually, density-wave formation with long-range order at least partially suppresses superconductivity such as in $2H - NbSe_2$ (see below). Then, additional modes appear as a result of the competition be-

tween CDW ordering and superconductivity, and collective modes appear as one modulates either one or both order parameters.

Littlewood and Varma (1981, 1982) and Browne and Levin (1983) considered a direct coupling between charge density and superconducting gap amplitudes, modulated for example by a CDW phonon, although this was not specified. They obtained an additional "gap" mode below 2Δ. Yet this mode was only considered in the $L = 0$ channel, and Coulomb interactions once again remove this mode. Lei *et al.* (1985) considered an effective CDW-SC coupling via a phonon and realized that in anisotropic systems such collective modes in $L \neq 0$ channels may appear. Finally, Tüttő and Zawadowski (1992) treated electron-phonon and CDW amplitude-phonon coupling on equal footing in finite angular momentum channels, showing generally that the collective modes in these channels are unaffected by Coulomb screening. The modes obtained split off from the gap edge and appear as excitations below the quasiparticle spectrum, much like excitons in semiconductors. Evidence of mixed CDW-SC pairing may be seen in Raman experiments via the presence or absence of these modes. This has recently been extended by Zeyher (2003) to MgB_2, having multiple energy gaps on different electron bands.

The collective mode spectrum of coupled $d-$wave charge density and superconductivity was investigated by Zeyher and Greco (2002) along the lines developed by Tüttő and Zawadowski (1992) for conventional CDW and superconducting systems. As for $s-$wave CDW superconductors, collective modes split off from the maximum of the gap edge. As an important difference in $d-$wave systems, the modes distinctly affect the various symmetry channels. Besides the reorganization of A_{1g} spectral weight, additional modes alter the B_{1g} spectrum, as shown in Figure 23.

Density waves instabilities need not necessarily compete with superconductivity but rather can provide an effective coupling mechanism (Castellani *et al.*, 1995; Perali *et al.*, 1996) as long as quantum and thermal fluctuations suppress long range order. Then, collective modes may appear as fluctuation-induced modes. The Raman scattering is usually determined from Aslamazov-Larkin fluctuation diagrams considered for the conductivity (Aslamazov and Larkin, 1968). To overcome the $\mathbf{q} = 0$ phase space limitations, the Raman response is given by the exchange of two fluctuations modes at wavevectors $\mathbf{Q}_c$ and $-\mathbf{Q}_c$, yielding generally a mode at energies of twice the mass of the fluctuation propagator. Once again the polarization dependence can select different fluctuation modes corresponding to different ordering wavevectors coupling to either charge or spin density modes. This was investigated for spin (Brenig and Monien, 1992) and charge (Caprara *et al.*, 2005) fluctuations in the normal state, and for novel spin resonances in the superconducting state of the cuprates (Chubukov *et al.*, 1999, 2006; Venturini *et al.*, 2000).

Lastly, we remark that many other types of collective modes are possible if one considers more exotic ground states with different symmetry classifications. For example, a chiral spin liquid has been investigated by Khveshchenko and Wiegmann (1994) in which helical excitations were conjectured to exist and are in principle measurable in A_{2g} orientations which can be projected out via proper sums of spectra taken with both linearly and circularly polarized light. Other examples are modes induced by magnetic fields or optical modes resulting from Dzyaloshinskii-Moriya interactions in Heisenberg antiferromagnets as observed recently in lightly doped $La_{2-x}Sr_xCuO_4$, $0 \leq x \leq 0.03$ (Gozar *et al.*, 2005b) and discussed by Silva Neto and Benfatto (2005), directly demonstrating the importance of spin coupling to the local environment.

III. FROM WEAKLY TO STRONGLY INTERACTING ELECTRONS

In this section we review experimental results in systems other than doped semiconductors (see reviews by, e.g., Abstreiter *et al.* (1984) and Pinczuk and Abstreiter (1989)) and cuprates (see section IV) with a view towards signatures in the Raman spectra arising from the development of strong electronic correlations. We discuss various types of superconductors and summarize results on correlated metals and other strongly interacting systems.

The light scattering cross section in absorbing media, such as systems with free carriers, is generally weak since the interaction volume is small for the short penetration
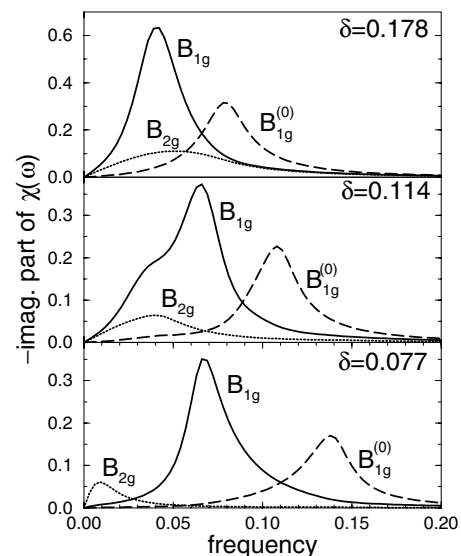

FIG. 23 Electronic Raman spectra of B symmetries for three different doping levels including coupling of d-CDW and d-superconducting amplitudes. The superscript 0 denotes the spectra in the absence of collective modes. From Zeyher and Greco (2002).

depth of visible light, $\delta \ll \lambda_i = 2\pi c/\omega_i$. As a consequence, the momentum perpendicular to the surface is not conserved, and the transfer $\mathbf{q}$ is not given any more by the difference of the vacuum momenta of the involved photons $\mathbf{k}_i - \mathbf{k}_s$ but essentially by $\delta = \lambda/(4\pi k)$ with k the imaginary part of the index of refraction (Abrikosov and Fal'kovskiĭ, 1961; Mills *et al.*, 1970). Even in strongly absorbing materials with $k > 1$, $1/\delta \ll \pi/a$ holds where a is the lattice constant, and the limit of small momentum transfer is still effective. This introduces a new energy scale $\hbar v_F q \approx \hbar v_F/\delta$ with v_F and q being the magnitudes of the Fermi velocity and the momentum transfer, respectively. In all considerations, this scale must be put into relation to the other relevant energies, such as the electron scattering rate $\Gamma = \hbar/\tau$ in the normal and the gap Δ in the superconducting state. These apparent academic considerations have major impact on both the observability and the interpretation of electronic spectra.

A. Elemental Metals and Semiconductors

In addition to the small scattering volume due to the absorption of light by free carriers, a parabolic dispersion and a spherical Fermi surface reduce the cross section of single-electron excitations in metals and degenerate semiconductors strongly, since in such systems the associated density fluctuations are screened by the long-range Coulomb interaction. The few spectra we are aware of have been taken on elements with a more complex band structure such as Nb (Klein, 1982a; Klein and Dierker, 1984) or Dy (Klein *et al.*, 1991). In Dy a broad continuum similar to that in the high-T_c cuprates (Bozovic *et al.*, 1987) is found. In Nb the superconducting state was studied. Due to the low transition temperature T_c, the correspondingly small energy gap $\Delta(T)$ and the small ratio δ/ξ with δ the penetration depth of the light and ξ the superconducting coherence length (for details see section III.B) the characteristic redistribution of scattering intensity is very hard to observe. The peaks found at 1.8 K in the expected energy range close to $2\Delta(T)$ are very weak, and no normal state spectra have been measured for comparison (Klein, 1982a; Klein and Dierker, 1984).

In fact, superconductors rather than normal metals were the main focus in the early days of electronic Raman scattering. Only after the discovery of the cuprates (Bednorz and Müller, 1986), with generally complicated and sometimes very surprising electronic properties, did studies of the normal state become increasingly attractive (see section IV).

B. Conventional Superconducting Compounds

Among superconductors, intermetallic compounds like Nb_3Sn or V_3Si with A15 structure, can be considered conventional both above and below T_c. They are strictly

3D, superconductivity is mediated by phonons leading to an essentially isotropic s-wave gap, and correlations are believed to be of minor importance. This does not mean they are simple. For instance, the Fermi velocity is very small, close to the velocity of sound, and the Fermi surface is multi-sheeted. Sufficiently perfect single crystals of Nb_3Sn and V_3Si undergo a structural transformation from a cubic to a tetragonal lattice at low temperature. Nevertheless, A15 compounds are paradigms of strong-coupling s-wave superconductors with a high density of electronic states at E_F. Materials like the borocarbides, MgB_2 or $2H-NbSe_2$ are certainly more complex and correlations or multiband aspects come into play.

1. A15 compounds

Superconductivity induced structures close to twice the gap edge were found in mono-crystalline Nb_3Sn (Fig. 24) and V_3Si (Dierker *et al.*, 1983; Hackl *et al.*, 1982, 1983; Klein, 1982a) two years after the discovery of gap modes in $2H-NbSe_2$ by Sooryakumar and Klein (1980) (section III.C) and after an early but unsuccessful attempt in polycrystalline Nb_3Sn by Fraas (1970). For $T < T_c$ the scattering intensity is redistributed
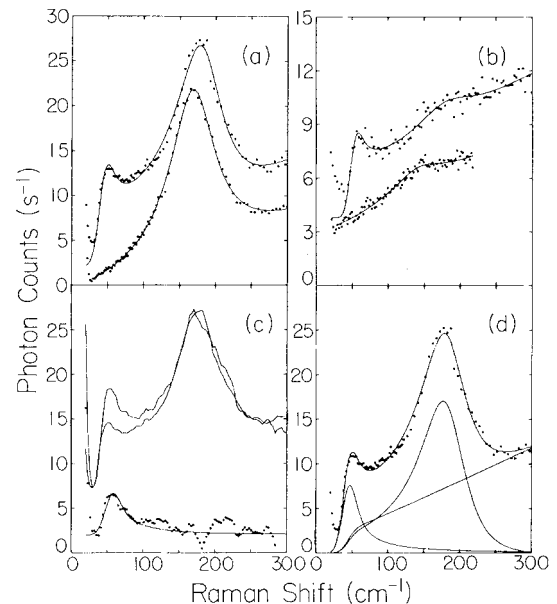

FIG. 24 Raman spectra of Nb_3Sn. Lower curves in (a) and (b) are at 40 K and upper curves are at 1.8 K. Data in (c) and (d) are at 1.8 K. Below $T_c = 18$ K the intensity at low energies is strongly suppressed with respect to the normal state. Beyond a threshold of approximately 50 cm^{-1} a new peak appears. The symmetries are E_g (a, d), T_{2g} (b), E_g+A_{1g} (c top), E_g (c middle), and A_{1g} (c bottom). The A_{1g} data in (c) are obtained by subtracting the middle from the upper curve. All solid lines except for the upper two in (c) are theoretical fits to a broadened Maki-Tsuneto function (see section II.D.6). From Dierker *et al.* (1983).

with a suppression below and a pile-up at approximately $2\Delta \simeq 50$ cm^{-1}. The well-defined peak in E_g symmetry follows the BCS prediction for the temperature dependence of the gap up to approximately $0.85\ T_c$ (Hackl *et al.*, 1983, 1989). Somewhat unexpectedly, the peak frequencies of the superconductivity-induced features depend on the selected symmetry (Table II). Independent of minor differences in the absolute numbers stemming from the data analysis the E_g peaks are significantly below those having A_{1g} and T_{2g} symmetries. At first glance one could think of a gap anisotropy to manifest itself. However, there is no support from the tunneling results which rather indicate the possible gap anisotropy to be opposite in V$_3$Si and Nb$_3$Sn and very large or from calorimetric studies which should track the smallest gap (Table II). In addition, the shapes of the Raman spectra are strongly symmetry dependent in that the E_g peak is much narrower than the others. The meaning of this anisotropy was a matter of intense discussion.

The results in A_{1g} scattering symmetry in Nb$_3$Sn (Dierker *et al.*, 1983; Klein, 1982a) and later in V$_3$Si (Hackl and Kaiser, 1988a) demonstrate clearly that the structures below T_c originate in light scattering from Cooper pairs (Fig. 24), since there exist no Raman active excitations at this symmetry, such as phonons or other bosonic modes in the A15 structure from which the electrons can borrow intensity. There is not even an electronic continuum above T_c (see Fig. 24 (c) and Hackl and Kaiser (1988a)). In spite of similar band structures and densities of states at the Fermi level, $N(E_F)$, (Klein *et al.*, 1978) the intensities of the modes are quite different in the two compounds as is the overall scattering cross section. For this reason, the weak A_{1g} mode in V$_3$Si escaped detection for a while (Hackl and Kaiser, 1988a). Since there is nothing to interact with the peak frequencies, the A_{1g} structures should be close to the energy gap in the respective material. One actually observes coincidence of both the A_{1g} and T_{2g} Raman energies with those of bulk methods such as calorimetry and neutrons, while the E_g energies are substantially lower (Table II).

We first note that surface sensitive methods such as tunneling return somewhat smaller gap energies than bulk methods. Optical spectroscopy results are also smaller most likely due to surface treatment. Strain or disorder can indeed reduce T_c in A15 materials since $N(E_F)$ decreases rapidly (Mattheiss and Weber, 1982). Similar reasons might apply for the Raman data in Nb$_3$Sn of Dierker *et al.* (1983) although the fits (see Figure 24) reveal gap values slightly below (5–10 %) the peak positions. Spectra of cleaved surfaces, such as those of V$_3$Si and Nb$_3$Sn taken by Hackl and Kaiser (1988a) and Hackl *et al.* (1989), respectively, apparently give gaps closer to the bulk values.

For these reasons, it seems worthwhile to look for other sources of the anisotropy, and we consider an interpretation in terms of final state interactions (Bardasis and Schrieffer, 1961; Klein and Dierker, 1984; Zawadowski *et al.*, 1972). This means that the two single electrons of

Sample	Raman Energy (cm^{-1})			Reference Data (cm^{-1})		
	A_{1g}	E_g	T_{2g}			
Nb$_3$Sn	52	41	50	a	50	tunneling	e
	67	48	70	b	35–13	tunneling	f
					53	tunneling	g
					62	calorimetric	h
					56	neutrons	i
V$_3$Si	-	40	-	c	37	tunneling	j
	55	42	52	d	40–50	tunneling	k
					46	IR	l
					41	IR	m
					49	calorimetric	h

TABLE II Gap energies in A15 compounds as measured by Raman scattering and other methods. a and c refer to results from fits (see Fig. 24 and section II.D.6), b and d are peak frequencies. In two cases an anisotropy was found by tunneling being indicated by a range (f and k). The first and the second numbers are for [100] and [111] directions, respectively. Results of the following publications are used: a (Dierker *et al.*, 1983), b (Hackl *et al.*, 1989), c (Klein and Dierker, 1984), d (Hackl and Kaiser, 1988a), e (Rudman and Beasley, 1984), f (Hoffstein and Cohen, 1969), g (Geerk *et al.*, 1984), h (Junod *et al.*, 1983), i (Axe and Shirane, 1973), j (Moore *et al.*, 1979), k (Morita *et al.*, 1984), l (Tanner and Sievers, 1973), m (Perkovitz *et al.*, 1976).

a broken Cooper pair can still interact in channels orthogonal to the pairing channel. The strongly coupled E_g phonon (Schicktanz *et al.*, 1980, 1982; Weber, 1984; Wipf *et al.*, 1978) is in fact orthogonal to the fully symmetric (s-wave) pairing channel. Hence, it is capable of forming a bound state below the pair-breaking threshold,
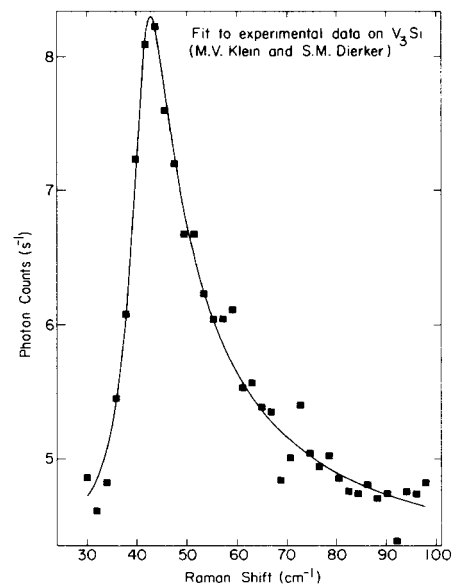

FIG. 25 Raman spectra in E_g symmetry of V$_3$Si. From Monien and Zawadowski (1990).

explaining both the reduced energy and the linewidth of the E_g gap mode (Monien and Zawadowski, 1990). Fits to the results in V_3Si are substantially improved by including the bound state (Fig. 25) in comparison to those neglecting it (Klein and Dierker, 1984). Additional experimental support comes from the evolution with temperature of the spectra in V_3Si and Nb_3Sn (Hackl *et al.*, 1983, 1989). In either compound, the integrated spectral weight in A_{1g} symmetry increases significantly because a new scattering channel opens up below T_c due to the formation of Cooper pairs while staying essentially constant in E_g symmetry because the weight is being transferred from the phonon to the bound state (Fig. 26).

In contrast to E_g symmetry, the pair-breaking features in T_{2g} symmetry are weak and essentially at the A_{1g} position. The question arises as to why there is no bound state although there exists a phonon. Clearly, the T_{2g} phonon intensity is weak and the line width is small, reflecting the moderate coupling as opposed to E_g symmetry where the complete line width and the asymmetric Fano shape stem from the coupling to conduction electrons (Weber, 1984; Wipf *et al.*, 1978). The bound state's energy split-off by approximately 30 % indicates that the very strong interaction drives the system close to an instability of the s-wave ground state. On the other hand, the T_{2g} mode is only weakly coupled and the interaction with the conduction electrons is not strong enough to substantially renormalize the spectrum.

Symmetry arguments, the unique line shape and the intensity transfer in E_g symmetry, as well as the comparison to calorimetric results, make us believe that the formation of a bound state is more likely an interpretation of the E_g results in A15 compounds than the manifestation of a gap anisotropy or a two-gap scenario. In contrast, both effects may cooperate in 2D MgB_2 discovered to be a superconductor just recently by Nagamatsu *et al.* (2001).

2. MgB_2 and the Borocarbides

Electronic Raman studies on MgB_2 have explored the superconducting energy gap and changes in phonon lineshapes occurring below T_c, starting with the work of Chen *et al.* (2001) and followed thereafter by Quilty *et al.* (2002, 2003). Here the symmetry dependence of the response allowed a direct observation of the pairing gap on the two-dimensional σ bands and the 3D π bands. By orienting the light polarizations along the c-axis of MgB_2 (perpendicular to the hexagonal planes) the σ bands cannot be probed for having little dispersion and thus the π bands are projected out, giving a value $2\Delta_\pi = 29$ cm^{-1}. Other polarizations are able to detect a larger pairing gap $2\Delta_\sigma = 100$ cm^{-1}. zz-polarized spectra in the superconducting state are shown in Figure 27 along with fits from the theory for disordered $s-$wave superconductors.

The gap values are consistent with those from other techniques, yet the fit yields values of the disorder-related scattering rate different from those of the resistivity by a factor of 2 (Quilty *et al.*, 2003). Zeyher (2003) has reanalyzed the fit where the direct coupling of light to the σ band is zero and the σ gap appears as a result of a coupling to the Raman active E_{2g} phonon, believed to be largely responsible for pairing. The xx spectrum in the superconducting state can be understood then as a superposition of a phonon line, a background, and a collective bound state due to residual interactions between electrons, similar to that observed in A15 compounds (see Figures 25 and 26 (a)).

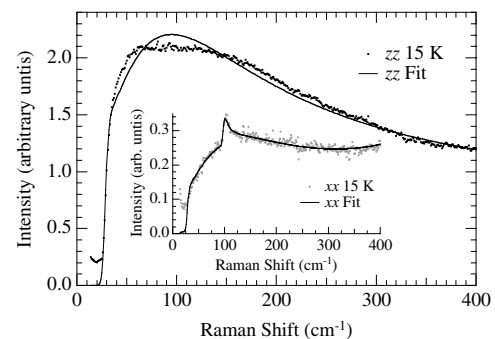The superconducting energy gap has also been stud-

FIG. 26 Raman spectra of Nb_3Sn at E_g (a) and A_{1g} (b) symmetries. The integrated spectral weight (limits indicated by arrows) stays constant to within 3 % in E_g symmetry while increasing by a factor of 3 in A_{1g} symmetry on cooling from T_c to 6 K. For clarity the data points are omitted and only the results of a smoothing procedure are displayed. The scatter of the data is smaller than 0.1 units around the lines. From Hackl *et al.* (1989), reproduced with permission from Elsevier, © 1989.

FIG. 27 Raman spectra for xx and zz polarization geometries in the superconducting state of MgB_2 taken by Quilty *et al.* (2003). The solid lines are fits to the data using the theory of Devereaux (1992) for disordered $s-$wave superconductors using a single gap and two gap model for zz and xx polarizations. The xx spectrum has also been interpreted in terms of a collective bound state by Zeyher (2003).

ied in some detail in the borocarbide superconductors $R\mathrm{Ni}_2\mathrm{B}_2C$ (R=Y, Lu) by Yang $et\ al.$ (2000a,b). Sharp 2Δ peaks were observed in A_{1g} and B_{2g} symmetries, while the maximum in B_{1g} symmetry is less pronounced and 20% higher in energy. All peaks showed a typical BCS-type temperature dependence and disappeared above the upper critical field H_{c2}. Due to the high surface quality and improved instrumentation, the residual scattering intensity below the gap edge is much smaller than, e.g., in the A15 compounds but finite with an approximately linear variation with energy.

Since a direct coupling to a Raman active mode was not found in the borocarbides, it is more complicated than in the A15 compounds or in MgB_2 to sort out whether a gap anisotropy, multi-gap superconductivity or collective modes are responsible for the variations in energy and line shape at the different symmetries. Of course, the existence of bound states is not related to Raman-active modes; only the experimental verification is more indirect, e.g., via the line shape (see Figure 25). Similarly, the linear low-energy scattering can suggest either the presence of strong inelastic scattering due to large coupling constants λ (Allen and Rainer, 1991; Yang $et\ al.$, 2000b) or gap nodes in pairing states with lower symmetry, such as $s+g$-wave superconductivity (Lee and Choi, 2002). A quantitative analysis on the basis of a realistic band structure could possibly help clarify these, at present, open issues.

While superconductivity was the dominant correlation in the A15 compounds, MgB_2 was more complex due to the interplay between 2D and 3D behavior. In the borocarbides magnetic order as a second instability competing with superconductivity comes into play (Canfield $et\ al.$, 1998). Although the Raman studies were performed on non-magnetic compounds (Yang $et\ al.$, 2000a,b) the vicinity of different types of order is characteristic for this and the following classes of systems.

C. Charge Density Wave Systems

The competition or coexistence of different ground states was studied intensively in layered dichalcogenides in the 1970s and 1980s. The interest in these charge density wave (CDW) systems was revived after the discovery of superconductivity in the cuprates for two reasons: in both compound classes superconductivity competes with one or more other instabilities, and, secondly, the dramatically improved instrumentation allowed qualitatively new and unexpected insights into materials like $2H-\mathrm{NbSe}_2$. As an example, the electronic scattering rate τ^{-1} exhibits marginal (Varma $et\ al.$, 1989a) rather than Fermi liquid like temperature and energy dependences (for a discussion and for references see, e.g., Castro Neto (2001)).

1. $2H-\mathrm{NbSe}_2$

$2H-\mathrm{NbSe}_2$ is a layered, though 3D, superconductor with an in-plane coherence length $\xi_{\parallel}$ of approximately 70 Å and $\xi_{\perp} = 25$ Å (de Trey $et\ al.$, 1973). The penetration depth for visible light δ is of the order of 200 Å, hence $\xi_{\perp} \ll \delta$. The discontinuity at 2Δ is expected to increase with $2\Delta/(\hbar v_F q) \approx \delta/\xi$ (Klein and Dierker, 1984). In addition, the material can be cleaved easily, facilitating the preparation of atomically flat surfaces from which diffuse scattering of laser light is minimized. These are favorable (though not easy!) conditions for observing gap structures close to the elastic line.

In Fig. 28, the first observation of the redistribution of scattering intensity in the superconducting state of $2H-\mathrm{NbSe}_2$ with the sample immersed in superfluid He is reproduced. The effect is measured for two samples with slightly different impurity concentrations. In either case, the fully symmetric A and the E responses are shown.[13] The peaks have slightly different energies, and are located at 18 and 15 cm^{-1}, respectively, close to the essentially $\mathbf{k}$ independent leading edge gaps found in recent photoemission experiments (Valla $et\ al.$, 2004). In the normal state at 9 K the new low energy modes are absent, while the maximum related to the CDW state is still present.
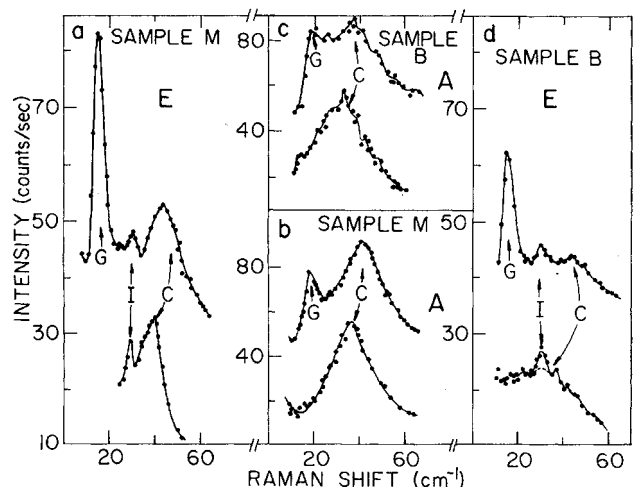

FIG. 28 Raman spectra of $2H-\mathrm{NbSe}_2$ above and below T_c. The lower curves of each panel are taken in the normal state (9 K) the upper ones at 2 K well below T_c with the sample immersed in superfluid He. At the A ($\parallel - \perp$) and the E ($\perp$) symmetry the superconducting spectra are offset by 40 and by 20 counts, respectively. According to the strength of the CDW mode (labeled by C) Sample B and M have slightly different impurity concentrations. From Sooryakumar and Klein (1980).

---

[13] In the (incommensurate) CDW phase the symmetry representations A_{1g} etc. of the D_{6h} point group do not apply any more.
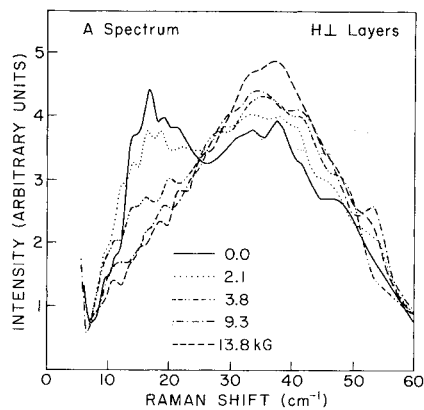
FIG. 29 Raman spectra in A symmetry of $2H-\text{NbSe}_2$ (sample B) in various magnetic fields at 2 K. From Sooryakumar and Klein (1980).

As can be seen in all panels, the CDW mode hardens below the superconducting transition.

The difference between the two samples is apparently the impurity concentration affecting the strength of both the CDW and the gap mode. In fact, the CDW transition can be suppressed by either pressure or an increasing number of defects, which may be quantified by the residual resistance ratio (Huntley and Frindt, 1974). In a systematic study of impurity effects, Sooryakumar et al. (1981) showed that the gap excitations go away along with the CDW mode while the superconducting transition temperature is essentially unchanged. It is tempting to assume that the gap modes are directly coupled to the CDW mode and exist only along with it. This interpretation is supported by results obtained in a magnetic field (Fig. 29). Upon increasing the field the gap feature in A symmetry is gradually suppressed while the CDW mode gains intensity leaving the energy integral over the Raman response $\chi''(\omega)$ constant to within 7% (Sooryakumar and Klein, 1981). In E symmetry no clear sum rule could be found (Sooryakumar and Klein, 1981), and it is possible that some of the gap intensity appears independent of the CDW.

Particularly the result in A symmetry (Fig. 29), where the gap mode gains intensity at the expense of the CDW mode, triggered the theoretical work to follow.[14] The available data are not supportive of a sum rule in E sym-

metry (see Fig. 28 a), demonstrating similarities with the A15 compounds where also both electronic scattering and coupling to phonons was observed. In order to bring some light into the rather involved discussion, it is worthwhile to reconsider the influence of impurities (Sooryakumar et al., 1981).

At first glance, the reaction to disorder points in the same direction as the results in magnetic fields. However, defects not only suppress the formation of the CDW (Huntley and Frindt, 1974) but also, independently, reduce the intensity close to 2Δ (Devereaux, 1992, 1993) while normally leaving the transition temperature T_c of a conventional s-wave superconductor unchanged (Anderson, 1959)[15]. For $\hbar v_F/\delta \ll \Delta$, $\hbar/\tau$ the intensity at 2Δ is proportional to $\tau\Delta$ (Devereaux, 1992, 1993). In this respect Raman is just opposite to the optical conductivity where the gap can be observed only if $\hbar/\tau$ is of the order of Δ or larger (Mattis and Bardeen, 1958). This implies that the Raman gap feature can be wiped out by impurities while T_c remains essentially constant; at the same time, though independently, the CDW transition is suppressed. Hence, it is possible that the gap features in $2H-\text{NbSe}_2$ exist on their own as pair-breaking effect but the interaction with the CDW leads to a bound state.

Most of the other CDW systems are not superconducting, but show very interesting behavior around the transition to the charge-ordered phase. Some of them have been studied earlier using light scattering. Here we briefly discuss a recent study of the temperature-pressure phase diagram of the CDW state.

2. $1T$-TiSe$_2$

In $1T$-TiSe$_2$ a commensurate CDW is established below $T_{\text{CDW}} \simeq 200$ K. The amplitude of the CDW couples to zone-boundary acoustic phonons which are folded to the center below T_{CDW} (Snow et al., 2003). Pronounced soft-mode behavior can be observed as a function of temperature. In the limit $T \to 0$ two strong lines at 115 and 75 cm^{-1} in A_{1g} and E_g symmetry, respectively, dominate the low-energy spectra. By increasing the pressure the CDW state first stiffens along with the lattice then disappears rapidly in the pressure range of 5 to 25 kbar. Above 25 kbar a quantum disordered (essentially isotropic) metallic or semi-metallic state is found although the Raman continuum typical for a metal is not reported. The quantum mechanical melting of the CDW order is in many ways similar to classical 2D melting, with the appearance of crystalline and disordered CDW regimes, as well as an intermediate "soft" CDW

---

[14] For convenience we again give the related references being discussed thoroughly in the context of collective modes and in the previous paragraph: (Balseiro and Falicov, 1980; Browne and Levin, 1983; Klein and Dierker, 1984; Lei et al., 1985; Littlewood and Varma, 1981, 1982; Monien and Zawadowski, 1990; Tüttő and Zawadowski, 1992). We would like to draw the readers's attention also to the closely related Raman experiments in superfluid ^{4}He (Greytak and Yan, 1969) and their theoretical description (Zawadowski et al., 1972).

[15] In A15 compounds the high density of electronic states at E_F (partially responsible for the high T_c) depends sensitively on disorder (Mattheiss and Weber, 1982). Hence, disorder reduces T_c fast as opposed to what one would expect from the Anderson theorem.

regime in which the CDW exhibits strong fluctuations and loses stiffness. Here, measurements on the development and polarization dependence of the electronic continuum raises the possibility of following quantum critical behavior in other systems with competing orders. This is a promising direction for future studies.

D. Kondo or Mixed-Valent Insulators

All correlations discussed so far are related to electron-lattice interactions in systems with screening lengths of the order of the interatomic spacing. With decreasing electronic density, new phenomena develop originating from the competition between kinetic and potential energy of the conduction electrons. Well known examples are the Mott metal-insulator transition or Wigner crystallization. In either case, the material becomes an insulator at low temperature due to "immobilization" of electrons rather than an energy gap as in band insulators.

Raman scattering on band insulators and semiconductors has been well-documented, with a focus placed on high energy charge transfer excitations. Yet the development of the Raman response at low frequencies can in principle shed light on the development of electronic correlations with temperature and/or doping.

Experiments by Nyhus et $al.$ (1995a) on Kondo insulating FeSi shown in Fig. 30 and Nyhus et $al.$ (1995b, 1997a) on mixed-valent SmB_6 have indeed shown the transfer of spectral weight from low to high energies as the temperature is lowered into the insulating state. This "universality" suggests that there is a common mechanism governing the electronic transport in correlated insulators. As these materials are cooled, they all show a pileup of spectral weight for moderate photon energy losses with a simultaneous reduction of the low-frequency spectral weight. This spectral weight transfer is slow at high temperatures and then rapidly increases as the temperature is lowered towards a putative quantum-critical point corresponding to a metal-insulator transition.

A characteristic energy appears which separates the region of intensity depletion from intensity enhancement with temperature. This characteristic frequency is essentially independent of temperature and is thus called an isosbestic point in the spectra (as shown in Figure 30). Finally, it is often observed that the range of frequency where the Raman response is reduced as T is lowered is an order of magnitude or more larger than the temperature at which the low-frequency spectral weight disappears. As discussed in the Section II.D.4 these findings are consistent with the loss of low-frequency scattering due to the thermal depletion of excited states. The channel-dependence has not yet been a focus of interest. If it were measured, important information concerning the evolution of the potential energy with doping could be inferred (Freericks et $al.$, 2005).
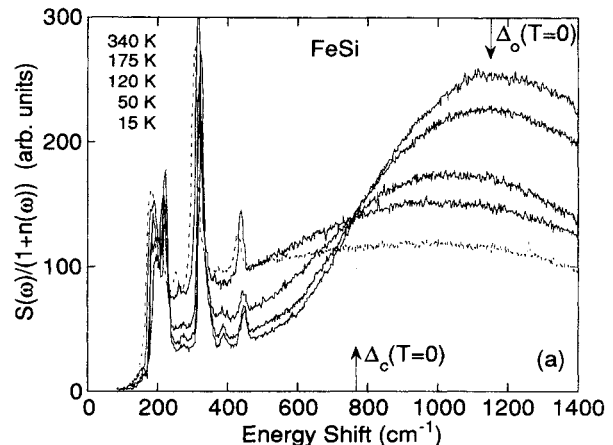

FIG. 30 Temperature dependence of the Raman response measured in FeSi by Nyhus et $al.$ (1995a). Here Δ_c denote the position of energy gap developing in the continuum at low temperatures, transferring spectral intensity into the peak at energy Δ_0 . The sharp low energy features are phonons.

E. Magnetic, charge and orbital ordering: Raman scattering in Eu-based compounds, Ruthenates, and the Manganites.

There has been a great deal of interest in the relationship between diverse and exotic low-temperature phases of strongly correlated systems (Dagotto, 2005). In particular, the manganites, ruthenates, Eu-oxides, and hexaborides display charge ordered, paramagnetic insulating, and ferromagnetic metallic phases as a function of doping, temperature, and/or temperature. Due to the complex interplay between spin, charge, and orbital degrees of freedom, these systems present a battleground where different ordered phases compete for primacy as knobs of the Hamiltonian are changed (Imada et $al.$, 1998).

The phase diagram of strongly correlated materials is more complex in systems having strong electron-lattice interactions as well as orbital ordering tendencies. Raman spectroscopy in systems such as the manganites and ruthenates have provided important information on the evolution of lattice, charge, and spin dynamics across phase boundaries. In many cases the transitions can be induced by applying pressure.

While Raman scattering from phonons has traditionally provided important information concerning the development of locally or globally symmetry-broken states accompanied by the formation of static charge ordering, electronic Raman spectroscopy can be brought to bear on this problem as it can detect both fluctuating or static charge and/or spin ordering, and may reflect on the tendency toward orbital ordering as well. In addition, the polarization dependence can shed light on the types of excitations that are created in or near the ordered phases which may serve as signatures that certain interactions are more prominent than others. Thus Raman is

a powerful spectroscopic method by which the dynamics across quantum phase transitions can be investigated in correlated systems.

Recent Raman studies on EuB_6 (Nyhus *et al.*, 1997b), $Eu_{1-x}La_xB_6$, EuO (Snow *et al.*, 2001), and $Eu_{1-x}Gd_xO$ (Rho *et al.*, 2002), show that the metal-semiconductor transition in these materials is accompanied by distinct changes of the electronic continuum. A high-temperature paramagnetic semimetallic phase is well characterized by scattering from diffusive charge excitations which become less diffusive at lower temperatures when correlation effects have not yet set in. However, the diffusive scattering rate, when fit with Eq. (49), increases with decreasing temperature and scales with the magnetic susceptibility as the system begins to develop short-range magnetic order, typical of insulating behavior, as shown in Figures 19 and 30. Finally, at low temperatures, a ferromagnetic metallic phase occurs, showing a flat continuum characteristic of a strongly correlated metal. The doping, polarization, and magnetic field dependence of the spectra implies that the metal-semiconductor transition is precipitated by the formation of bound magnetic polarons above the ferromagnetic ordering temperature.

Concerning the ruthenates, recently Snow *et al.* (2002) and Rho *et al.* (2003) have studied the evolution of the spin and lattice dynamics through the pressure-tuned collapse of the antiferromagnetic Mott-like phases of Ca_2RuO_4, $Ca_3Ru_2O_7$, and $Ca_{2-x}Sr_xRuO_4$ into a ferromagnetic and possibly orbitally ordered metallic state at low temperatures. The studies have shown many characteristic features resulting from the interplay of strong electron-lattice and electron-electron interactions. These include (i) evidence of an increase of the electron-phonon interaction strength, (ii) an increased temperature dependence of the two-magnon energy and linewidth in the antiferromagnetic insulating phase, (iii) evidence of a charge gap development significantly below the metal-insulator transition (T_{MI}), and (iv) a hysteresis associated with the structural phase change. The latter two effects are indicative of a first-order metal-insulator transition and a coexistence of metallic and insulating components for $T < T_{MI}$. The measurements have not yet been extended to probe the unconventional superconducting state at low temperatures.

Raman measurements on cubic and layered manganites have been used to explore the interplay of spin, charge and orbital degrees of freedom. Yamamoto *et al.* (2000) and Romero *et al.* (2001) observe a suppression of the low-energy continuum at B_{1g} symmetry upon entering the charge- and orbital-ordered state. The interpretation is not yet settled. Possible candidates are spin density or dynamical charge-orbital fluctuations (Yamamoto *et al.*, 2000) or a collective CDW excitation Romero *et al.* (2001). The controversy can probably not be solved without a quantitative theoretical description.

Björnsson *et al.* (2000) have measured cubic $La_{1-x}Sr_xMnO_3$ and via phonon lineshape analysis have shown strong electron-phonon interactions involving lo-

cal lattice distortions in the high temperature paramagnetic state which gradually vanish below the ferromagnetic transition. A broad hump in the electronic spectra develops at low temperatures in the metallic state around 400 cm^{-1} for x=0.2, and weakens in intensity and shifts to higher energies for x=0.5. Although a polaronic peak would weaken with increasing carrier density, the shift towards higher energies with doping was interpreted rather as a low-energy plasma excitations within the ferromagnetic metallic phase. Since recent ARPES studies on the same compound (Mannella *et al.*, 2004) and bi-layer manganite (Mannella *et al.*, 2005) have revealed coexistence of quasiparticle and polaron features in the metallic phase and do not show evidence for low energy plasma excitations, more work is needed to clarify this issue.

A comprehensive study via reflectance and Raman measurements on $Pr_{0.7}Pb_{0.21}Ca_{0.09}MnO_3$, $La_{0.64}Pb_{0.36}MnO_3$, $La_{0.66}Pb_{0.23}Ca_{0.11}MnO_3$, and $Pr_{0.63}Sr_{0.37}MnO_3$, by Yoon *et al.* (1998), have shown that the electronic continuum displays a change from diffusive polaronic peaks at high temperature to a flat featureless continuum, similar to that observed in the cuprates, in the low temperature ferromagnetic phase. A broad polaronic peak around 1200 cm^{-1} shifts to lower energies with increases doping indicative of weakened polaron binding energies. This is consistent with a crossover from a small-polaron-dominated regime at high temperatures to a large-polaron-dominated low-temperature regime. The low temperature phase also provided evidence for the coexistence of large and small polarons, also in agreement with the ARPES results.

Recent work on $Bi_{1-x}Ca_xMnO_3$ ($x < 0.5$) by Yoon *et al.* (2000) is of particular interest in connection with polarization studies for the evidence of charge ordering. As shown in Figure 31, Raman scattering offers a unique means of probing the unconventional spin and/or charge dynamics that arise when charge carriers are placed in the complex spin environment of a charge-ordered systems. Using circularly (LL) in addition to linearly (xx and yy) polarized light anti-symmetric components of the Raman tensor were isolated. In cubic crystals such as $Bi_{1-x}Ca_xMnO_3$ they transform as the T_{1g} irreducible representation (equivalent to A_{2g} in tetragonal materials like the cuprates). Upon entering the charge-ordered phase a quasielastic scattering response appears with the T_{1g} symmetry of the spin-chirality operator. Thus it was conjectured that the chiral excitations were signatures of either a chiral spin-liquid state associated with the Mn core spins, or of closed-loop charge motion caused by the constraining environment of the complex orbital and Néel textures. A possible path for charge motion is shown in Figure 31, emphasizing the circular nature of charge transfer. It is remarkable, that the spectral shape and the temperature variation of the characteristic energy are quite similar to the low-energy response in the cuprates (see section IV.D.3) although a state with static order is entered in $Bi_{1-x}Ca_xMnO_3$. It is interesting

and perhaps important how the two types of response are related.

Recently Saitoh *et al.* (2001) have performed Raman measurements on detwinned and orbitally ordered LaMnO$_3$ and have observed multiple peak structures which they interpret as orbital excitations or "orbitons". While this has been challenged by Grüninger *et al.* (2002) on the basis of selection rules, more recent measurements by Krüger *et al.* (2004) related the peak features to second order phonon scattering activated via the Franck-Condon mechanism (Perebeinos and Allen, 2001). Even

T*(n)

AF

T*(p)

SC

0
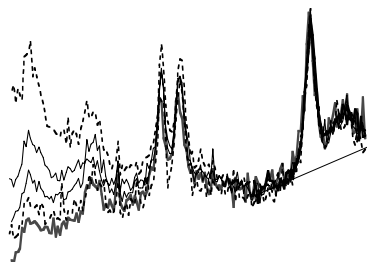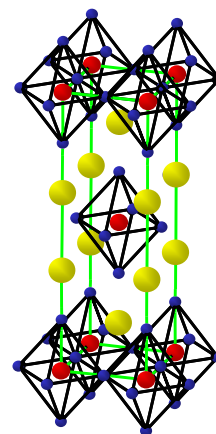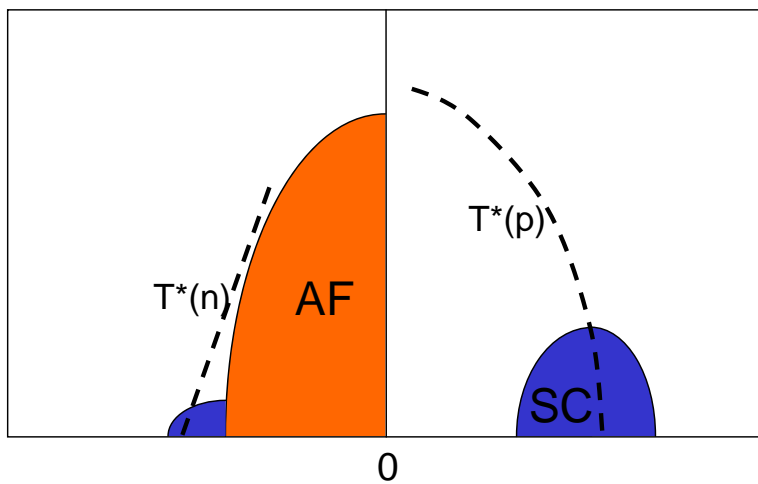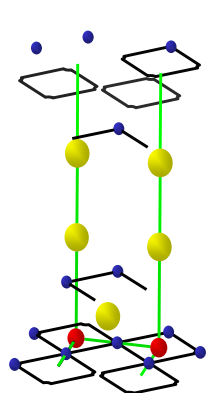
Slakey *et al.*, 1990b) visualized strong anisotropic interactions in these materials. Specifically, the observation of a polarization-dependent gap opening in the spectra below T_c was instrumental in solidifying the symmetry and orientation of the superconducting order parameter. Finally, more recent work has focused on elucidating the behavior of competing orders and complexity which come hand-in-hand with strong correlations.

It is safe to say that no other system has been studied so intensely via a bevy of experimental tools in recent years as the cuprates. This is certainly true for Raman spectroscopy, where the light scattering cross sections have been analyzed in a rich number and quality of materials. In this section, we discuss Raman results on the cuprates and related materials, with an overview of relating findings to the physics uncovered in other systems. We show issues in which consensus has been reached and other issues which are controversial and require further analysis.

A. From a Doped Mott Insulator to a Fermi Liquid

The so-called parent compounds of the cuprate superconductors are antiferromagnetic Mott insulators. At half filling, charges are completely localized and excited states are separated by the Coulomb energy U prohibiting double occupancy in the Hubbard model.[18] The ground state is a Heisenberg antiferromagnet which develops 3D long-range order below a Néel temperature of typically 300 K. The excitations are spin waves with a very small (in-plane) anisotropy gap at $\mathbf{q} = 0$ and a nearest-neighbor exchange coupling J. The spin waves have been studied right at the beginning by Raman scattering, and J was determined from the two-magnon peak to be of order 100 meV.[19] Very early the existence of chiral spin excitations, i.e. excitations where the spins are rotated out of the easy (CuO_2) plane, was demonstrated (Sulewski *et al.*, 1991). The resonance profile[20] has been described in terms of the triple resonance theory of Chubukov and Frenkel (1995a,b). Very recently, one magnon excitations at $\mathbf{q} = 0$ were observed in the Néel state of $La_{2-x}Sr_xCuO_4$ (Gozar *et al.*, 2004) and related to Dzyaloshinskii-Moriya and XY optical modes resulting from a spin gap by Silva Neto and Benfatto (2005). The experiments are the $\mathbf{q} = 0$ and $\hbar\Omega \to 0$ manifestation of canted spins which give also rise to scattering in the two-spin-flip channel at large energies in A_{2g} symmetry (Sulewski *et al.*, 1991). Here, a lot more information,

such as the Dzyaloshinskii-Moriya vector, the size of the anisotropy gap, and the spin-lattice interaction strength, could be derived (Gozar *et al.*, 2005b).

If the insulator is doped off half filling, antiferromagnetic long range order disappears quickly with hole doping but survives up to higher electron doping levels (Figure 32). Yet short ranged antiferromagnetic correlations are not quenched even at high doing levels, as seen by the persistence of the two-magnon peak in B_{1g} Raman scattering experiments on both the hole-doped (Blumberg *et al.*, 1994; Reznik *et al.*, 1993; Rübhausen *et al.*, 1999; Sugai *et al.*, 2003) and the electron-doped side (Onose *et al.*, 2004) of the phase diagram. This is summarized in Figure 33 for a number of compounds and shows how the two-magnon peak softens and broadens with doping, eventually merging into the continuum at higher doping levels. Since the two-magnon intensity is dominated by a double spin flip of nearest neighbors, it can be observed even for small magnetic correlation lengths ξ_m of the order of few lattice constants (see Figure 17). The two-magnon peak persists at least up to optimal doping for hole-doped systems (Fig. 33). The position of the maximum and the peak intensity decrease by factors of roughly 2 and 20, respectively, for $0 \leq p \leq 0.16$. Consistent with the Raman results, neutron scattering experiments in $La_{2-x}Sr_xCuO_4$ revealed magnetic excitations in the complete superconducting range (Wakimoto *et al.*, 2004).

The broadening of the two-magnon response with doping and temperature has been studied theoretically on clusters for the $t - J$ model (Prelovšek and Jaklič, 1998) and by quantum Monte Carlo (QMC) techniques (Sandvik *et al.*, 1998), respectively. Knoll *et al.* (1990) analyzed their experiments at elevated temperatures in terms of spin-lattice coupling. While many features of the data at 1/2 filling for undoped cuprates can be captured by studies of H_{ELF} Eq. (46), in general the evolution of the magnon lineshape with doping and temperature and its full polarization dependence is not very well understood. In particular, it is an unsettled issue, how, when a more metallic state develops for higher doping levels, the magnon line merges into the relatively featureless continuum (shown in Figures 33 and 34) that extends well-beyond all relevant energy scales such as $\hbar q v_F$, the superconducting energy gap Δ or the maximal phonon energy $\hbar\omega_D$. In strongly overdoped yet superconducting samples ($0.20 < p < 0.27$), the physical properties in the normal state are still not those of a conventional metal. The continuum itself displays significant polarization and doping dependence, which will be addressed in section IV.D.

For $p > 0.05$ ($n > 0.12$), superconductivity emerges and reaches a maximal T_c at approximately $p = 0.16$ ($n = 0.14$). In the Raman spectra, superconductivity induced peaks emerge out of the flat continuum in the normal state, accompanied by spectral weight reorganization for temperatures below T_c, as shown for $Bi_2Sr_2CaCu_2O_{8+\delta}$ in Figure 34.

---

[18] The subject has been reviewed in detailed articles and books (Fulde, 1995; Gebhard, 1997)

[19] (Blumberg *et al.*, 1996; Knoll *et al.*, 1990; Lyons *et al.*, 1988, 1989; Rübhausen *et al.*, 1997; Sugai *et al.*, 1988; Sulewski *et al.*, 1990, 1991)

[20] A selection of references is (Blumberg *et al.*, 1996; Knoll *et al.*, 1996; Lyons *et al.*, 1988; Rübhausen *et al.*, 1997).
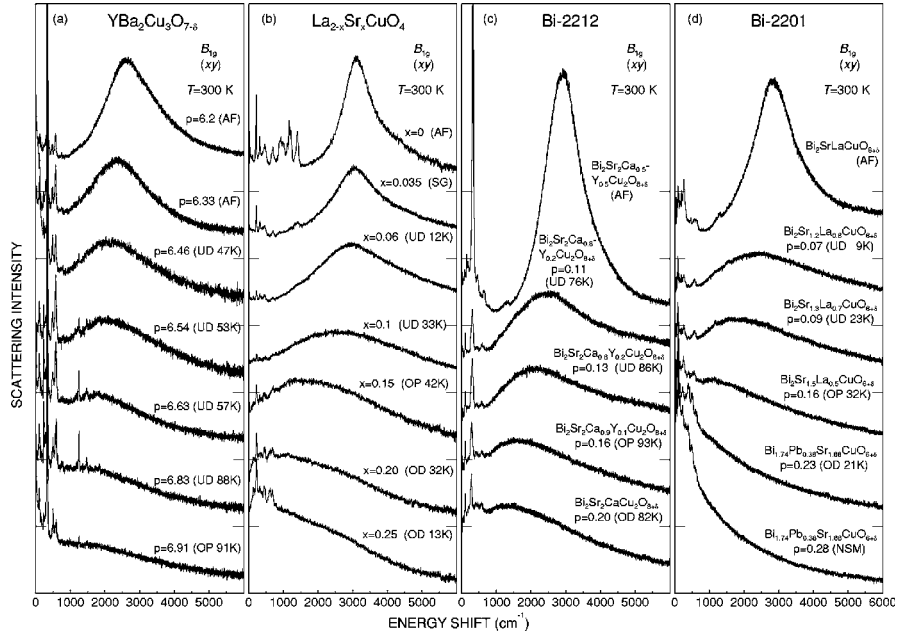
FIG. 33 Doping dependence of the two-magnon B_{1g} spectra in a number of compounds at 300 K. From Sugai *et al.* (2003).

In the following section we focus on the polarization dependence of the Raman response below T_c in both hole- and electron-doped cuprates. We summarize how symmetry arguments can be used to obtain the momentum dependence of electronic properties in general and, specifically, that of the energy gap $\Delta(\mathbf{k})$. The doping dependence in hole-doped systems is postponed and will be discussed in detail in section IV.C.

FIG. 34 Raman spectra in the normal state (a) and superconducting state (b) for $A_{1g} + B_{2g}$ (left panel) and B_{1g} ($+A_{2g}$) (right panel) orientations in $Bi_2Sr_2CaCu_2O_{8+\delta}$. From Yamanaka *et al.* (1988).

B. Superconducting Energy Gap and Symmetry

Early Raman results for the electronic continuum showed only little difference between the normal and the superconducting states (Lyons *et al.*, 1987). We know now that the relatively high defect concentration in the first samples suppressed the structures related to the gap. The synthesis of flux-grown $YBa_2Cu_3O_7$ with a sufficiently small number of defects (Kaiser *et al.*, 1987; Schneemeyer *et al.*, 1987) improved the situation rapidly, and a clear indication of the pair-breaking effect was obtained by Cooper *et al.* (1988a) on $YBa_2Cu_3O_7$, showing the emergence of a peak and reorganized spectral weight occurring for temperatures below T_c as expected from theory. Soon thereafter a strong polarization dependence of the Raman spectra was observed (Fig. 34), which can be considered the first spectroscopic evidence of a gap anisotropy (Cooper *et al.*, 1988b; Hackl *et al.*, 1988b; Slakey *et al.*, 1990a; Yamanaka *et al.*, 1988). In contrast to conventional materials (see, e.g., Fig. 24), there is no sharp onset of the scattering intensity at a threshold. As an explanation of the continuous increase of the scattering intensity at small frequencies the possibility of nodes was discussed early (Hackl *et al.*, 1988b; Monien and Zawadowski, 1989). Originally shown in $Bi_2Sr_2CaCu_2O_{8+\delta}$ and $YBa_2Cu_3O_7$, the studies were quickly extended to other optimally hole doped cuprates. It was shown by Kang *et al.* (1996, 1997) that magnetic fields suppress the peaks, independently indicating their relationship to superconductivity.
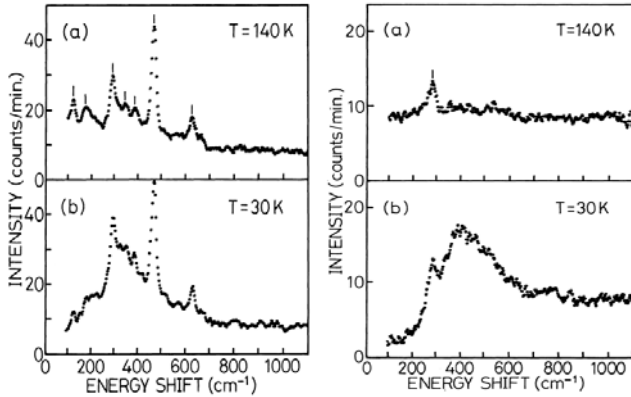
1. Symmetry: B_{1g} and B_{2g}

The polarization dependence of both the peak frequencies and the low-energy slopes of the superconducting spectra had been a vexing problem for several years following the first observation of the reorganized spectral weight and the polarization-dependent response. As shown in Figure 34, the peak in the B_{1g} response developed at roughly 30 percent higher energies than for B_{2g} or A_{1g} polarization geometries, and the low frequency spectra rose as Ω^3 for B_{1g} and linearly with Ω for other channels. In addition, the temperature dependent depletion at low frequency shifts was faster in B_{1g} symmetry than in other channels.

The satisfactory description emerged as soon as the momentum dependences of the Raman vertices of different symmetries μ, $\gamma_\mu(\mathbf{k})$, and of the energy gap $\Delta(\mathbf{k})$ were properly taken into account, as outlined in Section II.D.6. As indicated by a few experiments before (Hardy *et al.*, 1993; Shen *et al.*, 1993) and corroborated by many more later (Scalapino, 1995), a gap with $d_{x^2-y^2}$ symmetry is the most compatible with the results in the cuprates (Devereaux *et al.*, 1994a).

The predictions of $d-$wave theory - such as frequency power-laws, temperature dependences, and relative peak positions - were found to be consistent with many optimally hole-doped compounds, such as YBa$_2$Cu$_3$O$_7$ (Chen *et al.*, 1994a; Devereaux and Einzel, 1995a), Bi$_2$Sr$_2$CaCu$_2$O$_{8+\delta}$ (Blumberg *et al.*, 1997a; Devereaux *et al.*, 1994a; Devereaux and Einzel, 1995a), La$_{2-x}$Sr$_x$CuO$_4$ (Chen *et al.*, 1994b), Tl$_2$Ba$_2$CuO$_6$ (Blumberg *et al.*, 1997b; Devereaux and Einzel, 1995a; Kang *et al.*, 1996, 1997), Bi$_2$Sr$_2$CuO$_{6+\delta}$ (Einzel and Hackl, 1996), Tl$_2$Ba$_2$CaCu$_2$O$_8$ (Kang *et al.*, 1997; Maksimov *et al.*, 1990), Tl$_2$Ba$_2$Ca$_2$Cu$_3$O$_1$0 (Hoffmann *et al.*, 1994), and later HgBa$_2$Ca$_2$Cu$_3$O$_{8+\delta}$ (Sacuto *et al.*, 1998, 2000), Bi$_2$Sr$_2$Ca$_2$Cu$_3$O$_{10+\delta}$ (Limonov *et al.*, 2002a) and Hg.
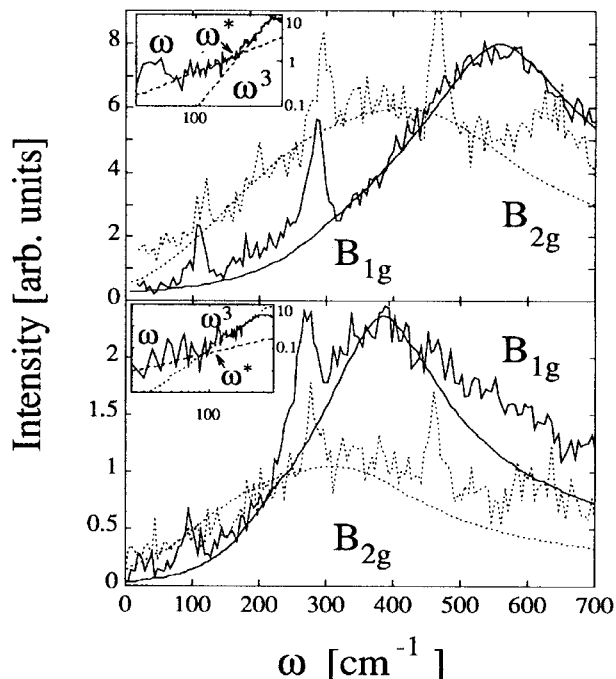

FIG. 35 Fit to the B_{1g} and B_{2g} data on as-grown (T$_c$=86 K, top panel) and oxygen-annealed (T$_c$=79 K, bottom panel) Bi$_2$Sr$_2$CaCu$_2$O$_{8+\delta}$ from Staufer *et al.* (1992). The inset is a log-log plot of the low frequency B_{1g} response, showing a cross-over from linear to cubic behavior at a characteristic frequency ω^*/Δ_0=0.38 and 0.45 for the top and bottom panels, respectively. From Devereaux (1995b).

Additional attributes have been intensely investigated, such as the agreement of the effective mass approximation calculated within LDA for $d-$wave superconductors in YBa$_2$Cu$_3$O$_7$ (Strohm and Cardona, 1997), effects of orthorhombicity and mixing of $s-$wave components allowed by symmetry (Nemetschek *et al.*, 1998; Strohm and Cardona, 1997), as well as the issue of the A_{1g} peak seen in the superconducting state (Krantz and Cardona, 1994), which is among the complicated though eventually crucial problems on the way to a better understanding of the cuprates.

2. The A_{1g} problem – Zn, Ni and Pressure

While the B_{1g} and the B_{2g} spectra are in reasonable agreement with the predictions on the basis of d-wave pairing various problems arose in A_{1g} symmetry which slowed down the acceptance of the model in the beginning. One of the objections was the strong intensity found in the A_{1g} channel. As discussed in Section II.D.6, the A_{1g} response is complicated due to the backflow terms which are as singular as the bare terms for frequencies at the gap edge, leading to cancellations of diverging intensities. For both a cylindrical Fermi surface and a tight-binding band structure (Devereaux *et al.*, 1994b; Krantz and Cardona, 1994), the effective mass approximation predicts a suppression of the A_{1g} intensity in comparison to other channels, in contrast to what is found experimentally, as shown in Figures 34 and 38. Since the effective mass approximation is of questionable utility in highly correlated systems like the cuprates, this objection was not as serious, as an overall comparison of spectral intensities is not possible without detailed knowledge of the Raman scattering matrix elements given in Eq. (36). Good fits to the data of the A_{1g}, B_{2g} and B_{1g} symmetries (with the overall intensities as free parameters) could be obtained (Devereaux and Einzel, 1995a). However, a sensitivity to band structure and higher harmonics of the energy gap and Raman vertices found in the calculations implied a similar sensitivity to details of the materials which was not observed in the data.

Further, it was argued by Krantz and Cardona (1994) that scattering in a multi-band system - such as in the CuO$_2$ bilayer - would yield a sharp intensity at twice the gap edge, which was again inconsistent with the data on single- and double-layer systems available at that time.

The issue of multiband scattering was partially resolved by Devereaux *et al.* (1996). It was found that if the energy gaps were equal on at least two sheets of the Fermi surface split by bi-layer hopping, a diverging intensity would be possible. However the intensity is only proportional to the difference of the individual Raman vertices of the bands. This is a qualitative reason why the multi-band case would give peaks only under quite special conditions, implying that the fits obtained from the single band case are still valid. Yet, it does not satisfactorily explain the sensitivity of the A_{1g} response to

band and energy gap anisotropy factors.

A recent undertaking to understand the origin of the A_{1g} intensity has involved the response of the peak to partial replacement (up to a few percent) of Cu by Zn and/or Ni in YBa$_2$Cu$_3$O$_{7-\delta}$ (Gallais *et al.*, 2002; Le Tacon *et al.*, 2005; Limonov *et al.*, 2002b; Martinho *et al.*, 2004). Martinho *et al.* (2004) found that the intensity of the A_{1g} peak was insensitive to either Ni or Zn doping, while the peak in B_{1g} is suppressed by Zn, in agreement with earlier results (Limonov *et al.*, 2002b). As shown in Figure 36, Gallais *et al.* (2002) found that the peak position in A_{1g} was reduced by Ni impurities and made the important observation that it followed that of the magnetic spin resonance mode (Sidis *et al.*, 2004). Le Tacon *et al.* (2005) found that Zn doping increased the low frequency spectral weight and suppressed the B_{1g} peak without changing its position. It is not clear why the position of the B_{1g} peak does not change while T_c decreases. Possible explanations are an inhomogeneous distribution of the impurities or an accidental cancellation effect between the decreasing $2\Delta(T_c)$ and an increase of the peak energy $\hbar\Omega_{\text{peak}}^{B_{1g}}$ because of defects (Devereaux, 1995b). The shift of the A_{1g} peak with Zn argued for a two-component picture including a contribution from a collective mode such as the π resonance in the spin wave spectrum (Hinkov *et al.*, 2004).

Two approaches concerning the presence of a collective mode in the spectra superimposed upon a well-screened background have been put forward recently by Venturini
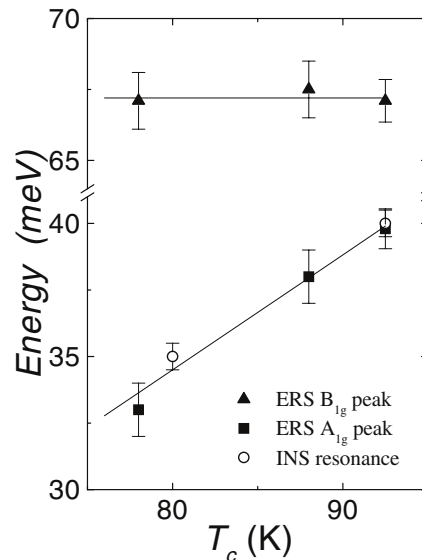

FIG. 36 Raman and neutron-resonance peak energies as a function of the critical temperature T_c in YBa$_2$(Cu$_{1-x}$Zn$_x$)$_3$O$_{6.95}$ for x = 0, 0.01, and 0.03. The horizontal line for the B_{1g} peak positions is just a guide to the eye, while the A_{1g} peak and the neutron resonance are fitted by a straight line representing $5k_BT_c$. From Gallais *et al.* (2002).

et al. (2000) and Zeyher and Greco (2002). Venturini *et al.* (2000) showed that a collective mode, uniquely appearing in A_{1g} and not other channels due to symmetry, emerges due to coupling to the 41 meV spin resonance mode seen in neutron scattering measurements in a number of compounds (Sidis *et al.*, 2004). Zeyher and Greco (2002) argued that the peak in the B_{1g} channel may be identified as a collective mode split off from 2Δ (Blumberg *et al.*, 1997a) as a consequence of the simultaneous presence of long-range d-CDW and d-superconducting order and that the A_{1g} peak may be related to a superconducting amplitude mode. In either case the sensitivity to parameters characterizing the anisotropies of energy gap, band structure, and Raman vertices were not present, yet it is still unclear which, if either, are able to explain the A_{1g} peak in the superconducting state.

Yet a remarkable set of experiments by Goncharov and Struzhkin (2003) plotted in Figure 37 highlights some
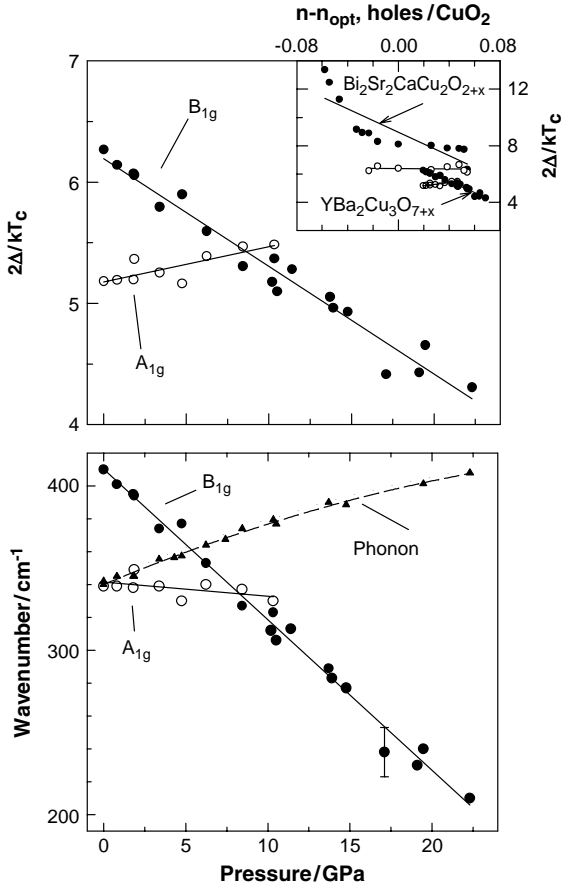
FIG. 37 Pressure dependences of the superconducting peaks in $YBa_2Cu_3O_{6.95}$ for B_{1g} (full circles) and A_{1g} (open circles) symmetries. The position of the B_{1g} phonon is also indicated (triangles). The inset shows a comparison to the Raman data on $Bi_2Sr_2CaCu_2O_{8+\delta}$ samples at ambient pressure with different doping levels (Kendziora and Rosenberg, 1995). From Goncharov and Struzhkin (2003). Reproduced with permission from Wiley © 2003.

shortcomings in the above mentioned scenarios. Upon pressure the peak in the B_{1g} channel and T_c move downward in a similar fashion as upon overdoping (discussed in detail in Section IV.C), and the B_{1g} phonon hardens as expected, while the peak position in A_{1g} remains remarkably constant. This implies that the B_{1g} peak is intimately tied to superconductivity and the A_{1g} peak has a substantial contribution from a channel which is relatively insensitive to pressure and changes in superconducting properties. In the discussions of possible candidates for the mode highlighted above, the pressure sensitivity of spin, charge, and superconducting order would all be expected to be large. Thus the origin of this peak remains presently unclear. One can speculate that it may be related to possible phonon modes involving mixed Bi-O and Ba-O which have been indicated to be less sensitive to pressure, but clearly further work is needed to clarify this matter (Goncharov and Struzhkin, 2003).

In multi-layer compounds with more than 2 adjacent CuO_2 planes, a strong A_{1g} peak in the superconducting state occurs at roughly the peak frequency of the B_{1g} channel, as shown in Figure 38 for $Bi_2Sr_2Ca_2Cu_3O_{10+\delta}$. In addition, strong phonon resonances were found here and for multilayer Hg compounds (Hadjiev *et al.*, 1998), where some A_{1g} c-axis phonons shift by as much as 20 cm^{-1} at the superconducting transition, more than in any other high T_c compound, implying a strong renormalization of the A_{1g} continuum below T_c.

Recently, Munzar and Cardona (2003) argued that a $c-$axis plasma mode would be expected to be Raman active in cuprate materials with more than 2 CuO_2 planes, giving rise to an additional contribution in the A_{1g} channel only due to mass fluctuations with opposite sign on different CuO_2 layers. The position of the plasma resonance was predicted to lie in a frequency range close to the continuum peak, as shown in Figure 38.

3. Resonance Effects

As another experimental knob to turn, resonance studies of the peaks developing in the superconducting state provide information on the character and the interactions of the quasiparticles forming the condensate. For this reason, studies of the gap feature as a function of the incoming photon energy were pursued. Effects in the energy range of the gap were observed in various compounds with one (Blumberg *et al.*, 2002; Kang *et al.*, 1996) more than one CuO_2 layer (Budelmann *et al.*, 2005; Hadjiev *et al.*, 1998; Limonov *et al.*, 2002a; Rübhausen *et al.*, 1999; Sacuto *et al.*, 1998). There are two distinct, though not necessarily independent, effects: (i) the spectral weight and the shape of some phonons of predominantly A_{1g} symmetry change more or less dramatically below T_c (Hadjiev *et al.*, 1998; Limonov *et al.*, 2002a), and (ii) the intensity of the electronic continuum is amplified in the vicinity of $2\Delta_{max}$ (Fig. 38) (Blumberg *et al.*, 2002; Limonov *et al.*, 2002a; Rübhausen *et al.*,
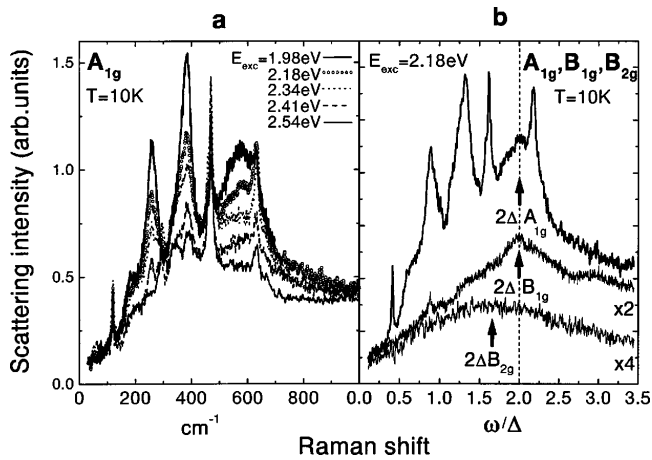
FIG. 38 Resonance enhancement of the of the A_{1g} Raman response in $Bi_2Sr_2Ca_2Cu_3O_{10+\delta}$ at 10 K. From Limonov *et al.* (2002a).

1999). The resonance effects typically occur for excitation energies of 2 ± 0.2 eV and are particularly strong in compounds with 3 or 4 CuO_2 layers (Limonov *et al.*, 2002a).[23] Importantly, the normal state is only weakly affected. Hence, although the resonance energy is close to the 1.6 eV absorption edge (Singley *et al.*, 2001; Uchida *et al.*, 1991), constraints are imposed on explanations in terms of interband transitions between the lower and the upper Hubbard band (c.f., Eq. (44) and Shastry and Shraiman (1990)), since the width of the resonance is much larger than $2\Delta_{max}$. At least in the triple-layer compounds, an additional channel can be opened up below T_c due to the c-axis plasma resonance (Munzar and Cardona, 2003) which may interact with low-energy phonons and renormalize their shape and intensity substantially. The existence of a resonating continuum in double-layer compounds is still a matter of debate. Some authors find the pair-breaking peaks to resonate (Blumberg *et al.*, 1997a; Budelmann *et al.*, 2005; Rübhausen *et al.*, 1999), while others do not (Limonov *et al.*, 2002a; Venturini *et al.*, 2002c).

Given this background, the strong resonance effects in electron-doped $Nd_{2-x}Ce_xCuO_4$ were a quite interesting and somewhat unexpected feature (Blumberg *et al.*, 2002). While the B_{2g} response in the superconducting state is strongly enhanced toward the red, neither the B_{1g} spectra below T_c nor the normal state spectra in general are particularly sensitive to the energy of the exciting light. An explanation in terms of Hubbard physics is certainly tempting but, for the symmetry and temperature dependence, not completely exhaustive. In our opinion, the subject needs further experimental and theo-

retical clarification before arriving at a level of predictive power.

After the observation of resonance effects in $Nd_{2-x}Ce_xCuO_4$ and along with an improved material quality the number of studies in electron-doped systems increased continuously and facilitated several interesting insights which will be summarized in the following paragraph.

4. Electron versus Hole-Doped Materials

Some cuprates such as $Nd_{2-x}Ce_xCuO_4$ crystallize in the T' structure which is characterized by missing oxygen octahedra (see Figure 32) and, as a consequence, a short c-axis (Tokura *et al.*, 1989). The maximal T_c of approximately 30 K is obtained in thin films of $La_{2-x}Ce_xCuO_4$ (Naito and Hepp, 2000). None of the electron-doped cuprates is completely ordered, and oxygen appearing in an apex position is the main defect (Radaelli *et al.*, 1994) even in superconducting samples.

Phonons (Heyen *et al.*, 1991) and crystal-field excita-
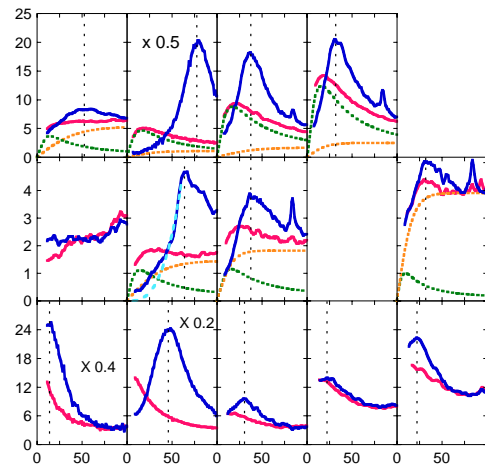
Ce CuO single crystals and thin films for B

B

power law is shown at   symmetry. From

[23] It is interesting to note that the resonance of the two-magnon peak is close to the charge transfer gap of 2.5 eV or higher (Blumberg *et al.*, 1997a; Knoll *et al.*, 1996; Rübhausen *et al.*, 1997).

tions (Jandl *et al.*, 1993) in $Nd_{2-x}Ce_xCuO_4$ were studied soon after the discovery (Tokura *et al.*, 1989) and explained thoroughly. An exception was the A_{1g} line at 590 cm^{-1}, assigned by Heyen *et al.* (1991) as a localized mode of interstitial oxygen in apex position (cf. Fig. 32). Later on, Onose *et al.* (1999) could indeed demonstrate that the mode is suppressed after annealing the samples in reducing atmosphere in order to induce or enhance T_c. The first electronic Raman spectra in the superconducting state of slightly overdoped $Nd_{1.84}Ce_{0.16}CuO_4$ showed a small gap anisotropy (Stadlober *et al.*, 1995). The ratio $4.1 \leq 2\Delta/k_BT_c \leq 4.9$ is similar to that of strong-coupling conventional superconductors like Pb, Nb or Nb_3Sn (see Table II). The temperature dependence of the gap is relatively close to the BCS prediction (Blumberg *et al.*, 2002; Stadlober *et al.*, 1995). This motivated an interpretation in terms of an anisotropic *s*-wave gap, yielding a reasonable description of both the shape and the positions of the B_{1g} and B_{2g} pair-breaking peaks (Stadlober *et al.*, 1995).

Similar spectral shapes were also found at other doping levels for both $Nd_{2-x}Ce_xCuO_4$ and $Pr_{2-x}Ce_xCuO_4$, as shown in Figure 39. The low-energy sides of the peaks were found to be almost doping independent and closer to those of hole-doped cuprates than to those in conventional superconductors when samples and instrumentation facilitated improved measurements close to $\Omega = 0$.

Recent ARPES (Armitage *et al.*, 2001; Matsui *et al.*, 2005) and interferometric experiments (Chesca *et al.*, 2003; Tsuei and Kirtley, 2000) provided evidence of a *d*-type gap bringing antiferromagnetic spin fluctuations back into play as a possible coupling mechanism. Since the diameter of the Fermi surface encircling (π, π) is smaller here than in hole-doped systems, the antiferromagnetic ordering vector $\mathbf{Q}_{AF} = (\pi, \pi)$ connects spots close to $(\pi/2, \pi/2)$ rather than in the vicinity of $(\pi, 0)$ for *p* doping and the gap is expected to have a maximum at the hot spots and to decrease towards $(\pi, 0)$.

On this basis Blumberg *et al.* (2002) proposed a novel type of non-monotonic *d*-wave gap with maxima only approximately 15° away from the diagonal. An explicit calculation using the suggested $\Delta(\mathbf{k})$ (Blumberg *et al.*, 2002) in a one-band model approximately reproduces the overall line shapes but reveals discrepancies in the peak positions (Venturini *et al.*, 2003) (see also Blumberg *et al.* (2003)). Better agreement between experiment and theory can be obtained with a monotonic $d-$wave gap in a two band picture (Liu *et al.*, 2005) for which evidence has been found by magnetotransport (Fournier *et al.*, 1997).

Four remarks are to be considered: (i) In ARPES, the gap maximum is found approximately at the hot spot where a pseudogap is observed above T_c (Matsui *et al.*, 2005). (ii) No quasiparticle peaks indicating coherence in the superconducting state are resolved in ARPES (Armitage *et al.*, 2001; Matsui *et al.*, 2005). (iii) Twice the gap energy observed by ARPES is $\sim 40\%$ smaller than that derived from the Raman spectra (Matsui *et al.*, 2005). (iv) Phase-sensitive experiments (Alff *et al.*, 1999)

and results on the magnetic penetration depth (Kokales *et al.*, 2000; Skinta *et al.*, 2002a) are supportive of an *s*-type gap.

Hence in spite of mounting evidence of *d*-wave pairing, explanations for the symmetry dependence of the Raman spectra and several other experiments are still missing. A possible explanation could lie in a crossover from *d* to *s* pairing upon increasing doping (Skinta *et al.*, 2002b). However, Raman data from differently doped $Pr_{2-x}Ce_xCuO_4$ (see Figure 39) do not show a variation of the lineshape and sufficiently strong symmetry dependence of the pair-breaking features in the proper doping range (Qazilbash *et al.*, 2005).

In the hole-doped systems, on the other hand, strong variations of the lineshapes at A_{1g} and B_{1g} symmetry are found although there is little doubt about the persistence of the (dominant) *d*-wave nature of the superconducting gap in the entire phase diagram (Tsuei and Kirtley, 2000). The doping and polarization dependence of the Raman spectra in superconducting *p*-type cuprates will be the subject of the next section.

C. Superconducting Gap: Doping Dependence

One of the early Raman experiments on doping effects in overdoped $Bi_2Sr_2CaCu_2O_{8+\delta}$ showed the energy of the pair-breaking peak in B_{1g} symmetry to decrease much faster than those at the other symmetries and T_c (Staufer *et al.*, 1992). The first systematic study was performed by Kendziora and Rosenberg (1995) on $Bi_2Sr_2CaCu_2O_{8+\delta}$, shown in the inset of Figure 37. The doping level in this material can be varied continuously and reliably between $0.15 \leq p \leq 0.23$ by changing the oxygen concentration (Kendziora *et al.*, 1993; Triscone *et al.*, 1991). At lower oxygen doping, the structure is possibly metastable or unstable, at higher doping the oxygen diffuses out even at room temperature. Underdoping is better achieved by replacing Ca with Y. As an essential result, the pair-breaking peaks at A_{1g}, B_{1g}, and B_{2g} symmetry are found to depend in different ways on doping and, consequently, on T_c. This doping dependence is shown in Figure 40 for recent measurements on $Bi_2Sr_2Ca_{1-x}Y_xCu_2O_{8+\delta}$ by Sugai *et al.* (2003). Most remarkably, the B_{1g} pair-breaking peak is proportional to $(1-p)$ rather than T_c in the doping range indicated, but fades in intensity for underdoped materials. The peak energies in B_{2g} symmetry however scale more or less with the transition temperature. For $p < 0.15$ the B_{1g} peak becomes very weak, yet a clear 2Δ peak survives in the B_{2g} channel for all doping levels.

In the decade to follow there were numerous studies on differently doped cuprates, including $Bi_2Sr_2CaCu_2O_{8+\delta}$,[24] $YBa_2Cu_3O_{6+x}$,[25]

---

[24] (Blumberg *et al.*, 1997a; Budelmann *et al.*, 2005; Hackl *et al.*,

La$_{2-x}$Sr$_x$CuO$_4$,[26] HgBa$_2$CuO$_4$,[27] HgBa$_2$Ca$_2$Cu$_3$O$_8$,[28] Tl$_2$Ba$_2$CuO$_6$,[29] Tl$_2$Ba$_2$CaCu$_2$O$_8$,[30] and Tl$_2$Ba$_2$Ca$_2$Cu$_3$O$_{10}$ [31]. A compilation of experimental results is shown in Fig. 41. The scatter of the data points partially reflects the development of the sample quality. However, there are also discrepancies between the results which are related to the interpretation of the experiments.
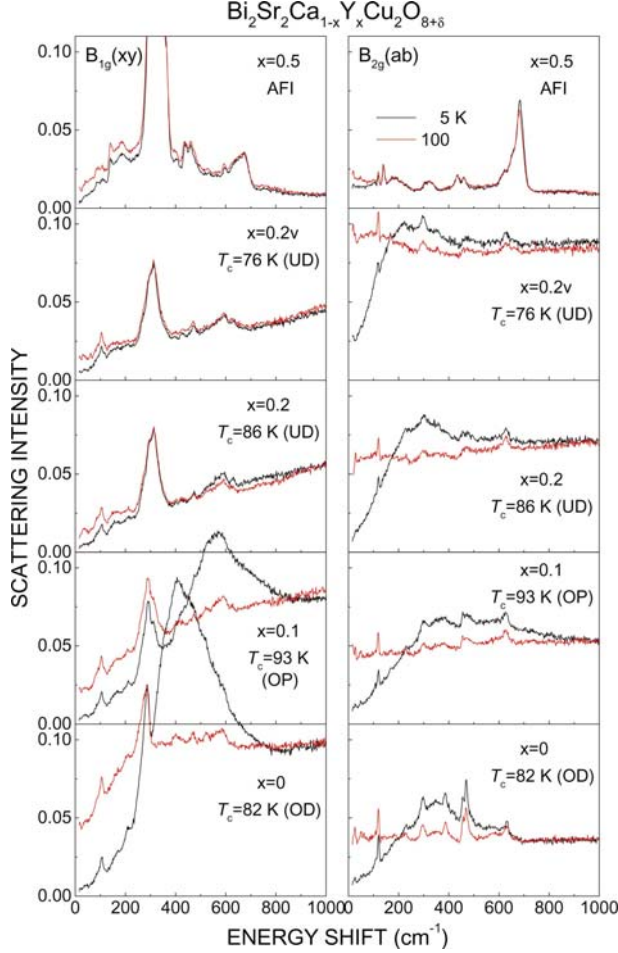

FIG. 40 Doping dependence of the B_{1g} and B_{2g} Raman spectra in Bi-2212 at 5 K and 100 K. From Sugai *et al.* (2003).

We first summarize the generally accepted features close to and above optimal doping:

- at $p \simeq 0.16$ the peaks in the three Raman active symmetries are in relative positions expected for d wave pairing, the ratio $2\Delta_{\mathrm{max}}/k_B T_c$ is approximately 8,[32]

- in the overdoped range, $p > 0.16$, the B_{1g} peak frequency decreases faster than T_c obeying $\Omega_{\mathrm{peak}}^{B_{1g}}/T_c^{\mathrm{max}} \approx 46(0.28 - p)$ (with $\Omega_{\mathrm{peak}}^{B_{1g}}$ and T_c^{max} in cm^{-1} and K, respectively),[33]
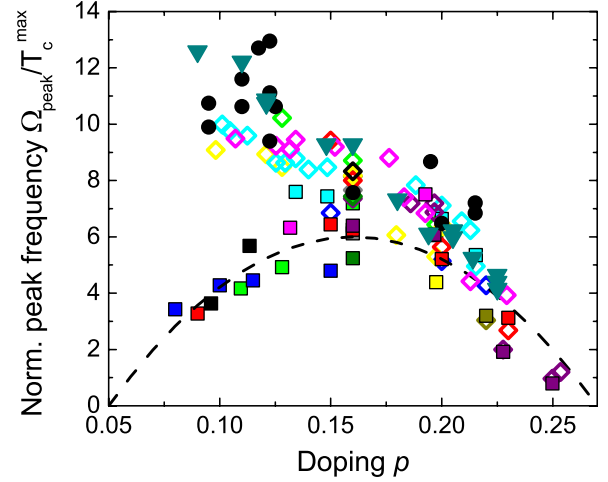

FIG. 41 Compilation of the position Ω_{peak} of the peak in the Raman response in the superconducting state normalized to T_c^{max}. B_{1g} (open diamonds) and B_{2g} (squares) orientations are shown for a variety of compounds. The respective references are color coded as follows: Bi-2212 [red (Venturini *et al.*, 2002c), green (Sugai and Hosokawa, 2000; Sugai *et al.*, 2003), cyan (Kendziora and Rosenberg, 1995), yellow (Blumberg *et al.*, 1997a; Liu *et al.*, 1999), pink (Hewitt and Irwin, 2002), and gold (Masui *et al.*, 2003)], LSCO [blue (Sugai *et al.*, 2003)], Bi-2223 [grey (Masui *et al.*, 2003)], Tl-2201 [purple (Gasparov *et al.*, 1997, 1998; Kang *et al.*, 1997; Nemetschek *et al.*, 1993)], Tl-2223 [olive (Hoffmann *et al.*, 1994; Stadlober *et al.*, 1994)], and Hg-1201 [black (Gallais *et al.*, 2005)]. The dashed black line is the interpolation formula $6T_c/T_c^{\mathrm{max}} = 6[1 - 82.6(p - 0.16)^2]$. For comparison, results for twice the maximal leading edge gap of ARPES (circles) (Campuzano *et al.*, 2002) and for the peak-to-peak energy in the tunneling density of states (triangles) (Zasadzinski *et al.*, 2002) are included.

1996; Hewitt and Irwin, 2002; Liu *et al.*, 1999; Opel *et al.*, 2000; Rübhausen *et al.*, 1999; Sugai and Hosokawa, 2000; Sugai *et al.*, 2003; Venturini *et al.*, 2003)

[25] (Altendorf *et al.*, 1992; Chen *et al.*, 1993; Cooper *et al.*, 1988b; Limonov *et al.*, 1998, 2000; Masui *et al.*, 2005; Nemetschek *et al.*, 1997; Opel *et al.*, 2000; Reznik *et al.*, 1993; Sugai *et al.*, 2003)

[26] (Chen *et al.*, 1994b; Naeini *et al.*, 1999; Venturini *et al.*, 2002a)

[27] (Gallais *et al.*, 2005; Le Tacon *et al.*, 2005)

[28] (Sacuto *et al.*, 1998, 2000)

[29] (Blumberg *et al.*, 1997b; Gasparov *et al.*, 1997; Kang *et al.*, 1996; Nemetschek *et al.*, 1993)

[30] (Kang *et al.*, 1997)

[31] (Gasparov *et al.*, 1997; Stadlober *et al.*, 1995)

[32] (Chen *et al.*, 1994b; Cooper *et al.*, 1988b; Devereaux *et al.*, 1994a; Gasparov *et al.*, 1997; Hackl *et al.*, 1988b; Yamanaka *et al.*, 1988)

[33] (Blumberg *et al.*, 1997a; Kendziora and Rosenberg, 1995; Masui *et al.*, 2003; Naeini *et al.*, 1999; Sugai *et al.*, 2003; Venturini *et al.*, 2002c)

- whenever the B_{2g} peak can be observed its maximum follows T_c, $\Omega_{\text{peak}}^{B_{2g}} \propto T_c$,[34]

- the A_{1g} peak frequency follows either the magnetic (π, π) mode[35] or, in the case of resonantly enhanced light scattering, $\Omega_{\text{peak}}^{B_{1g}}$.[36]

The gap close to the node, which is projected out in B_{2g} symmetry, is also found by penetration depth, low bias STM, and the Nernst effect to more or less follow the transition temperature for all doping levels (Deutscher, 1999, 2005; Panagopoulos and Xiang, 1998; Xu *et al.*, 2000). However it is inconsistent with peak-to-peak measurements of tunneling density of states(Zasadzinski *et al.*, 2002), the energy of the $(\pi, 0)$ peak in the spectral function(Campuzano *et al.*, 2002), and thermal conductivity (Sutherland *et al.*, 2005), which when interpreted in terms of $d-$wave quasiparticle picture (Durst and Lee, 2000) indicate that the gap energy continues to increase with decreased doping. This highlights one of the major issues in the cuprates of whether the superconducting pairing energy rises with underdoping or follows T_c, and this certainly requires further study.

In many experiments, a second energy scale is observed which varies approximately as $p_0 - p$, similar to $\Omega_{\text{peak}}^{B_{1g}}$. The majority of authors (Timusk and Statt, 1999) call it a pseudogap Δ^* opening below the crossover temperature T^* (see Fig. 32) with $\Delta^* \propto T^*$. The understanding of the pseudogap is a matter of intense research at present. A possible relation to the B_{1g} Raman data will be discussed below in section IV.C.

In the underdoped range, the interpretation is more controversial. The main issues are whether or not the B_{2g} pair-breaking peak can be observed at all doping levels and how the B_{1g} spectra evolve for $p < 0.16$.

The B_{2g} problem seems to converge with the improvement of the sample quality. The cleaner the samples, the clearer the B_{2g} pair-breaking peak, as expected theoretically (Devereaux, 1995b). The problem can be visualized in $YBa_2Cu_3O_{6+x}$ where oxygen tends to cluster and to form pinning centers if the Cu-O chains are not completely filled (Erb *et al.*, 1996b). However, in addition to fully oxygenated $YBa_2Cu_3O_7$, partially ordered phases exist for $x = 0.5$ with $T_c \simeq 60$ K and $x = 0.353$ with $T_c \to 0$ (Liang *et al.*, 2000, 2002) where every second and third chain is filled, respectively. Therefore, the maxima are pronounced in $YBa_2Cu_3O_{6.50}$ and $YBa_2Cu_3O_{6.98}$ (Opel *et al.*, 2000), while the peak is smeared out at optimal doping, $YBa_2Cu_3O_{6.93}$, and practically disappears slightly below (Sugai *et al.*, 2003). The problem of oxygen clustering exists also in $Bi_2Sr_2CaCu_2O_{8+\delta}$, but the

resulting potentials are weaker and essentially doping independent, as can be seen directly from the comparison of different overdoped samples (Opel *et al.*, 2000; Venturini *et al.*, 2002c) exhibiting nearly constant intensity of the B_{2g} pair-breaking features. In a similar fashion, partial replacement of Ca by Y does not create a strong impurity potential either. This was directly shown by electron spin resonance (ESR) (Jánossy *et al.*, 2003) in $YBa_2Cu_3O_{6.1}$, where Ca in place of Y is a very weak impurity which does not localize carriers even at low temperature and doping. We conclude that Y and O doping can be used more or less simultaneously in $Bi_2Sr_2CaCu_2O_{8+\delta}$ as long as Y is distributed statistically. The direct comparison of the data presented in Fig. 40 with those of Opel *et al.* (2000) and Venturini *et al.* (2002c) indeed shows that the B_{2g} pair-breaking peaks have doping and dopant (O, Y) independent intensities if a high sample quality can be maintained. Under these conditions, the B_{2g} maxima seem to exist at all doping levels and apparently scale with T_c. Since in $YBa_2Cu_3O_{6+x}$ and $La_{2-x}Sr_xCuO_4$ doping changes both carrier concentration p and mean free path ℓ, the pair breaking peaks appear and disappear depending on the doping-dependent order.

It is important to remember these considerations for the analysis of the B_{1g} data. This is particularly important when intensity issues are discussed. Therefore, we focus first on Y-under- and O-overdoped $Bi_2Sr_2CaCu_2O_{8+\delta}$ (Fig. 40) to determine the intensity evolution of the B_{1g} pair-breaking structure. It becomes very weak right below optimal doping while no significant weakening of the B_{2g} structures is observed. The gradual suppression of the B_{1g} coherence peaks in Raman goes along with the disappearance of the 2Δ peaks in scanning tunneling microscopy (McElroy *et al.*, 2003). This is corroborated by results in partially ordered $YBa_2Cu_3O_{6.5}$, in $La_{1.9}Sr_{0.10}CuO_4$, $HgBa_2CuO_4$, and $HgBa_2Ca_2Cu_3O_8$, where the B_{2g} structures are well resolved, while in B_{1g} symmetry, no pair-breaking effect could be found (Gallais *et al.*, 2005; Naeini *et al.*, 1999; Opel *et al.*, 2000; Venturini *et al.*, 2002b).

When the peak is observed in B_{1g} in the underdoped region, as shown in Figure 41, its position does not track T_c and lies within the scatter of points or slightly below the values of 2Δ generally obtained via ARPES (Campuzano *et al.*, 2002) and peak-to-peak positions in tunneling measurements (Zasadzinski *et al.*, 2002).[37] It has been argued by Chubukov *et al.* (1999, 2006) and Zeyher and Greco (2002) that the B_{1g} peak in Raman measurements in underdoped compounds may be due to a collective mode appearing below T_c from either spin-coupling

---

[34] (Gallais *et al.*, 2005; Kendziora and Rosenberg, 1995; Misochko *et al.*, 1999; Opel *et al.*, 2000; Venturini *et al.*, 2002b,c)
[35] (Gallais *et al.*, 2002; Le Tacon *et al.*, 2005)
[36] (Limonov *et al.*, 2002a)

[37] We point out however that there is considerable uncertainty in determining the gap from ARPES, as both the leading edge and the peak of the spectrum have been used. In either case, the antinodal spectral function is very broad in underdoped systems and identifying an energy scale from a broad feature is not without uncertainty.

or $d-$CDW order, respectively, split off from twice the gap maximum 2Δ. Yet this interpretation is inconsistent with the doping behavior of the pairing gap determined from B_{2g} symmetry, as discussed above. In addition, the findings of the doping behavior of the anti-nodal quasiparticles in the normal state (listed below in Section IV.C) indicate that anti-nodal quasiparticles have become incoherent already above optimal doping. Therefore it is not intuitively obvious how a propagating mode could emerge deep in a region of incoherence. An alternative scenario is that the peak observed in B_{1g} channels is strongly altered by incoherence and is a measure of the binding energy of localized anti-nodal electrons, such as via the formation of resonance-valence bond singlets or small polarons. Yet why a peak should appear remains to be understood. In any case, this issue highlights another vexing problem in the cuprates: how involved are the anti-nodal electrons in superconductivity for underdoped systems.

There were reports about B_{1g} pair-breaking peaks at low doping $p \leq 0.1$ (Blumberg et al., 1997a; Slakey et al., 1990b) appearing already above T_c, at a doping independent position of approximately 600 cm^{-1}. In the discussion of the existence of preformed pairs in the pseudogap state above T_c and of collective modes inside the gap (see Section II.D.7) that are indicative of the pairing potential, this result has obviously some importance. However, in the vast majority of the experiments, the observation could not be confirmed. Further complication comes from the existence of an oxygen impurity mode in close vicinity (Hewitt et al., 1999; Quilty et al., 1998). Future studies have to clarify this issue.

In conclusion, Raman scattering experiments reveal two energy scales in the superconducting state which have a different dependence on doping: while the peaks in B_{2g} symmetry follow the transition temperature, the maximum energy of those in B_{1g} symmetry decreases as $(p_0 - p)$. In the majority of the experiments, the coherence peaks in B_{1g} symmetry are found to fade away rapidly for $p < 0.16$. The origin of the features observed at small doping remains controversial.

D. Normal State: Dichotomy of Nodal and Anti-Nodal Electrons

The studies of the symmetry and doping dependence of the Raman spectra in the superconducting state are suggestive of interactions with a pronounced structure in momentum space which, in addition, vary with doping (see, e.g., Fig. 41). One of the key questions is therefore how the interactions renormalize the quasiparticles and their response functions in the normal state.[38] Owing to the

crystal structure of the cuprates, the anisotropy of the in-plane to the out-of-plane transport translates into a momentum dependence of the in-plane transport properties (Devereaux, 2003b; Forró, 1993; Turlakov and Leggett, 2001). Hence, Raman scattering can substantially supplement optical conductivity measurements above T_c. An anisotropy of the normal-state Raman spectra was actually observed soon after the gap anisotropy.[39]

1. Unconventional Metal-Insulator Transition

The momentum dependence of the transport as measured by Raman scattering is indeed dramatic. Generally, the nodal region along the diagonal of the Brillouin zone (B_{2g} symmetry) remain essentially unchanged at all doping levels, while the $(\pi,0)$ regions (B_{1g} symmetry) suffer an overall loss of oscillator strength by approximately an order of magnitude if the doping level is reduced from 0.22 to 0.10 (Fig. 42). When this doping dependence was first observed, Katsufuji et al. (1994) realized that the variation of the B_{1g} spectra with p cannot be explained by only changing the filling of a rigid band where the ratio of the B_{1g} to the B_{2g} scattering intensi-
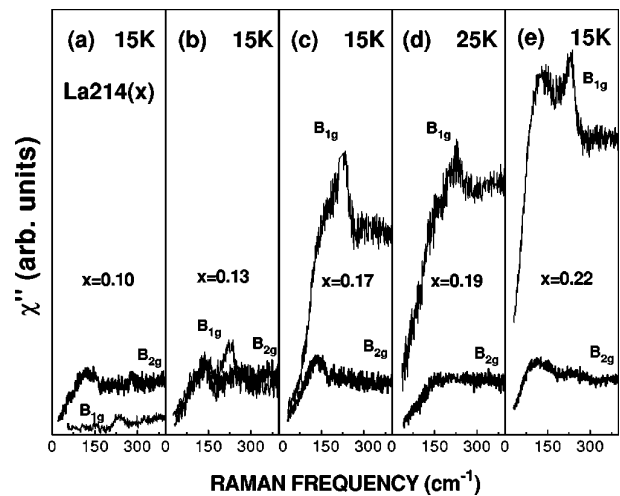

FIG. 42 Direct comparison of the low-energy B_{1g} and B_{2g} Raman response functions measured at temperatures indicated (all below T_c) in La$_{2-x}$Sr$_x$CuO$_4$ for different values of Sr doping. The scale is the same for all frames. From Naeini et al. (1999).

---

by Timusk and Statt (1999), Loram and Tallon (2001) and Basov and Timusk (2005). A thorough study of the dc and Hall transport properties in various compounds performed on high-quality samples of the last generation was presented recently by Ando et al. (2004)

[39] (Blumberg et al., 1999; Hackl et al., 1996; Katsufuji et al., 1994; Naeini et al., 1999; Opel et al., 2000; Reznik et al., 1993; Slakey et al., 1991; Staufer et al., 1990; Yamanaka et al., 1996)

[38] The properties of the normal state have been studied and reviewed extensively in the last two decades. Recent reviews are

ties is essentially determined by $(t/t')^2$ with t and t' the nearest and next-nearest neighbor hopping matrix elements, respectively (Einzel and Hackl, 1996). Changing the ratio (t/t') enough to account for the observed Raman intensities leads to unrealistic band structures. The suggested importance of correlation effects on the Raman intensities was pointed out early on.

The intensity changes of the B_{1g} spectra as a function of doping (Fig. 42) are accompanied by a qualitative change of the temperature dependence at a given doping level. For $Bi_2Sr_2CaCu_2O_{8+\delta}$, the effect is shown in the range $0.15 \leq p \leq 0.23$ (Fig. 43). For B_{2g} symmetry, there is little change of both the overall intensity and the initial slope which depends on temperature as expected for a metal. As opposed to B_{2g} symmetry, the temperature dependence of the B_{1g} spectra reverses sign (Fig. 43 (a)), indicating non-metallic behavior at $p = 0.15$. As outlined above (Eq. (55)), the initial slope of the response function is proportional to a transport lifetime τ or, equivalently, a conductivity. Accordingly, the inverse of it, $[\partial \chi''_\mu / \partial \Omega]^{-1}$ is a resistivity which, for the Raman selection rules, is momentum sensitive as indicated by the index μ.

It has been shown by Opel et $al.$ (2000) that both the energy dependences and the magnitudes of $\Gamma_\mu(\Omega, T) = \hbar/\tau_\mu(\Omega, T)$ and $m^*_\mu(\Omega, T)/m_b = 1 + \lambda_\mu(\Omega, T)$ can be determined from the spectra using a memory function analysis (Götze and Wölfle, 1972) in combination with an energy integral over χ''_μ / Ω ("sum rule"). By extrapolating the results to $\Omega = 0$, very reliable numbers for $\Gamma(\Omega \to 0, T)$ can be obtained.[40]

In Fig. 44, the "Raman resistivities" $\Gamma_\mu(\Omega, T)$ in the limit $\Omega = 0$ are plotted for $\mu = B_{1g}, B_{2g}$ at various temperatures and doping levels. The B_{2g} results compare well to conventional resistivities $\rho(T)$ using the Drude expression $\Gamma_\mu(\Omega = 0, T) = \varepsilon_0(\tilde\omega_{pl})^2 \rho(T)$ with the renormalized plasma frequency $\tilde\omega_{pl}$. With the plasma frequency in eV and the resistivity in $\mu\Omega$cm, one finds $\Gamma_\mu(T) \simeq 1.08(\tilde E_{pl})^2 \rho(T)$. At $p = 0.23$, the transport is essentially isotropic. Below $p = 0.22$, anisotropy develops quite abruptly, and for $p < 0.16$, the temperature dependence of the $\Gamma_{B_{1g}}(\Omega = 0, T)$ becomes non-metallic. This crossover behavior has been interpreted in

---

[40] The memory function or extended Drude analysis is particularly useful for a single-component response. Further details and limitations are discussed in the appendix of reference (Opel et $al.$, 2000). In Raman scattering the integral is as crucial as the plasma frequency in IR spectroscopy if magnitudes and energy dependences are to be derived in a similar way as in the analysis of the reflectivity (Basov and Timusk, 2005). "Sum rule" might be somewhat misleading and should be used with care since the integral over $\chi''_\mu(\Omega)/\Omega \propto \sigma'(\Omega)$ (see Eq. (6)) is not a conserved quantity like the number of carriers in the famous f-sum rule. Without the integral the energy dependence of one of the quantities must be dropped and/or a fit to model functions for $\Gamma_\mu(\Omega)$ and $1 + \lambda_\mu(\Omega)$ is required (Blumberg et $al.$, 1999; Hackl et $al.$, 1996; Naeini et $al.$, 1999; Slakey et $al.$, 1991; Yamanaka et $al.$, 1996).

terms of an unconventional metal-insulator transition at $0.20 < p < 0.22$, where the antinodal transport is gradually quenched while the nodal one remains essentially unaffected (Venturini et $al.$, 2002a).

Since the current vertex has a similar $\mathbf{k}$ dependence as the B_{2g} Raman vertex, IR spectroscopy and, similarly, dc transport project out mainly the nodal part of the Fermi surface (Devereaux, 2003b), and show therefore good qualitative agreement with the B_{2g} Raman results, which exhibit little variation with doping for $0.1 < p < 0.23$ beyond the change of $\tilde\omega_{pl}$, as shown in Figure 44. The suppression of the antinodal transport goes along with a reduction of the quasiparticle strength $Z_\mathbf{k}$ in the vicinity of $(\pi, 0)$ (Kim et $al.$, 2003), and a collapse of the Korringa law $(T_1 T)^{-1} = $ const as observed by NMR, where T_1 is the spin-lattice relaxation time (Alloul et $al.$, 1989; Billinge et $al.$, 2003).

Below $p \simeq 0.16$, insulating behavior can also be observed in conventional transport at low temperature if superconductivity is suppressed with high magnetic fields (Ando et $al.$, 2004a; Boebinger et $al.$, 1996). The logarithmic divergence of the resistivity in the limit $T \to 0$ indicates localization of the carriers. The crossover from metallic to non-metallic behavior occurs at temperatures $T < T_c$, well below those found in B_{1g} Raman scattering. This is consistent with the observation that the B_{2g} spectra do not show any anomaly in the normal state. The synopsis of NMR, conventional, and Raman transport leads to the quite consistent conclusion that carriers get gradually localized upon decreasing doping. According to the Raman results, the suppression of free-carrier transport starts at $p \simeq 0.21$ at the anti-nodal regions of the Fermi surface and gradually moves towards the nodal points with decreasing p. The conductivity apparently disappears only very close to or at zero doping, making connection to recent ARPES results which show quasiparticles along the nodal direction even at the lowest (yet finite) doping level (Yoshida et $al.$, 2003).

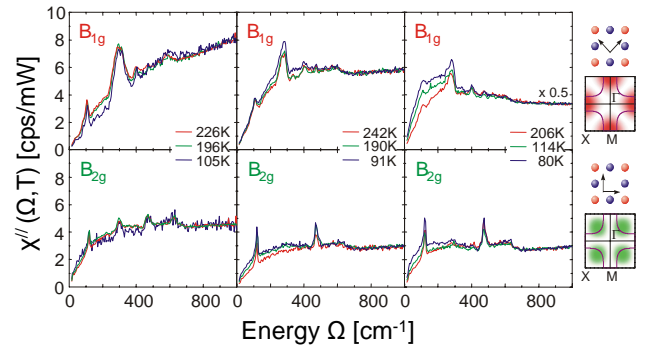Although there are no studies of both the doping and

FIG. 43 Direct comparison of the low-energy B_{1g} and B_{2g} Raman response functions measured at temperatures indicated (all above T_c) in $Bi_2Sr_2CaCu_2O_{8+\delta}$ for different doping levels $p = 0.15$, 0.20, and 0.22 (from left to right). From Venturini et $al.$ (2002a).

anen and Gunnarsson, 1989), charge ordering such as stripes or density waves (Andergassen *et al.*, 2001; Castellani *et al.*, 1995; Chakravarty *et al.*, 2001; Kivelson *et al.*, 2003) and Fermi surface deformation fluctuations (Metzner *et al.*, 2003). In all cases, static order is found only, if at all, at very low doping and/or in specifically modified structures such as $La_{2-y-x}Re_ySr_xCuO_4$ for $y \simeq 0.4$ and $Re = Nd, Eu$ (Klauss *et al.*, 2000; Tranquada *et al.*, 1995) or the nickelates. In $La_{1.775}Sr_{0.225}NiO_4$ (Pashkevich *et al.*, 2000) and $La_{1.67}Sr_{0.33}NiO_4$ (Blumberg *et al.*, 1998; Yamamoto *et al.*, 1998) the formation of static distortions due to the formation of stripes are big enough to split phonon and magnon lines due to zone doubling and to suppress the B_{1g} continuum at low energies.

Of course, static order is much easier to verify than fluctuating order. Nevertheless, fluctuating incommensurate spin order has been observed in $La_{2-x}Sr_xCuO_4$ for $x \geq 0.055$ (Fujita *et al.*, 2002), $YBa_2Cu_3O_{6.85}$, and $YBa_2Cu_3O_{6.6}$ (Hinkov *et al.*, 2004), while commensurate spin order is seen at low energies in $YBa_2Cu_3O_{6.353}$ (Stock *et al.*, 2006). This means that in a temperature dependent volume characterized by a coherence length $\xi_s(T)$ a superstructure of the antiferromagnetically ordered spins is established for higher doping levels. At the same time the charges which are expelled from the antiferromagnetic regions becoming spatially organized as well. This type of order has similarity with a liquid crystal and is sometimes referred to as nematic (Kivelson *et al.*, 1998, 2003). From these experiments it cannot be decided whether the fluctuating magnetic superstructure is a property of the spins or of the charges. For statically ordered $La_{2-y-x}Nd_ySr_xCuO_4$ with doping $x = 1/8$, Tranquada *et al.* (1995) showed that charge ordering precedes spin ordering when the temperature is reduced. It has indeed been shown that charge ordering fluctuations are quite common phenomena in correlated systems (Castellani *et al.*, 1995; Metzner *et al.*, 2003).

As long as there is no long range or static order which competes with superconductivity, the fluctuations can establish Cooper pairing (Chakravarty *et al.*, 2001; Perali *et al.*, 1996). For this reason, the understanding of the dynamics of incipient charge and spin order is a very interesting subject in the cuprates.

3. Role of Fluctuations and Incipient Ordering Phenomena at small doping

The study of dynamical order requires inelastic probes typically sensitive at finite **q**. In the case of charge ordering, resonant X-ray scattering is the most promising as it can provide direct evidence for the charge ordering at a particular wavevector (Abbamonte *et al.*, 2004), while neutrons can be used only if the charges modulate the lattice or the spin structure. While optical methods are confined to $\mathbf{q} = 0$ two excitations with opposite momenta can be created, such as multi-phonon or two magnon scattering. Therefore light can be scattered

from Cooper pairs or if an electron-hole pair couples to two excitations. It depends on the individual context how fluctuation phenomena are best studied.

In the copper-oxygen systems, an unexpected additional component in the B_{1g} spectra was observed in $La_{1.90}Sr_{0.10}CuO_4$: as shown in Figure 46, a peak is found in the $100~cm^{-1}$ range which gains intensity and moves to very low but finite energy with decreasing temperature (Tassini *et al.*, 2005; Venturini *et al.*, 2002b).[42] At high energy for all temperatures, and at high temperature for all energies, the spectra of the cuprates with $p \simeq 0.10$ in general are similar and show a strong anisotropy between nodal and anti-nodal regions in the Brillouin zone (see Fig. 42, 43, and 44). At low temperature the low energy feature is unique to $La_{1.90}Sr_{0.10}CuO_4$, while the spectra become flatter in $YBa_2Cu_3O_{6.5}$ and $Bi_2Sr_2(Y_{0.38}Ca_{0.62})Cu_2O_{8+\delta}$ (see Fig. 43). To appreciate the differences, one has to recall that the conventional transport properties of all these compounds are very similar (Ando *et al.*, 2004). Before we discuss possible inter-
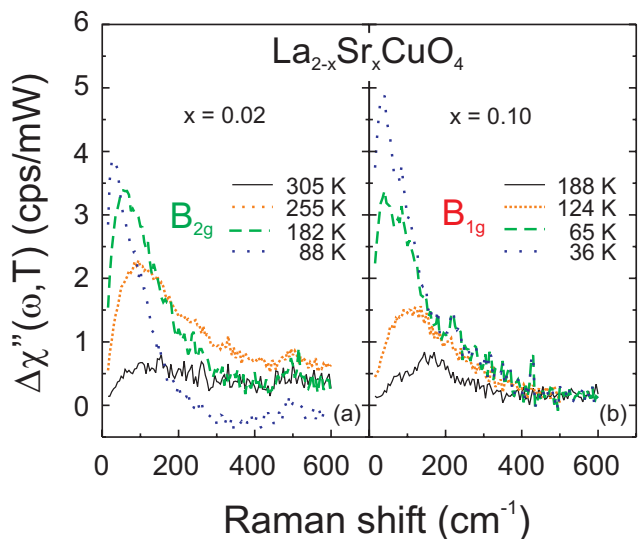

FIG. 46 Low energy response of underdoped $La_{2-x}Sr_xCuO_4$. A Drude-like peak (Zawadowski and Cardona, 1990) with a characteristic energy $\Omega_c(x,T)$ is revealed after subtraction of the 2D response of the CuO_2 planes. At $x = 0.02$ (a) and 0.10 (b) the additional response is observed in B_{2g} and B_{1g} symmetry, respectively. The styles of the lines (colours) do *not* correspond to similar temperatures but rather highlight the *scaling* of the response with temperature: similar spectra are obtained if the temperatures differ by approximately a factor of 2. From Tassini *et al.* (2005).

---

[42] We note that the the lines observed recently by Gozar *et al.* (2004) in $La_{2-x}Sr_xCuO_4$ ($x = 0, 0.01$) have nothing in common with the response discussed here and were clearly identified as one-magnon excitations (see also Silva Neto and Benfatto (2005)).

pretations we wish to compare results for different doping levels and materials.

From the comparison of the low energy peak to infrared results, a relationship to fluctuating stripe order was conjectured (Venturini *et al.*, 2002b). For further support, it seems worthwhile to exploit the selection rules Raman scattering offers. The effect in B_{1g} symmetry is indeed compatible with the orientation of stripes along the Cu–O bonds at $p = x = 0.10$ (Fujita *et al.*, 2002). This is simply because order along the principal axes of an essentially tetragonal lattice corresponds to an orthorhombic distortion. Fluctuations correspond to micro-twinning, meaning that x and y cannot be accessed individually. Hence, B_{1g} symmetry measuring only the difference $xx - yy$ (on a microscopic scale) projects out exactly this distortion. As a familiar example, we recall that fully oxygenated $YBa_2Cu_3O_7$ has Cu–O chains along the crystallographic b axis making $b > a$. Even if the sample is twinned, the chain contributions are always superimposed on the B_{1g} spectra, while the xx and yy spectra are equal (as opposed to a single-domain crystal). For $x < 0.055$, a reorientation by 45° is observed by neutron scattering (Fujita *et al.*, 2002). Since B_{1g} and B_{2g} are equivalent modulo a $\pi/4$ rotation in the basal plane of a tetragonal lattice, the related peak should now appear in B_{2g} rather than in B_{1g} symmetry. In fact, this has be observed in $La_{1.98}Sr_{0.02}CuO_4$, as shown in Figure 46 (Tassini *et al.*, 2005).

Spectra similar to those in $La_{1.98}Sr_{0.02}CuO_4$ (Fig. 46) are found in $(Y_{0.97}Ca_{0.03})Ba_2Cu_3O_{6.1}$ with $p \simeq 0.02$ (Fig. 47 (b)). Owing to the homogeneity of the sample, the peak is very narrow and well defined. As the low energy peak emerges, the intensity of the continuum is suppressed by roughly 30 % over an energy range of approximately 550 cm^{-1} in a similar though much stronger way than at higher doping (Nemetschek *et al.*, 1997; Opel *et al.*, 2000). In B_{1g} symmetry, there is an overall loss of spectral weight up to much higher energies, similar to $YBa_2Cu_3O_{6+x}$ and $Bi_2Sr_2CaCu_2O_{8+\delta}$ at higher dopings, demonstrating the transition to a correlated insulator (Freericks and Devereaux, 2001).

Simultaneously with the studies in $La_{1.90}Sr_{0.10}CuO_4$, the quasi 1D ladder compound $Sr_{14-x}Ca_xCu_{24}O_{41}$ was investigated (Blumberg *et al.*, 2002; Gozar *et al.*, 2003) which is considered a model system for the high-T_c cuprates (Dagotto and Rice, 1996; Dagotto, 1999; Sigrist *et al.*, 1994). At temperatures above approximately 450 K low energy spectral peaks similar to those in
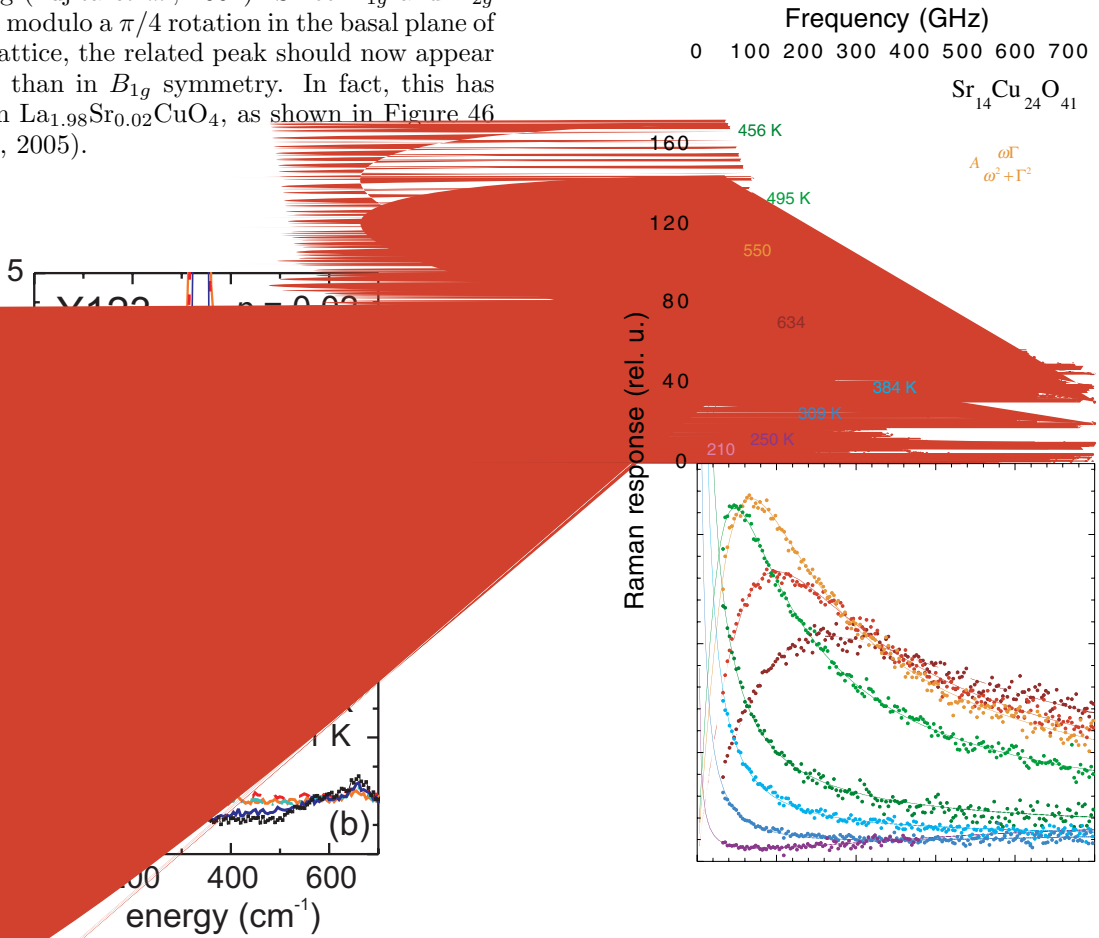
Raman response $\chi''_\mu(\omega, T)$ of $(Y_{0.97}Ca_{0.03})Ba_2Cu_3O_{6.1}$ in B_{1g} (a) and B_{2g} (b) symmetry. The doping level is close to $p = 0.02$. From Hackl *et al.* (2005).

$La_{1.90}Sr_{0.10}CuO_4$ are found (Fig. 48), although their energies and widths are an order of magnitude smaller. The width obeys an Arrhenius law with a doping independent activation energy Δ of approximately 2100 K. In the insulator ($x = 0$), the conductivity (for $T < 300$ K) reveals a similar Δ while for $x = 12$ the conductivity is metallic above 70 K (Gozar *et al.*, 2003; Gozar and Blumberg, 2005a). The position of the maximum and the width decrease upon cooling. In both cases, for $T < 450$ K the peaks move below the detection limit of 2 cm^{-1}. Below 250 K, no indication of the peaks can be detected any more. It is interesting to note that at least in undoped $Sr_{14}Cu_{24}O_{41}$ a charge-ordered state develops below $T_{CO} \approx 250$ K (Abbamonte *et al.*, 2004).

In the ordered state $Sr_{14}Cu_{24}O_{41}$ has an optical response which is well described by that of a pinned charge density wave (Blumberg *et al.*, 2002; Littlewood, 1987). For $T > 250$ K, the results are interpreted in terms of a damped plasma oscillation above T_{CO} (Blumberg *et al.*, 2002; Gozar *et al.*, 2003; Gozar and Blumberg, 2005a). Since free carriers damp the mode, the width is expected to increase proportional the conductivity just opposite to what one would expect from free carrier response. This complicates the interpretation of the results in metallic $Sr_2Ca_{12}Cu_{24}O_{41}$ where the width still increases with temperature while the conductivity decreases. Gozar *et al.* (2003) argue that different regions of the Fermi surface contribute to the transport and the damping in essentially 2D $Sr_2Ca_{12}Cu_{24}O_{41}$.

A comparison of panels (a) and (b) of Figure 48 shows that the continuum surviving at low temperature is significantly stronger in the metal (Fig. 48 (b)). We therefore think that the low-energy mode found at $T > 250$ K could also originate from incipient charge order. In $Sr_{14-x}Ca_xCu_{24}O_{41}$ the mode is then superimposed on a free electron response in a similar way as in the high-T_c cuprates.

It is interesting that similar types of spectra are also found in $Bi_{1-x}Ca_xMnO_3$ (see section III.E), exhibiting comparable temperature dependences. While the results in ladders are interpreted in terms of an overdamped plasma mode in a CDW system above the ordering temperature (Blumberg *et al.*, 2002; Gozar *et al.*, 2003; Gozar and Blumberg, 2005a), the response in the cuprates was proposed to originate from fluctuations of the charge density in the vicinity of a charge-ordering instability (Caprara *et al.*, 2005). Since the charge modulation observed e.g. by tunneling microscopy (Hoffman *et al.*, 2002; Howald *et al.*, 2003; Vershinin *et al.*, 2004) is at finite **q**, two fluctuations have to be exchanged to fulfill the $q = 0$ selection rule in Raman scattering (Caprara *et al.*, 2005; Venturini *et al.*, 2000). Caprara *et al.* (2005) have shown that charge ordering fluctuations at incommensurate wavevectors determined via neutron scattering (Fujita *et al.*, 2002) yield proper lineshapes and selection rules in $La_{1.90}Sr_{0.10}CuO_4$ and $La_{1.98}Sr_{0.02}CuO_4$. To which extent the spin channel is involved and whether similar considerations apply to other dopings and cuprate

families have not been explored yet and remain important future topics.

In contrast to $Sr_{14-x}Ca_xCu_{24}O_{41}$, the low energy peak is strongly doping dependent in $La_{2-x}Sr_xCuO_4$. The temperature scale is different by a factor of 2 for the two doping levels studied (Fig. 46), implying that $T^*(0.02) \approx 2T^*(0.10)$. The doping level p_c determined from extrapolating T^* to zero, $T^*(p_c) = 0$, yields $0.15 \leq p_c \leq 0.20$ in close vicinity of the QCP inferred from other experiments. It is therefore possible that the low energy response is related to the thermal and quantum fluctuations above a hidden critical point.

In summary, the comparison of the cuprates studied suggests that there is a superposition of two anomalies in B_{1g} symmetry: (i) below $p \simeq 0.22$ antinodal quasiparticles become localized in all compounds as can be observed at sufficiently high temperature; (ii) with decreasing temperature a well-defined peak develops in $La_{1.90}Sr_{0.10}CuO_4$ at low energy. Although nothing comparable can be resolved in Y- and Bi-based compounds at the same doping level, the additional response may not necessarily be absent. It rather can mean that the low energy features are broader and shifted to higher energies, hence becoming very similar in shape to the response from the 2D planes. Since the relationship between superconductivity and spin and/or charge fluctuations is a key issue in the cuprates further work seems worthwhile here.

V. CONCLUSIONS AND OPEN QUESTIONS

The results discussed in the course of this review demonstrate that Raman spectroscopy is and has been an invaluable tool to investigate the dynamics of strongly correlated electrons. Improvements in the experimental technique have opened up the field to a variety of new systems. Light scattering has offered unique insights into dynamics in different regions of the Brillouin zone, showing the development of ordering and the competition between various phases as the role of correlations increases. Materials such as superconductors with charge-density wave order, correlated insulators, ruthenates, manganites, and finally the superconducting cuprates show the rich variety of phenomena which have been unveiled via Raman investigations. Along the way, light scattering has considerably deepened our knowledge of dynamics and correlation effects, and has provided several key ingredients towards the development of a comprehensive theoretical description of these materials.

Summarizing the findings on correlated systems over the past several years, the key ingredients stemming from Raman investigations include: (i) The development of anisotropies as correlations are increased. Symmetry-selective measurements provide a tool to zoom in on the dynamics in different regions of the Brillouin zone. This is evidenced by Raman scattering studies on MgB_2 as well as the cuprates in the normal and superconducting

phases, and the ordered phases in the ruthenates and the manganites. (ii) The existence of collective modes. Using Raman techniques the prevalence of certain types of order as a consequence were identified. Evidence for the importance of collective modes comes from CDW-superconductors and magnon scattering in antiferromagnetic insulators, and implications for a number of possible fluctuation or ordering modes exist in the cuprates. (iii) A qualitative understanding of quantum critical behavior. The symmetry projection of parts of the Brillouin zone completes the picture of the battleground between competing orders concomitant with an underlying quantum phase transition. Here, spectral weight transfers as a function of temperature, doping, and pressure on a number of materials combined with polarization dependent studies have opened a new door in the area of quantum criticality.

It is clear that a number of issues are still of primary interest in correlated systems in general. These include (i) the origin of the electronic continuum in a number of compounds which look surprisingly similar at first pass. (ii) The origin of the polarization dependence in materials which exhibit instabilities towards ordered phases. (iii) The mapping of Brillouin zone-projected electron dynamics close to a quantum critical point.

The cuprates continue to provide a wealth of information and puzzles in the area of superconductivity and strong electronic correlations. Issues in which consensus has been reached include (i) the presence antiferromagnetic correlations over a wide range of doping levels evidenced from the two-magnon peak, (ii) the broad continuum in the normal state as a common feature of all the cuprates, (iii) the $d-$wave nature of the pair state below T_c in a number of hole-doped materials derived from the low frequency power laws and polarization dependences, (iv) the dichotomy between the dynamics of B_{1g} and B_{2g} quasiparticles at low dopings, where the low frequency anti-nodal B_{1g} behavior is governed by incoherence at the same time as the nodal B_{2g} quasiparticles show relatively doping-independent metallic character, similar to the findings of transport quantities, and (v) the disappearance of this dichotomy for appreciably doped samples.

In the cuprates there are still several unsettled questions. (i) What is the origin of the A_{1g} and/or B_{1g} peaks in the superconducting state? Do they originate from the redistribution of superconducting quasiparticles or are they collective modes or of lattice origin? (ii) How does the nodal/anti-nodal dichotomy picture of coherence/incoherence merge into metallic description at high doping, BCS superconductivity for temperatures below T_c, and antiferromagnetism near half filling? (iii) What is the microscopic origin for low energy peaks at low doping, and how from this can information be obtained on the competition between ordered phases?

These are issues which we believe will form the plan of development of Raman scattering in the cuprates as well as other materials in the years to come. The continuation of investigations on many new and well-characterized samples will further our knowledge of materials and correlations, and applications of the use of pressure and magnetic field will allow an exploration of quantum criticality and evolution of anisotropic electron dynamics in a variety of systems. The rapid development of Raman scattering as we have outlined indicate that the study of the electronic dynamics of complex materials will remain a vibrant and promising field of research.

References

Abbamonte, P., G. Blumberg, A. Rusydi, A. Gozar, P. G. Evans, T. Siegrist, L. Venema, H. Eisaki, E. D. Isaacs, and G. A. Sawatzky, 2004, Nature (London) **431**, 1078.

Abrashev, M. V., C. Thomsen, and M. Surtchev, 1997, Physica C **280**, 297.

Abrikosov, A. A., and L. A. Fal'kovskiĭ, 1961, Zh. Eksp. Teor. Fiz. **40**, 262 [Sov. Phys. JETP **13**, 179 (1961)].

Abrikosov, A. A., and V. M. Genkin, 1973, Zh. Eksp. Teor. Fiz. **65**, 842 [Sov. Phys. JETP **38**, 417 (1974)].

Abrikosov, A. A., and L. A. Fal'kovskiĭ, 1987, Pis'ma Zh. Eksp. Teor. Fiz. **46**, 236 [Sov. Phys. JETP Lett. **46**, 179 (1987)].

Abrikosov, A. A., and L. A. Falkovsky, 1988, Physica C **156**, 1.

Abrikosov, A. A., 1991, Physica C **182**, 191.

Abstreiter, G., M. Cardona, and A. Pinczuk, 1984, in *Light Scattering in Solids IV*, edited by M. Cardona and G. Güntherodt (Springer-Verlag, Berlin), p. 5.

Alff, L., S. Meyer, S. Kleefisch, U. Schoop, A. Marx, H. Sato, M. Naito, and R. Gross, 1999, Phys. Rev. Lett. **83**, 2644.

Alff, L., Y. Krockenberger, B. Welter, M. Schonecke, R. Gross, D. Manske, and M. Naito, 2003, Nature (London) **422**, 698.

Allen, J. W. and J. C. Mikkelsen, 1977, Phys. Rev. B **15**, 2952.

Allen, P., 1976, Phys. Rev. B **13**, 1416.

Allen, P., and D. Rainer, 1991, Nature (London) **349**, 369.

Allen, P. B., and V. Perebeinos, 2001, Phys. Rev. B **64**, 085118.

Alloul, H., T. Ohno, and P. Mendels, 1989, Phys. Rev. Lett. **63**, 1700.

Altendorf, E., J. C. Irwin, R. Liang, and W. N. Hardy, 1992, Phys. Rev. B **45**, 7551.

Andergassen, Y., S. Caprara, C. Di Castro, and M. Grilli, 2001, Phys. Rev. Lett. **87**, 056401.

Andersen, O. K., A. I. Liechtenstein, O. Jepsen, and F. Paulsen, 1995, J. Phys. Chem. Solids **56**, 1573.

Anderson, P. W., 1958, Phys. Rev. **112**, 1900.

Anderson, P. W., 1959, J. Phys. Chem. Solids **11**, 26.

Ando, Y., S. Komiya, K. Segawa, S. Ono, and Y. Kurita, 2004, Phys. Rev. Lett. **93**, 267001.

Ando, Y., S. Ono, X. F. Sun, J. Takeya, F. F. Balakirev, J. B. Betts, and G. S. Boebinger, 2004a, Phys. Rev. Lett. **92**, 247004.

Armitage, N. P., D. H. Lu, D. L. Feng, C. Kim, A. Damascelli, K. M. Shen, F. Ronning, Z.-X. Shen, Y. Onose, Y. Taguchi, and Y. Tokura, 2001, Phys. Rev. Lett. **86**, 1126.

Ashcroft, N. W., and N. D. Mermin, 1976, *Solid State Physics* (Holt-Saunders, Philadelphia).

Aslamazov, L. G., and A. I. Larkin, 1968, Sov. Phys. Sol. State **10**, 875.

Axe, J. D., and G. Shirane, 1973, Phys. Rev. Lett. **30**, 214.

Balseiro, C. A., and L. M. Falicov, 1980, Phys. Rev. Lett. **45**, 662.

Bang, Y., 1993, Physica C **218**, 251.

Bardasis, A., and J. R. Schrieffer, 1961, Phys. Rev. **121**, 1050.

Basov, D. N., and T. Timusk, 2005, Rev. Mod. Phys. **77**, 721.

Bednorz, J. G., and K. A. Müller, 1986, Z. Phys. B **64**, 189.

Benfatto, L., S. Caprara, and C. Di Castro, 2000, Eur. Phys. J. B **17**, 95.

Billinge, S. J. L., M. Gutmann, and E. S. Božin, 2003, Int. J. Mod. Phys. B **17**, 3640.

Björnsson, P., M. R. Rübhausen, J. Bäckström, M. Käll, S. Eriksson, J. Eriksen, and L. Börjesson, 2000, Phys. Rev. B **61**, 1193.

Blum, F. A., 1970, Phys. Rev. B **1**, 1125.

Blumberg, G., R. Liu, M. V. Klein, W. C. Lee, D. M. Ginsberg, C. Gu, B. W. Veal, and B. Dabrowski, 1994, Phys. Rev. **49**, 13295.

Blumberg, G., P. Abbamonte, M. V. Klein, W. C. Lee, D. M. Ginsberg, L. L. Miller, and A. Zibold, 1996, Phys. Rev. **53**, 11930.

Blumberg, G., M. Kang, M. V. Klein, K. Kadowaki,and C. Kendziora, 1997a, Science **278**, 1427.

Blumberg, G., M. Kang, and M. V. Klein, 1997b, Phys. Rev. Lett. **78**, 2461.

Blumberg, G., M. V. Klein, and S.-W. Cheong, 1998, Phys. Rev. Lett. **80**, 564.

Blumberg, G., and M. V. Klein, 1999, J. Low Temp. Phys. **117**, 1001.

Blumberg, G., A. Koitzsch, A. Gozar, B. S. Dennis, C. A. Kendziora, P. Fournier, and R. L. Greene, 2002, Phys. Rev. Lett. **88**, 107002.

Blumberg, G., A. Koitzsch, A. Gozar, B. S. Dennis, C. A. Kendziora, P. Fournier, and R. L. Greene, 2003, Phys. Rev. Lett. **90**, 149702.

Bock, A., S. Ostertun, R. Das Sharma, M. Rübhausen, K.O. Subke, and C. T. Rieck, 1999, Phys. Rev. B **60**, 3532.

Boebinger, G. S., Y. Ando, A. Passner, T. Kimura, M. Okuya, K. Kishio, K. Tamasaku, N. Ichikawa, and S. Uchida, 1996, Phys. Rev. Lett. **77**, 5417.

Bogoliubov, N. N., V. V. Tolmachev, and D. V. Shirkov, 1959, *A New Method in the Theory of Superconductivity*, (Bureau, New York).

Borkowski, L. S., and P. J. Hirschfeld, 1994, Phys. Rev. B **49**, 15404.

Bozovic, I., D. Kirillov, A. Kapitulnik, K. Char, M. R. Hahn, M. R. Beasley, T. H. Geballe, Y. H. Kim, and A. J. Heeger, 1987, Phys. Rev. Lett. **59**, 2219.

Branch, D., and J. P. Carbotte, 1995, Phys. Rev. B **52**, 603.

Branch, D., and J. P. Carbotte, 1996, Phys. Rev. B **54**, 13288.

Brenig, W., and H. Monien, 1992, Solid State Commun. **83**, 1009.

Brenig, W., P. Knoll, and M. Mayer, 1997, Physica B **237**, 95.

Browne, D. A., and K. Levin, 1983, Phys. Rev. B **28**, 4029.

Budelmann, D., B. Schulz, M. Rübhausen, M. V. Klein, M. S. Williamsen, and P. Guptasarma, 2005, Phys. Rev. Lett. **95**, 057003.

Campuzano, J. C., M. R. Norman, and M. Randeira, 2002, in *The Physics of Supreconductors Vol. II*, edited by K. H. Bennemann and J. B. Ketterson (Springer-Verlag, Berlin), p. 167.

Canali, C. M., and S. M. Girvin, 1992, Phys. Rev. B **45**, 7127.

Canfield, P. C., P. L. Gammel, and D. J. Bishop, 1998, Physics Today **51** (10), 40.

Cappelluti, E., and R. Zeyher, 1999, Phys. Rev. B **59**, 6475.

Caprara, S., C. Di Castro, S. Fratini, and M. Grilli, 2002, Phys. Rev. Lett. **88**, 147001.

Caprara, S., C. Di Castro, M. Grilli, and D. Suppa, 2005, Phys. Rev. Lett. **95**, 117004.

Castellani, C., C. Di Castro, and M. Grilli, 1995, Phys. Rev. Lett. **75**, 4650.

Castellani, C., C. Di Castro, and M. Grilli, 1997, Z. Phys. B

103, 137.

Castro Neto, A. H., 2001, Phys. Rev. Lett. **86**, 4382.

Cava, R. J., R. B. van Dover, B. Batlogg, and E. A. Rietman, 1987, Phys. Rev. Lett. **58**, 408.

Cerdeira, F., T. A. Fjeldly, and M. Cardona, 1973, Phys. Rev. B **8**, 4734.

Chakravarty, S., R. B. Laughlin, D. K. Morr, and C. Nayak, 2001, Phys. Rev. B **63**, 094503.

Chandrasekhar, M., M. Cardona, and E. O. Kane, 1977, Phys. Rev. B **16**, 3579.

Chen, X. K., E. Altendorf, J. C. Irwin, R. Liang, and W. N. Hardy, 1993, Phys. Rev. B **48**, 10530.

Chen, X. K., J. C. Irwin, R. Liang, and W. N. Hardy, 1994a, Physica C **227**, 113.

Chen, X. K., J. C. Irwin, H. J. Trodahl, T. Kimura, and K. Kishio, 1994b, Phys. Rev. Lett. **73**, 3290.

Chen, X. K., M. J. Konstantinović, J. C. Irwin, D. D. Lawrie, and J. P. Franck, 2001, Phys. Rev. Lett. **87**, 157002.

Chesca, B., K. Ehrhardt, M. Mößle, R. Straub, D. Koelle, R. Kleiner, and A. Tsukada, 2003, Phys. Rev. Lett. **90**, 057004.

Choi, K.-Y., P. Lemmens, T. Sahaoui, G. Güntherodt, Yu. G. Pashkevich, V. P. Gnezdilov, P. Reutler, L. Pinsard-Gaudart, B. Büchner, and A. Revcolevschi, 2005, Phys. Rev. B **71**, 174402.

Chubukov, A. V., and D. M. Frenkel, 1995a, Phys. Rev. Lett. **74**, 3057.

Chubukov, A. V., and D. M. Frenkel, 1995b, Phys. Rev. B **52**, 9760.

Chubukov, A., D. Morr, and G. Blumberg, 1999, Sol. State Commun. **112**, 193.

Chubukov, A., T. P. Devereaux, and M. V. Klein, 2006, Phys. Rev. B **73**, 094512.

Cooper, S. L., M. V. Klein, B. G. Pazol, J. P. Rice, and D. M. Ginsberg, 1988a, Phys. Rev. B **37**, 5920.

Cooper, S. L., F. Slakey, M. V. Klein, J. P. Rice, E. D. Bukowski, and D. M. Ginsberg, 1988b, Phys. Rev. B **38**, 11934.

Dagan, Y., M. M. Qazilbash, C. P. Hill, V. N. Kulkarni, and R. L. Greene, 2004, Phys. Rev. Lett. **92**, 167001.

Dagotto, E., and T. M. Rice, 1996, Science **271**, 618.

Dagotto, E., 1999, Rep. Prog. Phys. **62**, 1525.

Dagotto, E., 2005, Science **309**, 257.

Dahm, T. P., D. Manske, and B. Tewordt, 1998, Phys. Rev. B **58**, 12454.

Dahm, T. P., D. Manske, and B. Tewordt, 1999, Phys. Rev. B **59**, 14740.

Damascelli, A., Z. Hussain, and Z.-X. Shen, 2003, Rev. Mod. Phys. **75**, 473.

Deutscher, G., 1999, Nature (London) **397**, 410.

Deutscher, G., 2005, Rev. Mod. Phys. **77**, 109.

Devereaux, T. P., 1992, Phys. Rev. B **45**, 12965.

Devereaux, T. P., 1993, Phys. Rev. B **47**, 5230.

Devereaux, T. P., D. Einzel, B. Stadlober, R. Hackl, D. Leach, and J. J. Neumeier, 1994a, Phys. Rev. Lett. **72**, 396.

Devereaux, T. P., D. Einzel, B. Stadlober, and R. Hackl, 1994b, Phys. Rev. Lett. **72**, 3291.

Devereaux, T. P., and D. Einzel, 1995a, Phys. Rev. B **51**, 16336 [*Erratum:* Phys. Rev. B **54**, 15547 (1996)].

Devereaux, T. P., 1995b, Phys. Rev. Lett. **74**, 4313.

Devereaux, T. P., A. Virosztek, and A. Zawadowski, 1996, Phys. Rev. B **54**, 12523.

Devereaux, T. P., and A. P. Kampf, 1997, Int. Journ. Mod. Phys. B **11**, 2093.

Devereaux, T. P., and A. P. Kampf, 1999, Phys. Rev. B **59**, 6411.

Devereaux, T. P., and A. P. Kampf, 2000, Phys. Rev. B **61**, 1490.

Devereaux, T. P., G. E. D. McCormack, and J. K. Freericks, 2003a, Phys. Rev. B **68**, 075105.

Devereaux, T. P., 2003b, Phys. Rev. B **68**, 094503.

Devereaux, T. P., G. E. D. McCormack, and J. K. Freericks, 2003c, Phys. Rev. Lett. **90**, 067402.

Dierker, S. B., M. V. Klein, G. W. Webb, and Z. Fisk, 1983, Phys. Rev. Lett. **50**, 853.

van Dongen, P. G. J., 1992, Phys. Rev. B **45**, 2267.

Durst, A., and P. Lee, 2000, Phys. Rev. B **62**, 1270.

Einzel, D., and R. Hackl, 1996, J. Raman Spectrosc. **27**, 307.

Einzel, D., and D. Manske, 2004, Phys. Rev. B **70**, 172507.

Eisaki, H., N. Kaneko, D. L. Feng, A. Damascelli, P. K. Mang, K. M. Shen, Z.-X. Shen, and M. Greven, 2004, Phys. Rev. B **69**, 064512.

Elliot, R. J., and R. Loudon, 1963, Phys. Lett. **3A**, 189.

Erb, A., E. Walker, and R. Flükiger, 1996a, Physica C **258**, 9.

Erb, A., J.Y. Genoud, F. Marti, M. Däumling, E. Walker, and R. Flükiger, 1996b, J. Low Temp. Phys. **105**, 1023.

Fabelinskiǐ, I. L., 1998, Physics Uspekhi **41** (12), 1229.

Falikov, L. M., and J. C. Kimball, 1969, Phys. Rev. Lett. **22**, 997.

Fal'kovskiǐ, L. A., 1989, Zh. Eksp. Teor. Fiz. **95**, 1145 [Sov. Phys. JETP **68**, 661 (1989)].

Fal'kovskiǐ, L. A., 1990, Usp. Fiz. Nauk. **160**, 71 [Sov. Phys. Usp. **33**, 296 (1990)].

Fal'kovskiǐ, L. A., 1991, Zh. Eksp. Teor. Fiz. **100**, 2045 [Sov. Phys. JETP **73**, 1134 (1991)].

Falkovsky, L. A., and S. Klama, 1990, Physica C **172**, 242.

Fano, U., 1961, Phys. Rev. **124**, 1866.

Fang, A. C., L. Capriotti, D. J. Scalapino, S. A. Kivelson, N. Kaneko, M. Greven, and A. Kapitulnik, 2006, Phys. Rev. Lett. **96**, 017007.

Fleury, P. A., S. P. S. Porto, L. E. Cheesman, and H. J. Guggenheim, 1966, Phys. Rev. Lett. **17**, 84.

Fleury, P. A., S. P. S. Porto, and R. Loudon, 1967, Phys. Rev. Lett. **18**, 658.

Fleury, P., and R. Loudon, 1968, Phys. Rev. **166**, 514.

Fleury, P. A., and H. J. Guggenheim, 1970, Phys. Rev. Lett. **24**, 1346.

Fleury, L., 1993, Phys. Lett. A **179**, 140.

Fournier, P. K., X. Jiang, W. Jiang, S. N. Mao, T. Venkatesan, C. J. Lobb, and R. L. Greene, 1997, Phys. Rev. B **56**, 14149.

Fraas, L. M., P. F. Williams, and S. P. S. Porto, 1970, Solid State Commun. **8**, 2113.

Freericks, J. K., and P. Miller, 2000, Phys. Rev. B **62**, 10022.

Freericks, J. K., and T. P. Devereaux, 2001a, Phys. Rev. B **64**, 125110.

Freericks, J. K., T. P. Devereaux, and R. Bulla, 2001b, Phys. Rev. B **64**, 233114.

Freericks, J. K., T. P. Devereaux, R. Bulla, and Th. Pruschke, 2003a, Phys. Rev. B **67**, 155102.

Freericks, J. K., and V. Zlatic, 2003b, Rev. Mod. Phys. **75**, 1333.

Freericks, J. K., T. P. Devereaux, M. Moraghebi, and S. L. Cooper, 2005, Phys. Rev. Lett. **94**, 216401.

Freitas, P. J., and R. R. P. Singh, 2000, Phys. Rev. B **62**, 5525.

Fujita, M., K. Yamada, H. Hiraka, P. M. Gehring, S. H. Lee, S.

Wakimoto, and G. Shirane, 2002, Phys. Rev. B **65**, 064505.

Fulde, P., and S. Strassler, 1965, Phys. Rev. **140**, A519.

Fulde, P., 1995, *Electronic Correlations in Solid and Molecules*, (Springer-Verlag, Berlin).

Gallais, Y., A. Sacuto, P. Bourges, Y. Sidis, A. Forget, and D. Colson, 2002, Phys. Rev. Lett. **88**, 177401.

Gallais, Y., A. Sacuto, and D. Colson, 2004, Physica C **408**, 785.

Gallais, Y., A. Sacuto, T. P. Devereaux, and D. Colson, 2005, Phys. Rev. B **71**, 012506.

Gasparov, L. V., P. Lemmens, M. Brinkmann, N. N. Kolesnikov, and G. Güntherodt, 1997, Phys. Rev. B **55**, 1223.

Gasparov, L. V., P. Lemmens, N. N. Kolesnikov, and G. Güntherodt, 1998, Phys. Rev. B **58**, 11753.

Gebhard, F., 1997, *The Mott Metal-Insulator Transition*, (Springer-Verlag, Berlin).

Geerk, J., H. Rietschel, and U. Schneider, 1984, Phys. Rev. B **30**, 459.

Ginzburg, V. L., 1998, Vest. Ross. Akad. Nauk **68**, 51 and private communication.

Götze, W., and P. Wölfle, 1972, Phys. Rev. B **6**, 1226.

Goncharov, A. F., and V. V. Struzhkin, 2003, J. Raman Spectrosc. **34**, 532.

Gozar, A., G. Blumberg, B. S. Dennis, B. S. Shastry, N. Motoyama, H. Eisaki, and S. Uchida, 2001, Phys. Rev. Lett. **87**, 197202.

Gozar, A., G. Blumberg, P. B. Littlewood, B. S. Dennis, N. Motoyama, H. Eisaki, and S. Uchida, 2003, Phys. Rev. Lett. **91**, 087401.

Gozar, A., B. S. Dennis, G. Blumberg, S. Komiya, and Y. Ando, 2004, Phys. Rev. Lett. **93**, 027001.

Gozar, A., and G. Blumberg, 2005a, in *Frontiers in Magnetic Materials*, edited by A. V. Narlikar (Springer-Verlag, Berlin), p. 653.

Gozar, A., S. Komiya, Y. Ando, and G. Blumberg, 2005b, in *Frontiers in Magnetic Materials*, edited by A. V. Narlikar (Springer-Verlag, Berlin), p. 755.

Greytak, T. J., and J. Yan, 1969, Phys. Rev. Lett. **22**, 987.

Grüninger, M., R. Rückamp, M. Windt, P. Reutler, C. Zobel, T. Lorenz, A. Freimuth,and A. Revcolevschi, 2002, Nature (London) **418**, 39.

Gurtubay, I. G., Wei Ku, and J. M. Pitarke, A. G. Eguiluz, B. C. Larson, J. Tischler, and P. Zschack, 2004, Phys. Rev. B **70**, 201201.

Hackl, R., R. Kaiser, and S. Schicktanz, 1982, in *Superconductivity in d- and f- band Metals IV*, edited by W. Buckel and W. Weber (Kernforschungzentrum, Karlsruhe), p. 559.

Hackl, R., R. Kaiser, and S. Schicktanz, 1983, J. Phys. C: Sol. State Phys. **16**, 1729.

Hackl, R., and R. Kaiser, 1988a, J. Phys. C: Solid State Phys. **21**, L453.

Hackl, R., W. Gläser, P. Müller, D. Einzel, and K. Andres, 1988b, Phys. Rev. B **38**, 7133.

Hackl, R., P. Müller, D. Einzel, and W. Gläser, 1989, Physica C **162-164**, 1241.

Hackl, R., M. Opel, P. F. Müller, G. Krug, B. Stadlober, R. Nemetschek, H. Berger, and L. Forró, 1996, J. Low Temp. Phys. **105**, 733.

Hackl, R., L. Tassini, F. Venturini, Ch. Hartinger, A. Erb, N. Kikugawa, and T. Fujita, 2005, in *Adv. in Solid State Phys.* **45** edited by B. Kramer (Springer-Verlag, Berlin), p. 225.

Hadjiev, V. G., X. Zhou, T. Strohm, M. Cardona, Q. M. Lin, and C. W. Chu, 1998, Phys. Rev. B **58**, 1043.

Halley, J. W., 1978, Phys. Rev. Lett. **41**, 1605.

Hanaguri, T., C. Lupien, Y. Kohsaka, D.-H. Lee, M. Azuma, M. Takano, H. Takagi, and J. C. Davis, 2004, Nature (London) **430**, 1001.

Hanamura, E., N. T. Dan, and Y. Tanabe, 2000, Phys. Rev. B **62**, 7033.

Hardy, W. N., D. A. Bonn, D. C. Morgan, R. Liang, and K. Zhang, 1993, Phys. Rev. Lett. **70**, 3999.

Hartschuh, A., E. J. Sanchez, X. S. Xie, and L. Novotny, 2003, Phys. Rev. Lett. **90**, 095503.

Hayes, W., and R. Loudon, 2005, in *Scattering of Light by Crystals*, (Dover Publications, New York).

He, H., P. Bourges, Y. Sidis, C. Ulrich, L. P. Regnault, S. Pailhès, N. S. Berzigiarova, N. N. Kolesnikov, and B. Keimer, 2002, Science **295**, 1045.

Hewitt, K. C., T. P. Devereaux, X. K. Chen, X.-Z. Wang, J. G. Naeini, A. E. Curzon, M. Irwin, and A. Martin, 1997, Phys. Rev. Lett. **78**, 4891.

Hewitt, K. C., N. L. Wang, J. C. Irwin, D. M. Pooke, A. E. Pantoja, and H. J. Trodahl, 1999, Phys. Rev. B **60**, R9943.

Hewitt, K. C., and J. C. Irwin, 2002, Phys. Rev. B **66**, 054516.

Heyen, E. T., R. Liu, M. Cardona, S. Piñol, R. J. Melville, E. Morán, and M. A. Alario-Franco, 1991, Phys. Rev. B **43**, 2857.

Hinkov, V., S. Pailhès, P. Bourges, A. Ivanov, A. Kulakov, C. T. Lin, D. P. Chen, C. Bernhard, and B. Keimer, 2004, Nature (London) **430**, 650.

Ho, C. M., V. N. Muthukumar, M. Ogata, and P. W. Anderson, 2001, Phys. Rev. Lett. **86**, 1626.

Hoffman, J. E., K. McElroy, D.-H. Lee, K. M. Lang, H. Eisaki, S. Uchida, and J. C. Davis, 2002, Science **297**, 1148.

Hoffmann, A., P. Lemmens, G. Güntherodt, V. Thomas, and K. Winzer, 1994, Physica C **235-240**, 1897.

Hoffstein, V., and R. W. Cohen, 1969, Phys. Lett. **29** A, 603.

Homes, C. C., P. B. Clayman, J. L. Peng, and R. L. Greene, 1997, Phys. Rev. B **56**, 5525.

Homes, C. C., S. V. Dordevic, M. Strongin, D. A. Bonn, R. Liang, W. N. Hardy, S. Komiya, Y. Ando, G. Yu, N. Kaneko, X. Zhao, M. Greven, D. N. Basov, and T. Timusk, 2004, Nature (London) **430**, 539.

Howald, C., H. Eisaki, N. Kaneko, M. Greven, and A. Kapitulnik, 2003, Phys. Rev. B **67**, 014533.

Huntley, D. J., and R. F. Frindt, 1974, Can. J. Phys. **52**, 861.

Imada, M., A. Fujimori, and Y. Tokura, 1998, Rev. Mod. Phys. **70**, 1039.

Ipatova, I. P., A. V. Subashiev, and V. A. Voitenko, 1981, Sol. State Commun. **37**, 893.

Ipatova, I. P., M. I. Kaganov, and A. V. Subashiev, 1983, Zh. Eksp. Teor. Fiz. **84**, 1830 [Sov. Phys. JETP **57**, 1066 (1983)].

Itai, K., 1992, Phys. Rev. B **45**, 707.

Jain, J. K., and S. Das Sarma, 1987, Phys. Rev. B **36**, 5949.

Jandl, S., M. Iliev, C. Thomsen, T. Ruf, M. Cardona, B. M. Wanklyn, and C. Chen, 1993, Solid State Commun. **87**, 609.

Jánossy, A., T. Fehér, and A. Erb, 2003, Phys. Rev. Lett. **91**, 177001.

Jiang, C., and J. P. Carbotte, 1996, Phys. Rev. B **53**, 11868.

Junod, A., T. Jarlborg, and J. Muller, 1983, Phys. Rev. B **27**, 1568.

Jurecka, C., V. Grützun, A. Friedrich, and W. Brenig, 2001, Eur. Phys. J. B **21**, 469.

Kaiser, D. L., F. Holtzberg, B. A. Scott, T. R. McGuire, and 1987, App. Phys. Lett. **51**, 1040.

Kampf, A. P., and W. Brenig, 1992, Z. Phys. B **89**, 313.

Kang, M., G. Blumberg, M. V. Klein, and N. N. Kolesnikov, 1996, Phys. Rev. Lett. **77**, 4434.

Kang, M., G. Blumberg, M. V. Klein, and N. N. Kolesnikov, 1997, Phys. Rev. B **56**, 11427.

Katanin, A. A., and A. P. Kampf, 2003, Phys. Rev. B **67**, 100404.

Katsufuji, T., Y. Tokura, T. Ido, and S. Uchida, 1994, Phys. Rev. B **48**, 16131.

Kee, H.-Y., K. Maki, and C. H. Chung, 2003, Phys. Rev. B **67**, 180504.

Kendziora, C., L. Forro, D. Mandrus, J. Hartge, P. Stephens, L. Mihaly, R. Reeder, D. Moecher, M. Rivers, and S. Sutton, 1992, Phys. Rev. B **45**, 13025.

Kendziora, C., M. C. Martin, J. Hartge, and L. Mihaly, 1993, Phys. Rev. B **48**, 3531.

Kendziora, C., and A. Rosenberg, 1995, Phys. Rev. B **52**, 9867.

Kendziora, C., R. J. Kelley, and M. Onellion, 1996, Phys. Rev. Lett. **77**, 727.

Khaǐkin, M. S., and V. P. Bykov, 1956, JETP **30**, 191 [Sov. Phys. JETP **3**, 119 (1956)].

Khveshchenko, D. V., and P. B. Wiegmann, 1994, Phys. Rev. Lett. **73**, 500.

Kim, T. K., A. A. Kordyuk, S. V. Borisenko, A. Koitzsch, M. Knupfer, H. Berger, and J. Fink, 2003, Phys. Rev. Lett. **91**, 167002.

Kirillov, D., J. P. Collman, J. T. McDevitt, G. T. Yee, M. J. Holcomb, and I. Bozovic, 1988, Phys. Rev. B **37**, 3660.

Kivelson, S. A., E. Fradkin, and V. J. Emery, 1998, Nature (London) **393**, 550.

Kivelson, S. A., I. P. Bindloss, E. Fradkin, V. Oganesyan, J. M. Tranquada, A. Kapitulnik, and C. Howald, 2003, Rev. Mod. Phys. **75**, 1201.

Klauss, H.-H., W. Wagener, M. Hillberg, W. Kopmann, H. Walf, F. J. Litterst, M. Hücker, and B. Büchner, 2000, Phys. Rev. Lett. **85**, 4590.

Klein, B. M., L. L. Boyer, D. A. Papaconstantopoulos, and L. F. Mattheiss, 1978, Phys. Rev. B **18**, 6411.

Klein, M. V., 1982a, in *Superconductivity in d- and f- band Metals IV*, edited by W. Buckel and W. Weber (Kernforschungzentrum, Karlsruhe), p. 539.

Klein, M. V., 1982b, in *Light Scattering in Solids III*, edited by M. Cardona and G. Güntherodt (Springer-Verlag, Berlin), p. 121.

Klein, M. V., 1982c, Phys. Rev. B **25**, 7192.

Klein, M. V., 1983, in *Light Scattering in Solids I*, edited by M. Cardona and G. Güntherodt (Springer-Verlag, Berlin), p. 147.

Klein, M. V., and S. B. Dierker, 1984, Phys. Rev. B **29**, 4976.

Klein, M. V., S. L. Cooper, A. L. Kotz, Ran Liu, D. Reznik, F. Slakey, W. C. Lee, and D. M. Ginsberg 1991, Physica C **185**, 72.

Knoll, P., C. Thomsen, M. Cardona, and P. Murugaraj, 1990, Phys. Rev. B **42**, 4842.

Knoll, P., M. Mayer, W. Brenig, and Ch. Waidacher, 1996, J. Low Temp. Phys. **105**, 383.

Koitzsch, A., G. Blumberg, A. Gozar, B. S. Dennis, P. Fournier, and R. L. Greene, 2003, Phys. Rev. B **67**, 184522.

Kokales, J. D., P. Fournier, L. V. Mercaldo, V. V. Talanov, C. A. Kendziora, R. L. Greene, and S. M. Anlage, 2000, Phys. Rev. Lett. **85**, 3696.

Kostur, V. N., and G. M. Éliashberg, 1991, Pis'ma Zh. Eksp. Teor. Fiz. **53**, 373 [Sov. Phys. JETP Lett. **53**, 391 (1991)].

Kostur, V. N., 1992, Z. Phys. B **89**, 149.

Kosztin, J., and A. Zawadowski, 1991, Sol. State Commun. **78**, 1029.

Kotani, A., and S. Shin, 2001, Rev. Mod. Phys. **73**, 203.

Kramer, B., and M. Sassetti, 2000, Phys. Rev. B **62**, 4238.

Kramers, H. A., and W. Heisenberg, 1925, Z. Phys. **31**, 681.

Krantz, M. C., and M. Cardona, 1994, Phys. Rev. Lett. **72**, 3290.

Krüger, R., B. Schulz, S. Naler, R. Rauer, D. Budelmann, J. Bäckström, K. H. Kim, S.-W. Cheong, V. Perebeinos, and M. Rübhausen, 2004, Phys. Rev. Lett. **92**, 097203.

Ku, W., W. E. Pickett, R. T. Scalettar, and A. G. Equiluz, 2002, Phys. Rev. Lett. **88**, 057001.

Landau, L. D., and E. M. Lifshitz, 1960, in *Electrodynamics of Continuous Media*, (Pergamon, Oxford), p. 377.

Landsberg, G. S., and L. I. Mandelstam, 1928, Naturwissenschaften **16**, 557.

Le Tacon, M., A. Sacuto, and D. Colson, 2005, Phys. Rev. B **71**, 100504.

Lee, H. C., and H.-Y. Choi, 2002, Phys. Rev. B **65**, 174530.

Lei, X. L., C. S. Ting, and J. L. Birman, 1985, Phys. Rev. B **32**, 1464.

Lemmens, P., G. Güntherodt, and C. Gros, 2003, Phys. Reports **375**, 1.

Liang, R., D. A. Bonn, and W. N. Hardy, 2000, Physica C **336**, 57.

Liang, R., D. A. Bonn, W. N. Hardy, J. C. Wynn, K. A. Moler, L. Lu, S. Larochelle, L. Zhou, M. Greven, L. Lurio, and S. G. J. Mochrie, 2002, Physica C **383**, 1.

Limonov, M., A. I. Rykov, S. Tajima, and A. Yamanaka, 1998, Phys. Rev. Lett. **80**, 825.

Limonov, M., S. Tajima, and A. Yamanaka, 2000, Phys. Rev. B **62**, 11859.

Limonov, M., S. Lee, S. Tajima, and A. Yamanaka, 2002a, Phys. Rev. B **66**, 054509.

Limonov, M., D. Shantsev, S. Tajima, and A. Yamanaka, 2002b, Phys. Rev. B **65**, 024515.

Lindroos, M., S. Sahrakorpi, and A. Bansil, 2002, Phys. Rev. B **65**, 054514.

Littlewood, P. B., 1987, Phys. Rev. B **36**, 3108.

Littlewood, P. B., and C. M. Varma, 1981, Phys. Rev. Lett. **47**, 811.

Littlewood, P. B., and C. M. Varma, 1982, Phys. Rev. B **26**, 4883.

Liu, R., D. Salamon, M. V. Klein, S. L. Cooper, W. C. Lee, S.-W. Cheong, and D. M. Ginsberg, 1993, Phys. Rev. Lett. **71**, 3709.

Liu, H. L., G. Blumberg, M. V. Klein, P. Guptasarma, and D. G. Hinks, 1999, Phys. Rev. Lett. **82**, 3524.

Liu, C. S., H. G. Luo, W. C. Wu, and T. Xiang, 2005, e-print, cond-mat/0512173.

van Loosdrecht, P. H. M., J. P. Boucher, G. Martinez, G. Dhalenne, and A. Revclovschi, 1996, Phys. Rev. Lett. **76**, 311.

Loram, J. W., and J. L. Tallon, 2002, Physica C **349**, 53.

Lorenzana, J., and G. A. Sawatzky, 1995, Phys. Rev. B **52**, 9576.

Löwdin, P.-O., 1951, J. Chem. Phys. **19**, 1396.

Lyons, K. B., S. H. Liou, M. Hong, H. S. Chen, J. Kwo, and T. J. Negran, 1987, Phys. Rev. B **36**, 5592.

Lyons, K. B., P. A. Fleury, J. P. Remeika, A. S. Cooper, and T. J. Negran, 1988, Phys. Rev. B **37**, 2353.

Lyons, K. B., P. E. Sulewski, P. A. Fleury, H. L. Carter, A. S. Cooper, G. P. Espinoza, Z. Fisk, and S.-W. Cheong, 1989,

Phys. Rev. B **39**, 9693.

Machida, K., 1989, Physica C **87**, 192.

Mahan, G. D., 2000, *Many-Particle Physics* (Kluwer Academic, New York).

Maki, K., and T. Tsuneto, 1962, Prog. Theor. Phys. (Kyoto) **28**, 163.

Maksimov, A. A., I. I. Tartakovskiĭ, V. B. Timofeev, and L. A. Fal'kovskiĭ, 1990, Zh. Eksp. Teor. Fiz. **97**, 1047 [Sov. Phys. JETP **70**, 588 (1990)].

Mandrus, D., L. Forró, D. Koller, and L. Mihály, 1991, Nature (London) **351**, 460.

Mannella, N., A. Rosenhahn, C. H. Booth, S. Marchesini, B. S. Mun, S.-H. Yang, K. Ibrahim, Y. Tomioka, and C. S. Fadeley, 2004, Phys. Rev. Lett. **92**, 166401.

Mannella, N., W. L. Yang, X. J. Zhou, H. Zheng, J. F. Mitchell, J. Zaanen, T. P. Devereaux, N. Nagaosa, Z. Hussain, and Z.-X. Shen, 2005, Nature **438**, 474.

Manske, D., C. T. Rieck, R. Das Sharma, A. Bock, and D. Fay, 1997, Phys. Rev. B **56**, 2940.

Manske, D., A. Bock, C. T. Rieck, and D. Fay, 1998, Phys. Rev. B **58**, 8841.

Martinho, H., A. A. Martin, C. Rettori, and C. T. Lin, 2004, Phys. Rev. B **69**, 180501.

Masui, T., M. Limonov, H. Uchiyama, S. Lee, S. Tajima, and A. Yamanaka, 2003, Phys. Rev. B **68**, 060506.

Masui, T., M. Limonov, H. Uchiyama, S. Tajima, and A. Yamanaka, 2005, Phys. Rev. Lett. **95**, 207001.

Matsui, H., K. Terashima, T. Sato, T. Takahashi, M. Fujita, and K. Yamada, 2005, Phys. Rev. Lett. **95**, 017003.

Mattheiss, L. F., and W. Weber, 1982, Phys. Rev. B **25**, 2248.

Mattis, D. C., and J. Bardeen, 1958, Phys. Rev. **111**, 142.

McElroy, K., R. W. Simmonds, J. E. Hoffman, D.-H. Lee, J. Orenstein, H. Eisaki, S. Uchida, and J. C. Davis, 2003, Nature (London) **422**, 592.

McElroy, K., H. Eisaki, S. Uchida, and J. C. Davis, 2005, Science **309**, 1048.

Metzner, W., D. Rohe, and S. Andergassen, 2003, Phys. Rev. Lett. **91**, 066402.

Migdal, A. B., 1958, Sov. Phys. JETP **7**, 996.

Millis, A. J., H. Monien, and D. Pines, 1990, Phys. Rev. B **42**, 167.

Mills, D. L., A. A. Maradudin, and E. Burstein, 1970, Annals of Physics **56**, 504.

Mishchenko, E. G., 1999, Phys. Rev. B **59**, 14892.

Misochko, O. V., K. Sakai, S. Nakashima, and G. Gu, 1999, Phys. Rev. B **60**, 1326.

Moler, K. A., D. J. Baar, J. S. Urbach, Ruixing Liang, W. N. Hardy, and A. Kapitulnik, 1994, Phys. Rev. Lett. **73**, 2744.

Monien, H., and A. Zawadowski, 1989, Phys. Rev. Lett. **63**, 911.

Monien, H., and A. Zawadowski, 1990, Phys. Rev. B **41**, 8798.

Monthoux, P., and D. J. Scalapino, 1994, Phys. Rev. Lett. **72**, 1874.

Mooradian, A., and G. B. Wright, 1966, Phys. Rev. Lett. **16**, 999.

Moore, D. F., R. B. Zubeck, J. M. Rowell, and M. R. Beasley, 1979, Phys. Rev. B **20**, 2721.

Morita, S., S. Imai, S. Yamashita, N. Mikoshiba, N. Toyota, T. Fukase, and T. Nakanomyo, 1984, Physica B+C **126**, 601.

Morr, D. K., A. V. Chubukov, A. P. Kampf, and G. Blumberg, 1996, Phys. Rev. B **54**, 3468.

Morr, D. K., and A. V. Chubukov, 1997, Phys. Rev. B **56**, 9134.

Munzar, D., and M. Cardona, 2003, Phys. Rev. Lett. **90**, 077001.

Nachumi, B., C. Kendziora, N. Ichikawa, Y. Nakamura, and S. Uchida, 2002, Phys. Rev. B **65**, 092504.

Naeini, J. G., X. K. Chen, J. C. Irwin, M. Okuya, T. Kimura, and K. Kishio, 1999, Phys. Rev. B **59**, 9642.

Naito, M., and M. Hepp, 2000, Jpn. J. Appl. Phys. **39**, L485.

Nagamatsu, J., N. Nakagawa, T. Muranaka, Y. Zenitani, and J. Akimitsu, 2001, Nature (London) **410**, 63.

Nambu, Y., 1960, Phys. Rev. **117**, 648.

Nemetschek, R., O. V. Misochko, B. Stadlober, and R. Hackl, 1993, Phys. Rev. B **47**, 3450.

Nemetschek, R., M. Opel, C. Hoffmann, P. F. Müller, R. Hackl, H. Berger, L. Forró, A. Erb, and E. Walker, 1997, Phys. Rev. Lett. **78**, 4837.

Nemetschek, R., R. Hackl, M. Opel, R. Philipp, M. T. Beal-Monod, J. B. Bieri, K. Maki, A. Erb, and E. Walker, 1998, Euro. Phys. J. B **5**, 495.

Nyhus, P., S. L. Cooper, and Z. Fisk, 1995a, Phys. Rev. B **51**, 15626.

Nyhus, P., S. L. Cooper, Z. Fisk, and J. Sarrao, 1995b, Phys. Rev. B **52**, 14308.

Nyhus, P., S. L. Cooper, Z. Fisk, and J. Sarrao, 1997a, Phys. Rev. B **55**, 12488.

Nyhus, P., S. Yoon, M. Kauffman, S. L. Cooper, Z. Fisk, and J. Sarrao, 1997b, Phys. Rev. B **56**, 2717.

Okamoto, S., S. Ishihara, and S. Maekawa, 2002, Phys. Rev. B **66**, 014435.

Opel, M., R. Nemetschek, C. Hoffmann, R. Philipp, P. F. Müller, R. Hackl, I. Tüttő, A. Erb, B. Revaz, E. Walker, H. Berger, and L. Forró, 2000, Phys. Rev. B **61**, 9752.

Onose, Y., Y. Taguchi, T. Ishikawa, S. Shinomori, K. Ishizaka, and Y. Tokura, 1999, Phys. Rev. lett. **82**, 5120.

Onose, Y., Y. Taguchi, K. Ishizaka, and Y. Tokura, 2001, Phys. Rev. lett. **87**, 217001.

Onose, Y., Y. Taguchi, K. Ishizaka, and Y. Tokura, 2004, Phys. Rev. B **69**, 024504.

Panagopoulos, C., and T. Xiang, 1998, Phys. Rev. Lett. **81**, 2336.

Parkinson, J. B., 1969, J. Phys. C **2**, 2012.

Pashkevich, Yu. G., V. A. Blinkin, V. P. Gnezdilov, V. V. Tsapenko, V. V. Eremenko, P. Lemmens, M. Fischer, M. Grove, G. Güntherodt, L. Degiorgi, P. Wachter, J. M. Tranquada, and D. J. Buttrey, 2000, Phys. Rev. Lett. **84**, 3919.

Pekker, S., A. Jánossy, and A. Rockenbauer, 1991, Physica C **181**, 11.

Perali, A., C., Castellani, C., Di Castro, and M. Grilli, 1996, Phys. Rev. B **54**, 16216.

Perkovitz, S., M. Merlin, and L. R. Testardi, 1976, Solid State Commun. **18**, 1059.

Pinczuk, A., and G. Abstreiter, 1989, in *Light Scattering in Solids V*, edited by M. Cardona and G. Güntherodt (Springer-Verlag, Berlin), p. 153.

Pines, D., 1963, *Elementary Excitations in Solids* (Benjamin, New York).

Pines, D., and P. Nozières, 1966, *The Theory of Quantum Liquids: Normal Fermi Liquids* (Addison-Wesley, New York).

Platzman, P. M., and N. Tzoar, 1964, Phys. Rev. **136**, A11.

Placzek, G., 1934, *Marx's Handbuch der Radiologie*, **6**, (Akademische Verlagsanstalt Leipzig, 209).

Platzman, P. M., 1965, Phys. Rev. **139**, A379.

Platzman, P. M., and E. D. Isaacs, 1998, Phys. Rev. B **57**, 11107.

Pleijel, H., 1930, *Presentation Speech of the Nobel Prize in*

Physics, (e-print, http://nobelprize.org/physics/).

Prelovšek, P., and J. Jaklič, 1996, Phys. Rev. B **53**, 15095.

Pruschke, T., M. Jarrell, and J. K. Freericks, 1995, Adv. Phys. **44**, 187.

Qazilbash, M. M., A. Koitzsch, B. S. Dennis, A. Gozar, Hamza Balci, C. A. Kendziora, R. L. Greene, and G. Blumberg, 2005, Phys. Rev. B **72**, 214510.

Quilty, J. W., H. J. Trodahl, and D. M. Pooke, 1998, Phys. Rev. B **57**, R11097.

Quilty, J. W., S. Tajima, S. Adachi, and A. Yamanaka, 2001, Phys. Rev. B **63**, 100508.

Quilty, J. W., S. Lee, A. Yamamoto, and S. Tajima, 2002, Phys. Rev. Lett. **88**, 087001.

Quilty, J. W., S. Lee, S. Tajima, and A. Yamanaka, 2003, Phys. Rev. Lett. **90**, 207006.

Radaelli, P. G., J. D. Jorgensen, A. J. Schultz, J. L. Peng, and R. J. Green, 1994, Phys. Rev. B **49**, 15332.

Raman, C. V., and K. S. Krishnan, 1928, Nature (London) **121**, 501.

Rashkeev, S. N., and G. Wendin, 1993, Phys. Rev. B **47**, 11603.

Renner, Ch., and Ø., Fischer, 1995, Phys. Rev. B **51**, 9208.

Reznik, D., S. L. Cooper, M. V. Klein, W. C. Lee, D. M. Ginsberg, A. A. Maksimov, A. V. Puchkov, I. I. Tartakovskii, S.-W. Cheong, and 1993, Phys. Rev. B **48**, 7624.

Rho, H., C. S. Snow, S. L. Cooper, Z. Fisk, A. Comment, and J.-P. Ansermet, 2002, Phys. Rev. Lett. **88**, 127401.

Rho, H., S. L. Cooper, S. Nakatsuji, H. Fukazawa, and Y. Maeno, 2003, Phys. Rev. B **68**, 100404.

Richards, D., 2000, Phys. Rev. B **61**, 7517.

Romero, D. B., Y. Moritomo, N. Dieckmann, J. F. Mitchell, and H. D. Drew, 2001, Phys. Rev. B **63**, 132404.

Roulin, M., A. Junod, A. Erb, and E. Walker, 2002, Phys. Rev. Lett. **80**, 1722.

Rübhausen, M., C. T. Rieck, N. Dieckmann, K. O. Subke, A. Bock, and U. Merkt, 1997, Phys. Rev. B **56**, 14797.

Rübhausen, M., P. Guptasarma, D. G. Hinks, and M. V. Klein, 1998, Phys. Rev. B **58**, 3462.

Rübhausen, M., O. A. Hammerstein, A. Bock, U. Merkt, C. T. Rieck, P. Guptasarma, D. G. Hinks, and M. V. Klein, 1999, Phys. Rev. Lett. **82**, 5349.

Rübhausen, M., A. Gozar, M. V. Klein, P. Guptasarma, and D. G. Hinks, 2001, Phys. Rev. B **63**, 224514.

Rudman, D. A., and M. R. Beasley, 1984, Phys. Rev. B **30**, 2590.

Sachdev, S., 1999, *Quantum Phase Transitions*, (Cambridge University Press, Cambridge).

Sacuto, A., R. Combescot, N. Bontemps, C. A. Müller, V. Viallet, and D. Colson, 1998, Phys. Rev. B **58**, 11721.

Sacuto, A., J. Cayssol, P. Monod, and D. Colson, 2000, Phys. Rev. B **61**, 7122.

Saitoh, E., S. Okamoto, K. T. Takahashi, K. Tobe, K. Yamamoto, T. Kimura, S. Ishihara, S. Maekawa, and Y. Tokura, 2001, Nature (London) **410**, 180.

Salamon, D., R. Liu, M. V. Klein, M. A. Karlow, S. L. Cooper, S.-W. Cheong, W. C. Lee, and D. M. Ginsberg, 1995, Phys. Rev. B **51**, 6617.

Sandvik, A., S. Capponi, D. Poilblanc, and E. Dagotto, 1998, Phys. Rev. B **57**, 8478.

Sassetti, M., and B. Kramer, 1998, Phys. Rev. Lett. **80**, 1485.

Sassetti, M., F. Napoli, and B. Kramer, 1999, Phys. Rev. B **59**, 7297.

Scalapino, D. J., 1995, Phys. Rep. **250**, 330.

Schicktanz, S., R. Kaiser, E. Schneider, and W. Gläser, 1980, Phys. Rev. B **22**, 2386.

Schicktanz, S., R. Kaiser, W. Weber, C. Politis, R. Flükiger, and P. Bujard, 1982, Phys. Rev. B **26**, 4909 and references therein.

Schneemeyer, L. F., J. V. Waszczak, T. Siegrist, R. B. van Dover, L. W. Rupp, B. Batlogg, R. J. Cava, and D. W. Murphy, 1987, Nature (London) **328**, 601.

Schulz, B., J. Bäckström, D. Budelmann, R. Maeser, M. Rübhausen, M. V. Klein, E. Schoeffel, A. Mihill, and S. Yoon, 2005, Rev. Sci. Inst. **76**, 073107.

Shastry, B. S., and B. I. Shraiman, 1991, Phys. Rev. Lett. **65**, 1068.

Shastry, B. S., and B. I. Shraiman, 1991, Int. Journ. Mod. Phys. B **5**, 365.

Shen, Z.-X., D. S. Dessau, B. O. Wells, D. M. King, W. E. Spcier, A. J. Arko, D. Marshall, L. W. Lombardo, A. Kapitulnik, P. Dickinson, S. Doniach, and J. DiCarlo, 1993, Phys. Rev. Lett. **70**, 1553.

Sherman, E. Ya., C. Ambrosch-Draxl, and O. V. Misochko, 2002, Phys. Rev. B **65**, 140510.

Sherman, E. Ya., O. V. Misochko, and P. Lemmens, 2003, in *Spectra of High T_c Superconductors: A Theoretical View.*, edited by N. M. Plakida (Taylor & Francis Publ., London and New York).

Shvaika, A. M., 2000, Physica C **341-348**, 177.

Shvaika, A. M., O. Vorobyov, J. K. Freericks, and T. P. Devereaux, 2004, Phys. Rev. Lett. **93**, 137402.

Shvaika, A. M., O. Vorobyov, J. K. Freericks, and T. P. Devereaux, 2005, Phys. Rev. B **71**, 045120.

Sidis, Y., S. Pailhès, B. Keimer, P. Bourges, C. Ulrich, and L. P. Regnault, 2004, Phys. Status Solidi B **241**, 1204.

Sigrist, M., T. M. Rice, and F. C. Zhang, 1994, Phys. Rev. B **49**, 12058.

Silva Neto, M. B., and L. Benfatto, 2005, Phys. Rev. B **72**, R140401.

Singh, R. R. P., P. A. Fleury, K. B. Lyons, and P. E. Sulewski, 1989, Phys. Rev. Lett. **62**, 2736.

Singley, E. J., D. N. Basov, K. Kurahashi, T. Uefuji, and K. Yamada, 2001, Phys. Rev. B **64**, 224503.

Skinta, J. A., T. Lemberger, T. Greibe, and M. Naito, 2002a, Phys. Rev. Lett. **88**, 207003.

Skinta, J. A., M. S. Kim, T. Lemberger, T. Greibe, and M. Naito, 2002b, Phys. Rev. Lett. **88**, 207005.

Slakey, F., M. V. Klein, E. D. Bukowski, and D. M. Ginsberg, 1990a, Phys. Rev. B **41**, 2109.

Slakey, F., M. V. Klein, J. P. Rice, and D. M. Ginsberg, 1990b, Phys. Rev. B **42**, 2643.

Slakey, F., M. V. Klein, J. P. Rice, and D. M. Ginsberg, 1991, Phys. Rev. B **43**, 3764.

Smekal, A., 1923, Naturwissenschaften **11**, 873.

Snow, C. S., S. L. Cooper, D. P. Young, Z. Fisk, A. Comment, and J.-P. Ansermet, 2001, Phys. Rev. B **64**, 174412.

Snow, C. S., S. L. Cooper, G. Cao, J. E. Crow, H. Fukazawa, S. Nakatsuji, and Y. Maeno, 2002, Phys. Rev. Lett. **89**, 226401.

Snow, C. S., J. F. Karpus, S. L. Cooper, T. E. Kidd, and T.-C. Chiang, 2003, Phys. Rev. Lett. **91**, 136402.

Sooryakumar, F., M. V. Klein, and C. Frindt, 1978, Ann. Phys. (N.Y.) **111**, 61.

Sooryakumar, F., and M. V. Klein, 1981, Phys. Rev. B **23**, 3213.

Sooryakumar, F., M. V. Klein, and R. F. Frindt, 1981, Phys. Rev. B **23**, 3222.

Sooryakumar, F. and M. V. Klein, 1980, Phys. Rev. Lett. **45**,

660.

Stadlober, B., R. Nemetschek, O. V. Misochko, R. Hackl, P. Müller, J. J. Neumeier, and K. Winzer, 1994, Physica B **194-196**, 1539.

Stadlober, B., G. Krug, R. Nemetschek, R. Hackl, J. L. Cobb, and J. T. Markert, 1995, Phys. Rev. Lett. **74**, 4911.

Staufer, T., R. Hackl, and P. Müller, 1990, Solid State Commun. **75**, 975.

Staufer, T., R. Nemetschek, R. Hackl, P. Müller, and H. Veith, 1992, Phys. Rev. Lett. **68**, 1069.

Stock, C., W. J. L. Buyers, Z. Yamani, C. L. Broholm, J.-H. Chung, Z. Tun, R. Liang, D. Bonn, W. N. Hardy, and R. J. Birgeneau, 2006, Phys. Rev. B **73**, 100504.

Strohm, T., and M. Cardona, 1997, Phys. Rev. B **55**, 12725.

Strohm, T., D. Munzar, and M. Cardona, 1998a, Phys. Rev. B **58**, 8839.

Sugai, S., S.-I. Shamoto, and M. Sato, 1988, Phys. Rev. B **38**, 6436.

Sugai, S., and T. Hosokawa, 2000, Phys. Rev. Lett. **85**, 1112.

Sugai, S., H. Suzuki, Y. Takayanagi, T. Hosokawa, and N. Hayamizu, 2003, Phys. Rev. B **68**, 184504.

Sulewski, P. E., P. A. Fleury, K. B. Lyons, S.-W. Cheong, and Z. Fisk, 1990, Phys. Rev. B **41**, 225.

Sulewski, P. E., P. A. Fleury, K. B. Lyons, and S.-W. Cheong, 1991, Phys. Rev. Lett. **67**, 3864.

Sutherland, M., S. Y. Li, D. G. Hawthorn, R. W. Hill, F. Ronning, M. A. Tanatar, J. Paglione, H. Zhang, L. Taillefer, J. DeBenedictus, R. Liang, D. A. Bonn, and W. N. Hardy, 2005, Phys. Rev. Lett. **94**, 147004.

Tanner, D. B., and H. J. Sievers, 1973, Phys. Rev. B **8**, 1978.

Tassini, L., Q. M. Zhang, F. Venturini, R. Hackl, F. Kikugawa, and S.-W. Fujita, 2005, Phys. Rev. Lett. **95**, 117002.

Thomsen, C., and M. Cardona 1989, in *Physical Properties of High Temperature Superconductors*, edited by D. M. Ginsberg (World Scientific, Singapore), p. 409.

Thomsen, C., 1991, in *Light Scattering in Solids VI*, edited by M. Cardona and G. Güntherodt (Springer-Verlag, Berlin), p. 285.

Tilley, D. R., 1972, Z. Physik **254**, 71.

Timusk, T., and B. W. Statt, 1999, Rep. Prog. Phys. **62**, 61.

Tohyama, T., H. Onodera, K. Tsutsui, and S. Maekawa, 2002, Phys. Rev. Lett. **89**, 2002.

Tokura, Y., H. Takagi, and S. Uchida, 1989, Nature (London) **337**, 345.

Tranquada, J. M., B. J. Sternlieb, J. D. Axe, Y. Nakamura, and S. Uchida, 1995, Nature (London) **375**, 561.

Tranquada, J. M., H. Woo, T. G. Perring, H. Goka, G. D. Gu, G. Xu, M. Fujita, and K. Yamada, 2004, Nature (London) **429**, 534.

de Trey, P., S. Gygax, , and J.-P. Jan, 1973, J. Low Temp. Phys. **11**, 421.

Triscone, G., J.-Y. Genoud, T. Graf, A. Junod, and J. Muller, 1991, Physica C **176**, 247.

Tsuei, C. C. and J. R. Kirtley, 2000, Rev. Mod. Phys. **70**, 969.

Tüttő, I., and A. Zawadowski, 1992, Phys. Rev. B **45**, 4842.

Turlakov, M., and A. Leggett, 2001, Phys. Rev. B **63**, 064518.

Uchida, S., T. Ido, H. Takagi, T. Arima, Y. Tokura, and S. Tajima, 1991, Phys. Rev. B **43**, 7942.

Valla, T., A. V. Fedorov, P. D. Johnson, P.-A. Glans, C. McGuinness, K. E. Smith, E. Y. Andrei, and H. Berger, 2004, Phys. Rev. Lett. **92**, 086401.

Van Harlingen, D. J., 1995, Rev. Mod. Phys. **67**, 515.

Varma, C. M., P. B. Littlewood, S. Schmitt-Rink, E. Abrahams, and A. E. Ruckenstein, 1989a, Phys. Rev. Lett. **63**, 1996.

Varma, C. M., 1989b, Physica C **162-164**, 303.

Varma, C. M., 1997, Phys. Rev. B **55**, 14554.

Venturini, F., U. Michelucci, T. P. Devereaux, and A. Kampf, 2000, Phys. Rev. B **62**, 15204.

Venturini, F., M. Opel, T. P. Devereaux, J. K. Freericks, I. Tüttő, B. Revaz, E. Walker, H. Berger, L. Forró, and R. Hackl, 2002a, Phys. Rev. Lett. **89**, 107003.

Venturini, F., Q.-M. Zhang, R. Hackl, A. Lucarelli, S. Lupi, M. Ortolani, P. Calvani, N. Kikugawa, and T. Fujita, 2002b, Phys. Rev. B **66**, 060502.

Venturini, F., M. Opel, R. Hackl, H. Berger, L. Forró, and B. Revaz, 2002c, Journ. Phys. Chem. Solids **63**, 2345.

Venturini, F., R. Hackl, and U. Michelucci, 2003, Phys. Rev. Lett. **90**, 149701.

Verkin, B. I., and B. G. Lazarev, 1948, Izv. Akad. Nauk SSSR Ser. Fiz. **12**, 598.

Vershinin, M., S. Misra, S. Ono, Y. Abe, Y. Ando, and A. Yazdani, 2004, Science **303**, 1995.

Virosztek, A., and J. Ruvalds, 1991, Phys. Rev. Lett. **67**, 1657.

Virosztek, A., and J. Ruvalds, 1992, Phys. Rev. B **45**, 347.

Vojta, M., 2003, Rep. Prog. Phys. **66**, 2069.

Wakimoto, S., H. Zhang, K. Yamada, I. Swainson, H. Kim, and R. J. Birgeneau, 2004, Phys. Rev. Lett. **92**, 217004.

Wang, D.-W., and S. Das Sarma, 1999, Phys. Rev. Lett. **83**, 816.

Wang, D.-W. and S. Das Sarma, 2002, Phys. Rev. B **65**, 125322.

Wang, D.-W., A. J. Millis, and S. Das Sarma, 2004, Phys. Rev. B **70**, 165101.

Weber, W., 1984, Physica B+C **126**, 217.

Worlock, J. M., A. Pinczuk, Z. J. Tien, C. H. Perry, H. L. Störmer, R. Dingle, A. C. Gossard, W. Wiegmann, and R. Aggarwal, 1981, Solid State Commun. **32**, 867.

Wipf, H., M. V. Klein, B. S. Chandrasekhar, T. H. Geballe, and J. H. Wernick, 1978, Phys. Rev. Lett. **41**, 1752.

Wolff, P. A., 1966, Phys. Rev. Lett. **16**, 225.

Wolff, P. A., 1968, Phys. Rev. **171**, 436.

Wu, M. K., J. R. Ashburn, C. J. Torng, P. H. Hor, R. L. Meng, L. Gao, Z. J. Huang, Y. Q. Wang, and C. W. Chu, 1987, Phys. Rev. Lett. **58**, 908.

Wu, W., and A. Griffin, 1995a, Phys. Rev. B **51**, 1190.

Wu, W., and A. Griffin, 1995b, Phys. Rev. B **52**, 7742.

Wu, W., and A. Griffin, 1996, Phys. Rev. B **54**, 6539.

Wu, W., and J. P. Carbotte, 1997, Phys. Rev. B **56**, 6327.

Wu, W. C., and J. P. Carbotte, 1998, Phys. Rev. B **57**, 5614.

Xu, Z. A., N. P. Ong, Y. Wang, T. Kageshita, and S. Uchida, 2000, Nature (London) **406**, 486.

Yamamoto, K., T. Katsufuji, T. Tanabe, and Y. Tokura, 1998, Phys. Rev. Lett. **80**, 1493.

Yamamoto, K., T. Kimura, T. Ishikawa, T. Katsufuji, and Y. Tokura, 2000, Phys. Rev. B **61**, 14706.

Yamanaka, A., T. Kimura, F. Minami, K. Inoue, and S. Takekawa, 1988, Jpn. J. Appl. Phys. **27**, L1902.

Yamanaka, A., H. Takato, F. Minami, K. Inoue, and S. Takekawa, 1992, Phys. Rev. B **46**, 516.

Yamanaka, A., N. Asayama, T. Furutani, K. Inoue, and S. Takekawa, 1996, SPIE Proceedings **2696**, 276.

Yang, I.-S., M. V. Klein, S. L. Cooper, P. C. Canfield, B. K. Cho, and S.-I. Lee, 2000a, Phys. Rev. B **62**, 1291.

Yang, I.-S., M. V. Klein, T. P. Devereaux, I. R. Fisher, and P. C. Canfield, 2000b, Physica C **341-348**, 2259.

Yoon, S., H. L. Liu, G. Schollerer, S. L. Cooper, P. D. Han, D. A. Payne, S.-W. Cheong, and Z. Fisk, 1998, Phys. Rev. B **58**, 2795.

Yoon, S., M. Rübhausen, S. L. Cooper, K. H. Kim, and S.-W. Cheong, 2000, Phys. Rev. Lett. **85**, 3297.

Yoshida, T., X. J. Zhou, T. Sasagawa, W. L. Yang, P. V. Bogdanov, A. Lanzara, Z. Hussain, T. Misokawa, A. Fujimori, H. Eisaki, Z.-X. Shen, T. Kakeshita, and S. Uchida, 2003, Phys. Rev. Lett. **91**, 027001.

Zaanen, J., and O. Gunnarsson, 1989, Phys. Rev. B **40**, 7391.

Zasadzinski, J., 2002, in *The Physics of Supreconductors Vol. I*, edited by K. H. Bennemann and J. B. Ketterson (Springer-Verlag, Berlin), p. 591.

Zawadowski, A., J. Ruvalds, and J. Solana, 1972, Phys. Rev. A **4**, 399.

Zawadowski, A., and M. Cardona, 1990, Phys. Rev. B **42**, 10732.

Zeyher, R., and A. Greco, 2002, Phys. Rev. Lett. **89**, 177004.

Zeyher, R., 2003, Phys. Rev. Lett. **90**, 107002.

Zhou, T., K. Syassen, M. Cardona, J. Karpinski, and E. Kaldis, 1996, Solid State Commun. **99**, 669.

Zhou, X. J., T. Yoshida, D.-H. Lee, W. L. Yang, V. Brouet, F. Zhou, W. X. Ti, J. W. Xiong, Z. X. Zhao, T. Sasagawa, T. Kakeshita, H. Eisaki, S. Uchida, A. Fujimori, Z. Hussain, and Z.-X. Shen, 2004, Phys. Rev. Lett. **92**, 187001.